Deposition of Newtonian Particles Entrained in a Turbulent Axisymmetric Free Jet

Zachary Burton Smith Robertson

Thesis submitted to the faculty of the Virginia Polytechnic Institute and State University in partial fulfillment of the requirements for the degree of

Master of Science
In
Mechanical Engineering

Kenneth S. Ball
Mark A. Pierson
Robert E. Masterson

April 23, 2012
Blacksburg, VA

Keywords: particle, deposition, axisymmetric jet, entrainment, turbulence

Deposition of Newtonian Particles Entrained in a Turbulent Axisymmetric Free Jet

Zachary Burton Smith Robertson

ABSTRACT

In the past 10 years there has been a significant amount of research into two-phase particle transport. The terrorist events of September 11, 2001 sparked a series of studies analyzing particle entrainment and deposition in turbulent airflows. One area of research needing further attention has been the study of particles entrained in axisymmetric air jets. An experimental rig was designed and built to study entrainment properties and deposition of Newtonian particles, after injection into a turbulent axisymmetric free air jet.

Newtonian spherical particles, ranging from 1mm to 6mm in diameter, were injected into a turbulent airstream and blown through a nozzle into a large, open space. As the particles fell out of the jet stream, their linear distances, from nozzle to initial-ground-contact, were recorded and analyzed.

The experiments conducted indicated particle size and density to be significant factors when considering Newtonian particle entrainment. Additionally, particle deposition distribution revealed a consistent positive skewness, as opposed to an expected Gaussian form.

The data presented in this paper provide a starting point for understanding entrainment of Newtonian spherical particles in jets. The simple experimental rig geometry and results also provide an opportunity for computational fluid dynamics models to be validated, answering a call from the 2006 Annual Review of Fluid Mechanics.

Dedication

This thesis is dedicated to my family, friends, and shipmates, for their unwavering love and support throughout all of my endeavors. The kindness, energy, and continuous sense of humor shared with me made this project possible.

Acknowledgements

First, I would like to thank the chairman of my committee, Dr. Ken Ball. As my advisor, Dr. Ball's insight and advice initiated this project, and his support made the completion a reality. Without Dr. Ball's ingenuity and enthusiasm, the Transport Phenomena and National Security Lab would not be in existence.

My committee members, Dr. Mark Pierson and Dr. Robert Masterson, both provided advice and knowledge that aided me through my degree process. Their abilities to make learning interesting and fun are renown throughout the Mechanical Engineering Department. Their teaching inspired me to seek out new areas of study and broaden my foundation of engineering knowledge.

A big thank you to the other members of the Transport Phenomena and National Security Lab. Chris Sebesta and Sandria Gray's advice and CFD support saved me weeks of work through their knowledge of ANSYS Fluent and other computer software.

Finally, I would like to acknowledge the incredible amount of support provided me by the United States Coast Guard. Specifically CAPT Matthew Miller, LT Alfred Giordano, SK1 Erik O'Brien, YN2 Stephanie Kerly, and the entire Marine Engineering Advanced Education program; without their financial and administrative support, it would not have been possible for me to attend Virginia Polytechnic Institute and State University.

All photos taken by the author, 2012.

Table of Contents

List of Figures

List of Tables

Nomenclature

SYMBOL	DESCRIPTION	UNITS
a	uncertainty value	
α	jet spread half-angle	^{o}
B	constant of decay	
C	critical value	
C_D	drag coefficient	
C_L	lift coefficient	
D	difference value	
d_n	nozzle diameter	m
d_p	particle diameter	m
$d_{P\sigma}$	particle diameter standard deviation	m
$d_{P\mu}$	mean particle diameter	m
F_B	buoyancy force	N
F_D	drag force	N
F_L	lift force	N
g	gravitational acceleration	m/s^2
k	velocity gradient	
m	mass	kg
m_p	particle mass	kg
μ_f	dynamic viscosity	kg/(m•s)
n	number of particles	
N_1	number of standard normal data points	
N_2	number of experimental data points	
π	pi	
ρ_f	fluid density	kg/m^3
ρ_p	particle density	kg/m^3
Re_p	particle Reynold's number	
T	temperature	K
U	centerline velocity	m/s
U_C	mean nozzle velocity	m/s
V	velocity	m/s
V_f	volume of fluid flow	m^3
V_p	particle volume	m^3
V_s	particle settling velocity	m/s
ν_f	kinematic viscosity	m^2/s
x	location along x-axis	m
Φ_p	volume fraction of particles	

CHAPTER 1 – Introduction

Motivation

Since the terrorist events of September 11, 2001 and the anthrax attacks of October 2001, there has been an increase of research in two-phase particle flow dynamics. The possibility of a chemical, biological, or radiological (CBR) threat being released to the public, as in New York City and Washington, DC, became a source of fear for the American people. This resulted in an increased demand for the development of new methods for locating, tracking, and predicting the spread of CBR particles, given a release in an urban environment [1]. Suddenly, a sub-field of study within the fluid mechanics community, "Homeland Security", was born. With this new field, research in multi-phase particulate flows was brought back to the front burner, as scientists and engineers tried to provide fast and accurate models to predict particle paths in various air flows [2].

Five years later, in 2006, Settles published an exceptional summary of this new field, entitled, "Fluid Mechanics and Homeland Security" [2]. This paper identified some of the great successes of the engineering community from 2001-2006, but also served as a call for further research in areas of need. One critical area of need was more experimental data to support and validate computer models, which would then predict the spread of CBR contaminants in urban environments. Settles recognized that although computer modeling of fluid flows is the way of the future for engineering, it cannot be considered accurate without adequate experimental test data to support its findings [2].

In 2010, Virginia Polytechnic Institute and State University's Mechanical Engineering Department created the Transport Phenomena and National Security (TPaNS) Lab. The TPaNS Lab joined the Homeland Security field in attempting to find an accurate model for identifying particle entrainment and dispersion characteristics for flows within building HVAC systems.

The research described in this paper comes from the TPaNS Lab, with the hope of creating a better understanding of what physical characteristics support particle entrainment, as

well as several data sets to be used for validation of computational fluid dynamics (CFD) codes, modeling particle transport in simple geometries. Specifically, this paper focuses on particle dispersion from an axisymmetric jet into an open environment. The particles studied will represent a selection from the Newtonian regime, as there has been very little research of this scale of particles in jet flows, and as start-up funding and facilities of the new TPaNS Lab is currently too limited to analyze those of the Stokes regime. The particle flow regimes are discussed in the next section.

This paper will describe a series of experiments, conducted to study the dispersion distance of Newtonian particles, injected into a pipe flow, and ejected in an axisymmetric jet, from a wall to an open space. This paper will study how a particle's diameter, mass, density, and injection-quantity, affects its ability to entrain in an axisymmetric jet flow.

Research Objectives

The primary objectives of this research project are:

- Create an experimental rig to study particle transport and the behavior of particles injected into axisymmetric jets
- Examine the relevant factors in maximizing entrainment by studying particle dispersion distance
- Provide experimental data to support the creation of a CFD code modeling particle transport in axisymmetric jets

Background

Particle Forces and Classification:

Particle Flow Regime

Ultimately, whether or not a particle will entrain is determined by an imbalance of forces in the upward-vertical direction. However, before the relevant forces acting on a particle can be identified, the flow regime of the particle must be determined. Particle flows are generally classified as existing in the Stokes, Transition, or Newtonian regime. This classification is determined by the particle Reynolds number (Re_p). Stokes's Law applies for $Re_p \leq 1$, Transition Regime for $1 < Re_p < 1000$, and Newton's Law exists for $Re_p \geq 1{,}000$ [3]. Particle Reynolds number can be determined from

$$\mathrm{Re}_p = \frac{V_s d_p}{\nu_f} \tag{1}$$

where V_s is the particle settling velocity, d_p is particle diameter, and ν_f is the kinematic viscosity of the fluid surrounding the particle [4]. Particle settling velocity has two main equations, one for particles in the Stokes regime and another for those in the Newtonian regime, as shown in Eq. (2) and (3), respectively.

$$V_s = \frac{\rho_p d_p^2 g}{18\mu_f} \tag{2}$$

$$V_s = \left(\frac{4\rho_p d_p g}{3C_D \rho_f} \right)^{1/2} \tag{3}$$

In these equations, ρ_p is particle density, ρ_f is fluid density, μ_f is dynamic viscosity of the fluid, C_D is drag coefficient, and g is gravitational acceleration. For a spherical Newtonian particle, $C_D \approx 0.44$ (note that this is not true for Transition or Stokes regimes) [3].

Drag & Lift Forces

Two equations exist for the calculation of drag force on a spherical particle. Stokes' Law provides one formula, best used with particles of $Re_p \leq 1$, shown below in Eq. (4) [3].

$$F_D = 3\pi\mu_f V d_p \tag{4}$$

Newton's Law provides the second formula, best used with particles in the Transition and Newtonian regimes [3]:

$$F_D = C_D \frac{\pi}{8} \rho_f V^2 d_p^2 \tag{5}$$

As with drag, there are two different equations used for lift. The first for those in the Stokes regime and the second in the Newtonian:

$$F_L = \frac{20.3 V d_p^2 k^{1/2} \mu}{\nu^{1/2}} \tag{6}$$

where k is the velocity gradient [5, 6]. To find the lift force on a particle with a $Re_p > 1$, the following formula is used [4]:

$$F_L = C_L \frac{\pi}{8} \rho_f V^2 d_p^2 \tag{7}$$

Formulas for lift of particles in the Stokes's region are more complicated and not relevant to the research in this paper. For further information of lift of Stokes particles, it is recommended to refer to P.G. Saffman's paper regarding lift on small spheres in slow shear flows [6].

Buoyancy Force

Another force relevant for smaller particles (primarily Stokes) is buoyancy. Although this value is relatively small compared to lift, drag, and gravity for large particles, it is very significant for particles less than 50 μm [5]. Spherical buoyancy force is [4]:

$$F_B = \frac{4}{3} \rho_f \pi \left(\frac{d_p}{2} \right)^3 \tag{8}$$

Other Forces

Gravitational force is the last known relevant force acting upon the particles in the flow. Adhesion and friction forces are not significant for the particles in this experiment, as they will not be entrained from a resting position [5]. Forces related to particle-particle interaction are not

known for this experiment, as particles will be Newtonian, and will be examined in the experiment.

Dispersion Classification

Particle collections can be classified as either polydisperse or monodisperse. When using spherical particles, monodisperse particles are those:

$$\frac{d_{p_\sigma}}{d_{p_\mu}} < 0.1 \tag{9}$$

where $d_{P\sigma}$ is particle diameter standard deviation and $d_{P\mu}$ is particle diameter mean value [7]. All other particle collections are considered polydisperse. There are other definitions for monodispersity, but this is the most conservative and widely used value in the Fluids community. The research in this paper was conducted using monodisperse particles. If results are compared to polydisperse experiments, a correction factor must be applied. This correction factor can be found in [8].

Phase Coupling

Coupling has been found to be an important classification of multi-phase turbulent flows. The term "coupling" refers to the relationships within the particles and fluids. The types of coupling and general behavior of each are listed in Table 1. Generally, the greater the volume fraction of particles (Φ_p), as defined in Eq. (10), the higher the coupling type [9]. This is important to the engineer, not only to better understand the physics of the flow, but as the computation time for a numerical analysis increases dramatically with each increase of coupling type [10]. Four-way coupling is especially challenging for most CFD models.

Coupling Type	Description
One-Way	Fluid Affects Particle
Two-Way	Fluid Affects Particle Particle Affect Fluid
Four-Way	Fluid Affects Particle Particle Affect Fluid Particle Affect Particles Particles Affect Particle

Table 1. Coupling Types & Description of Relationship

$$\Phi_p = \frac{nV_p}{V_f} \tag{10}$$

n: number of particles

V_p: particle volume (m^3)

V_f: volume of fluid flow (m^3)

When the volume fraction of particles is roughly greater than 10^{-3}, four-way coupling should be assumed. When lower than 10^{-6}, one-way coupling can be assumed [9]. These volume fraction values were set for Stokes regime particles and are not necessarily the same for those in the Newtonian regime.

Axisymmetric Jets

Turbulent axisymmetric free jets are the most common jets considered in multiphase flows. In studies of particles entrained in jets, axisymmetric free jets are considered almost exclusively. These jets are often chosen due to their frequent appearance in environmental, atmospheric, and mining studies. When identifying jet geometries and characteristics, it is important to understand the characteristics of the nozzle. Nozzle geometry and size are the most significant factors in jet stream shape and velocity.

There continues to be debate among researchers as to the angle of spread for axisymmetric jets (α, as seen below in Figure 1). Recent studies suggest same-fluid turbulent axisymmetric free jets have linear (or near-linear) spread half-angles of approximately 9.4º-11.8º [11-14]. However, Birkoff and Zarantonello, in the late 1950's, published half-angle ranges as high as 25º [15].

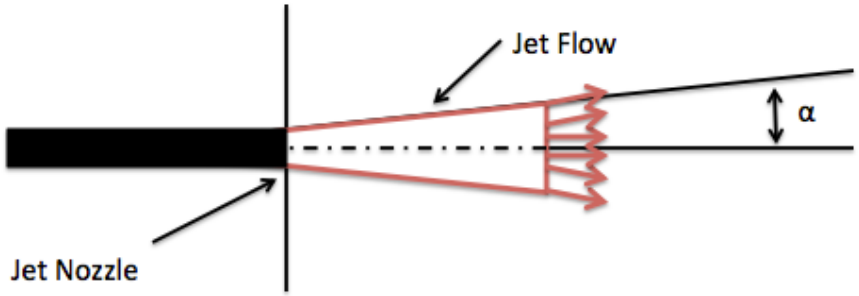

Figure 1. Axisymmetric Jet Spread Half-Angle, α

Regardless of the debate on the spread angles in Zaratonello's research, 11.8º is considered to be an appropriate broad-approximation for same-fluid turbulent axisymmetric jets. Additionally, it is well accepted that as long as a flow is turbulent, the spread angle of the jet is not dependent on Reynolds number [14]. Flow Reynolds, Froude, Weber, and Mach numbers all do have a significant effect on the breakup and length characteristics of the jet, so they cannot be immediately discarded [16].

With regard to jet spread and breakup, an important measure of jets is centerline velocity. To find centerline velocity at a given point, use

$$U_C = \frac{Bd_nU}{x} \tag{11}$$

where U_C is the centerline velocity of the jet, B is the constant of decay, d_n is the jet's nozzle diameter, U is the mean nozzle velocity, and x is location along the x-axis [17, 18]. Note that x is based off the reference location, "Virtual Orifice", as labeled in Figure 2, with the positive direction traveling with the jet flow [14, 17]. The constant of decay is an empirical constant found to be approximately B = 5.8 (experimental data ranges from 5.8 to 6.06) [14, 19, 20].

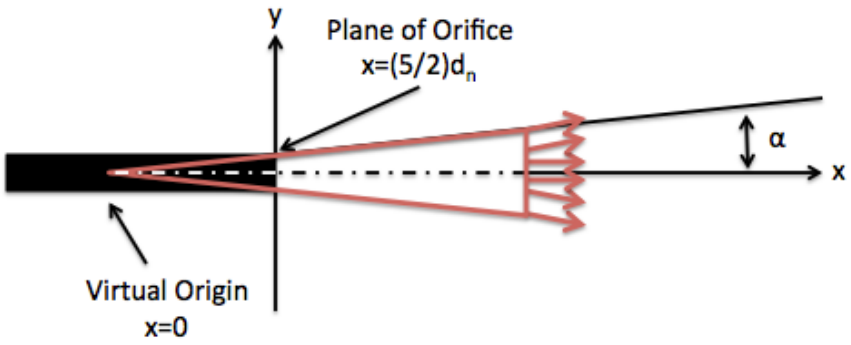

Figure 2. Axisymmetric Jet Virtual Orifice

Lagrangian vs. Eulerian Tracking

As a brief review of the two models for flow tracking, the Lagrangian method and Eulerian method must be identified. Researchers of fluid dynamics use these two methods to analyze and describe fluid flows. The Eulerian method involves monitoring fixed locations in space, as time progresses, and recording particle information as it passes through that location with the passage of time. The Lagrangian method involves monitoring fixed particles as they pass through space, as a function of time, recording data along the passage (velocity, position, pressure, density, etc.) [4, 21]. A common classroom visualization of this involves two scientists tracking migrating geese, known to travel from Baja California to Alaska. One scientist uses the Eulerian method by placing monitoring stations in Los Angeles, CA, Portland, OR, and Seattle, WA and recording the date, time, flight direction, and number of all geese passing overhead as they complete the migration. From this data he can create a plot showing their path and speed from Baja to Alaska. The second scientist uses the Lagrangian method by placing tracking tags on a dozen individual geese, randomly selected from those in Baja, before they depart. As they make their way to Alaska, the scientist can track their velocity vectors and path, and use the data to create a theory for the collective migration [22]. Both methods are valid, and both may produce the same result. However, resources, time, and environment must be evaluated before an experiment to determine which method will be the most effective for one's research. For the experiments in this paper, the Eulerian method has been chosen due to time and lab resources.

Literature Review:

Particles in jet flows were first studied numerically by Ricou and Spalding in 1961, and then followed up by Fields in the next couple of years [23, 24]. Both research groups published several papers regarding particles and entrainment in axisymmetric jets, using similar geometries to this paper, however they focused their studies on the entrainment properties of the fluid around the jet. They were looking for ways to increase thermal mixing, so the paths and direct behaviors of the particles were not of much concern [25].

Several papers have been published with computer models of particle transport of Stokes-regime contaminants in HVAC and other indoor environments. Although these indoor flow studies do not relate to the free jet scenario of this thesis, the results of these papers' models are helpful in understanding and approximating particle flows in turbulent environments. Chen [26], Gao [27], and Zhao [28, 29], presented papers describing particle transport in ventilation systems and single-room HVAC conditions. Sextro [30], Winters [31], and Musser [32], presented papers discussing room to room transport and HVAC systems reaching multiple building zones. Lastly, Zhao [33], and Zhang [34], compared Eulerian and Lagrangian methods for particle transport in enclosed spaces. Their descriptions of the Eulerian and Lagrangian methods are beneficial for anyone needing more information regarding the pros and cons of each method.

Useful experimental data on axisymmetric free jets has been collected and published by Panchapakesan [20], Hussein [19], Wygnanski [18], and Mi et al. [35]. The textbook, "Turbulent Flows", by Pope also serves as an excellent first-read on axisymmetric free jets [14].

Study of Stokes regime particle velocity vectors in turbulent round jets have been conducted by several researchers. Hardalups et al. [36], and Fleckhaus et al. [37], provide quality experimental, time-averaged data for CFD modelers to use as code validation. Longmire and Eaton also provide experimental data, not time-averaged, and include a large collection of clear flow visualization figures [38]. Casciola et al. [39], and Gualtieri [40], studied the inertial particle properties of these flows, demonstrating how particles do not always behave as tracer elements, resisting path change and congregating with other particles.

Chung and Troutt conducted the research most similar to this project in 1986, when they published an article in the Journal of Fluid Mechanics, "Simulation of particle dispersion in an axisymmetric jet" [41]. Their paper considered a numerical simulation, compared to experimental data reported by Crowe [42]. The information and results contained in those papers, while helpful for creating approximations for the particle paths in this experiment set, do not directly apply, as all of their data was for particles in the Stokes's regime [41].

CHAPTER 2 – Experimental Methods

Introduction:

To better understand the entrainment properties of Newtonian particles, an experimental rig was designed and built to propel particles mixed in a turbulent air flow through a smooth nozzle into an open space. After exiting the nozzle, located four feet above the ground, the stream becomes a turbulent jet flow. As the flow dissipates, the particles drop out of the jet stream and are trapped on the ground. Each particle's distance in the x direction (as shown in Figure 2) is measured and compared to other experimental initial conditions, to determine which particle factors most significantly affect entrainment.

Experimental Rig:

Overview

The experimental rig at the Transport Phenomena and National Security (TPaNS) Lab consists of two connected apparatuses:

- Jet Propulsion Apparatus
- Particle Entrapment System

The Jet Propulsion Apparatus creates the turbulent pipe airflow via a blower, flowmeter, PVC pipe system, particle injection system, and jet nozzle. The Particle Entrapment System consists of a large, open-end, 5-sided room for the jet-particle airstream, as well as the ground-level particle entrapment system. Overall, the rig measures 23 feet long, 8 feet tall, and 4 feet wide. Figure 3 shows the experimental rig, with both apparatuses labeled and identified.

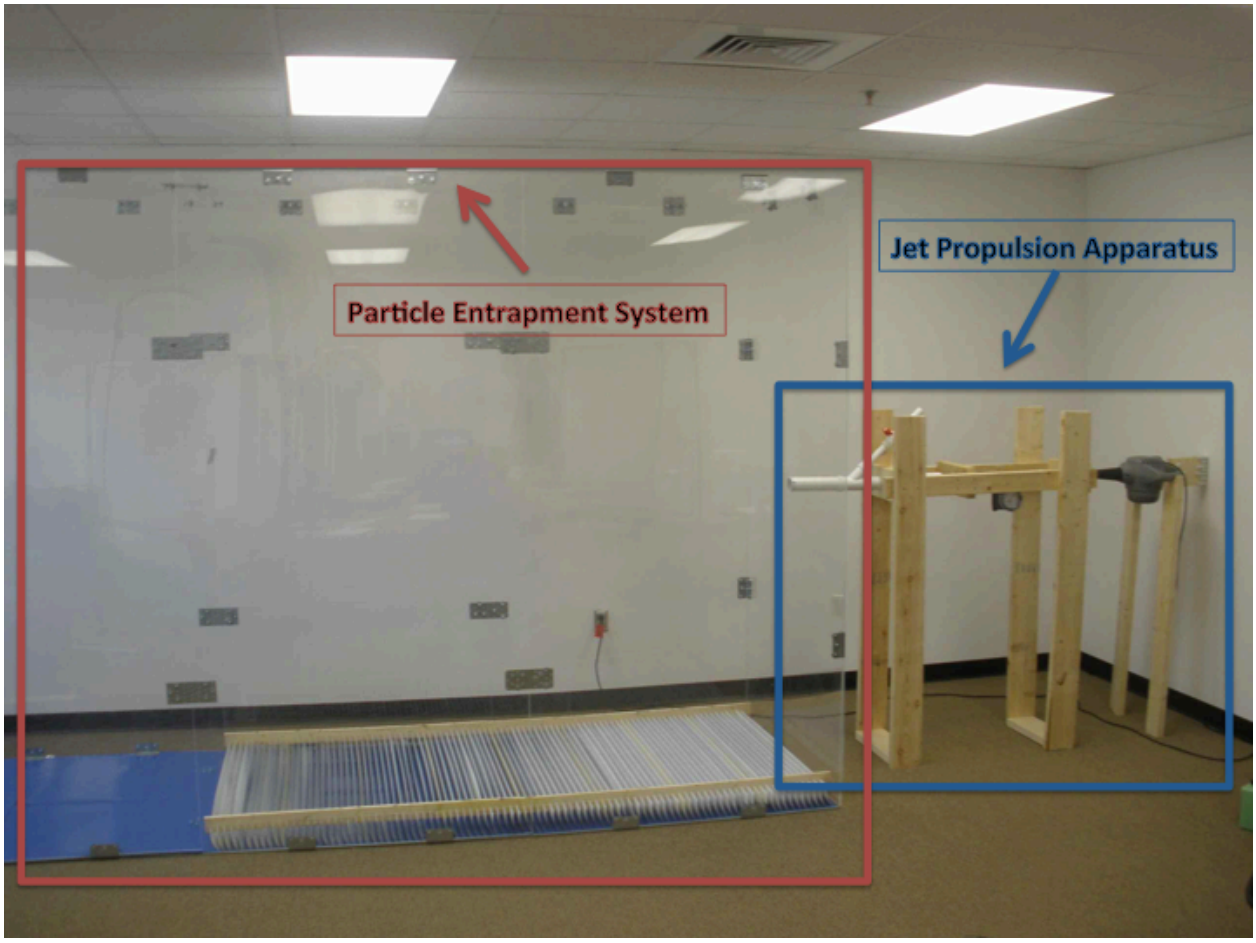

Figure 3. Experimental Rig & Labeled Apparatuses

Jet Propulsion Apparatus

The Jet Propulsion Apparatus (seen in Figure 4 below), like the rest of the experimental rig, was designed and built to allow easy adjustments for future experiments. All of the supports were made out of wood and screws, for fast and cheap modification. PVC components made customizing the flow piping possible without having to worry about any weld jobs. The only real limitation on the Jet Propulsion Apparatus was its length. As the experimental rig was 23 feet long, it would be difficult to add more than an inch or two to the system, unless moved to a larger lab space.

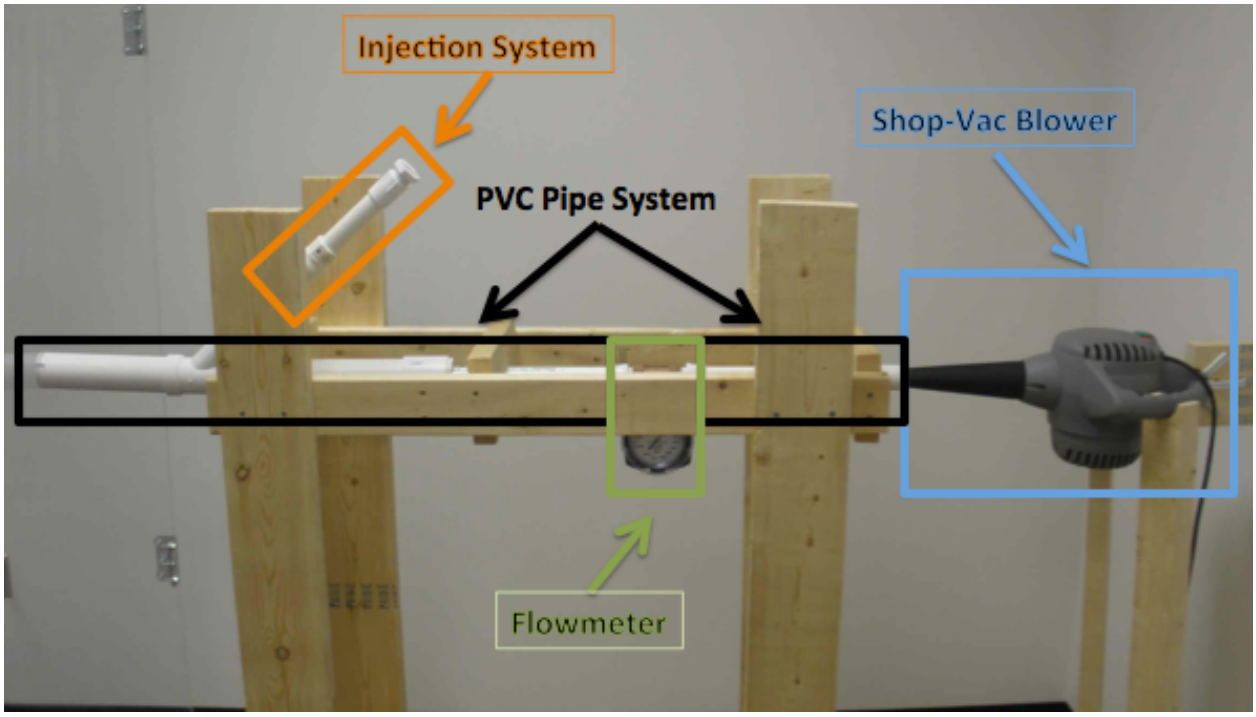

Figure 4. Jet Propulsion Apparatus & Labeled Systems

The blower selected for the experiment was a 6.5-hp, Shop-Vac detachable blower, purchased from Lowe's Companies, Inc. (seen in Figure 5). This Shop-Vac unit was rated for up to 210.0 CFM of airflow, although 146 SCFM was the highest attained in the TPaNS Lab environment [43]. While more powerful units were available from other common suppliers, such as McMaster-Carr, the Shop-Vac series was selected as the most affordable and the easiest to work with, given the round blower/suction ports. Most high-speed blowers have square or rectangular ports, which can be difficult to adapt to PVC pipe systems when a machine shop is not available.

Figure 5. Shop-Vac Blower Device

The 2.5-in blower port of the Shop-Vac transitions via a fabricated adaptor, down to a 1-in inner diameter (ID) PVC pipe. This pipe measures 12 inches long and connects to the dial-indicating flowmeter shown in Figures 6 and 13. Upon exiting the flowmeter, the air travels through another 12-in length of 1-in ID PVC pipe to an expansion device. This expansion device provided a sudden change from a 1-in ID pipe to a 2-in ID pipe. Figure 7 presents a sketch of the adaptor's change and Figure 6 shows the pipe system assembled, with the adaptor outlined in black dash marks.

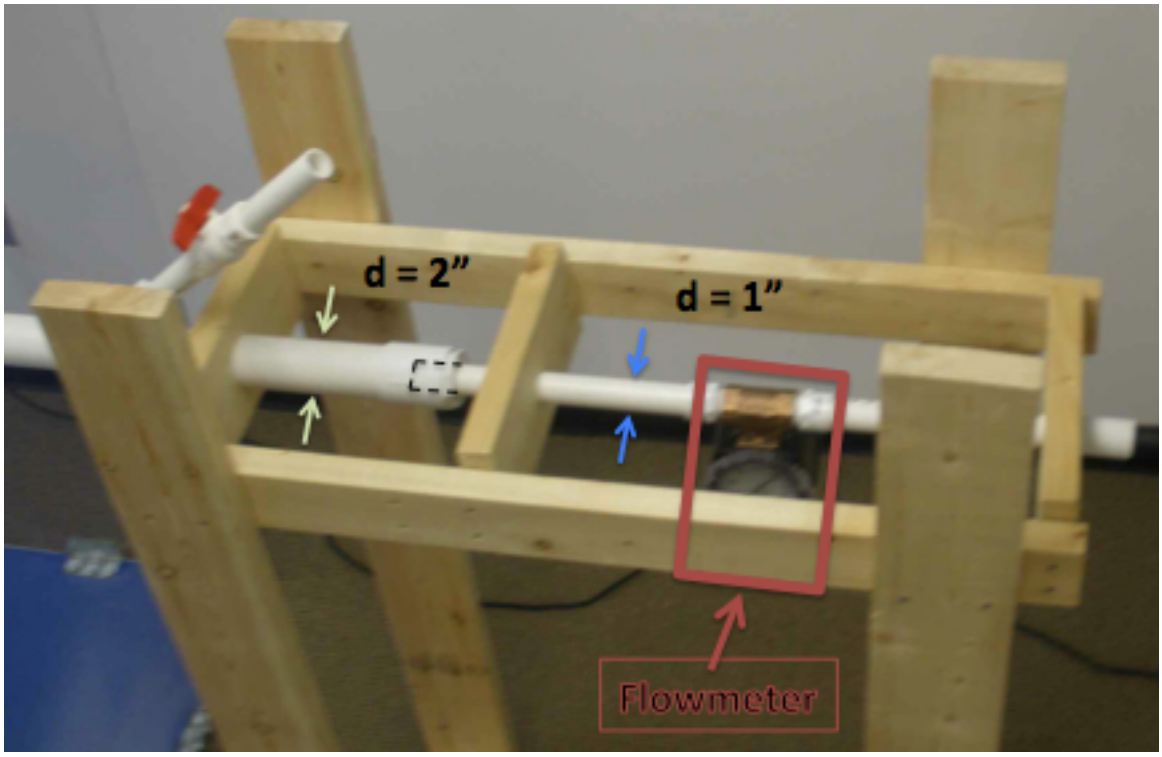

Figure 6. Flowmeter & PVC Pipe System

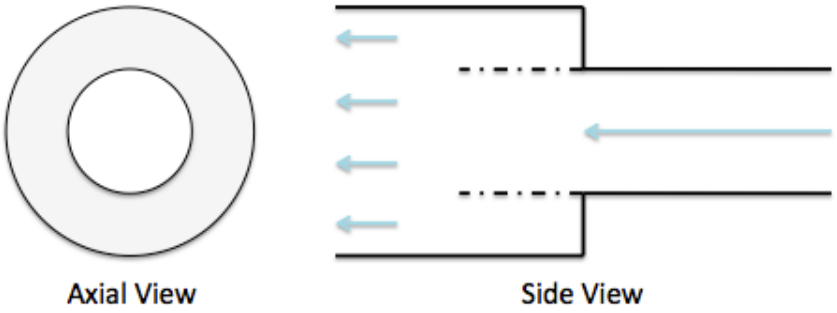

Figure 7. 1-in to 2-in PVC Adaptor

After expansion to the 2-in ID pipe, the airflow travels 13 inches to the 45º-wye connector, which connects the Particle Injection System (Figure 8) to the flow pipe.

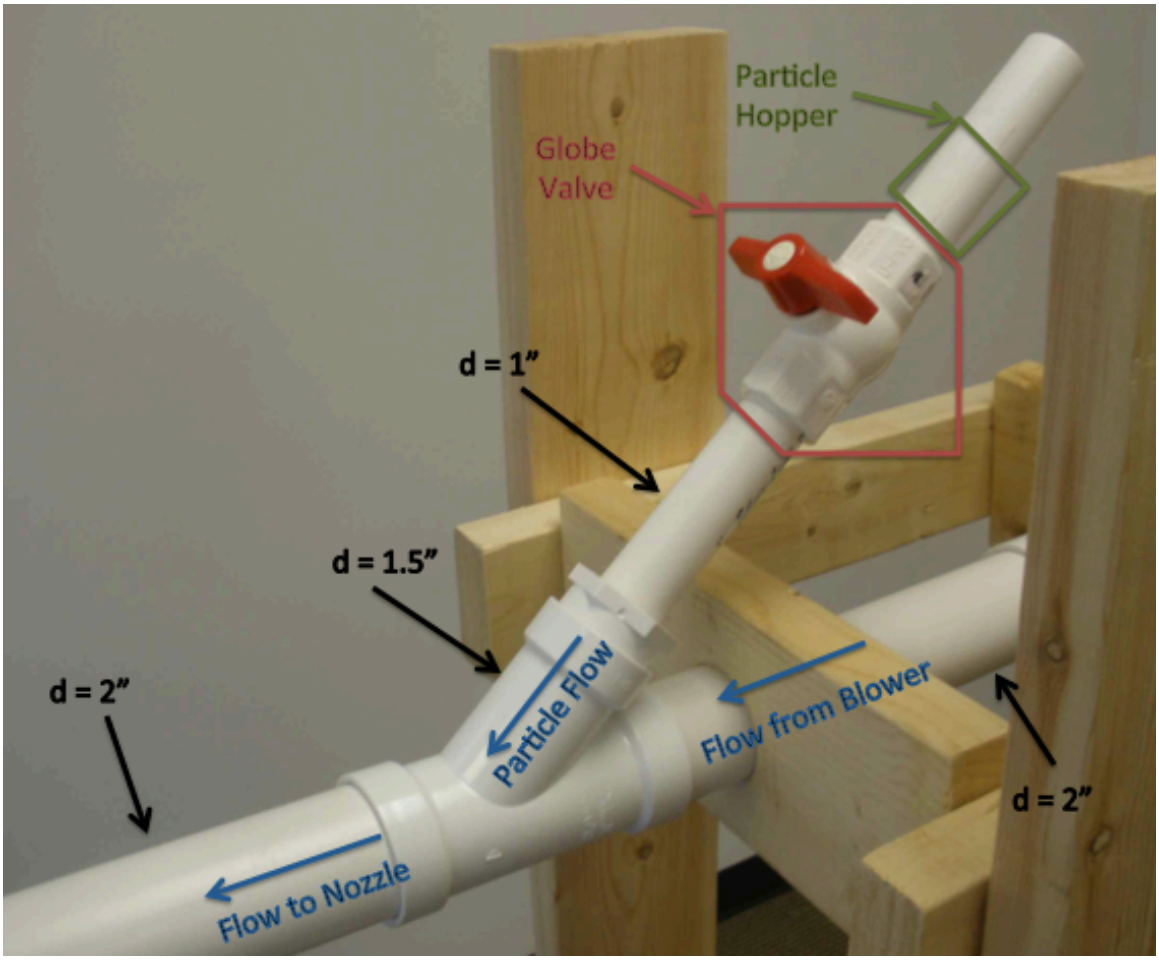

Figure 8. Particle Injection System

The Particle Injection System uses a 45º-wye with a 1.5-in ID vertical connection. The reverse angle and smaller diameter (1.5-in vs. the 2-in of the mainstream airflow), minimizes the amount of air flowing through the injection pipe. The 45º-wye is attached to a smooth-transition adaptor, which attaches to a 6 inch long piece of 1-in ID PVC pipe. This pipe is connected to the red-handled globe valve seen in Figure 8. The globe valve is used to seal off the last piece of 6 inch long, 1-in ID PVC pipe, which serves as the particle hopper, to hold the particles until ready for injection.

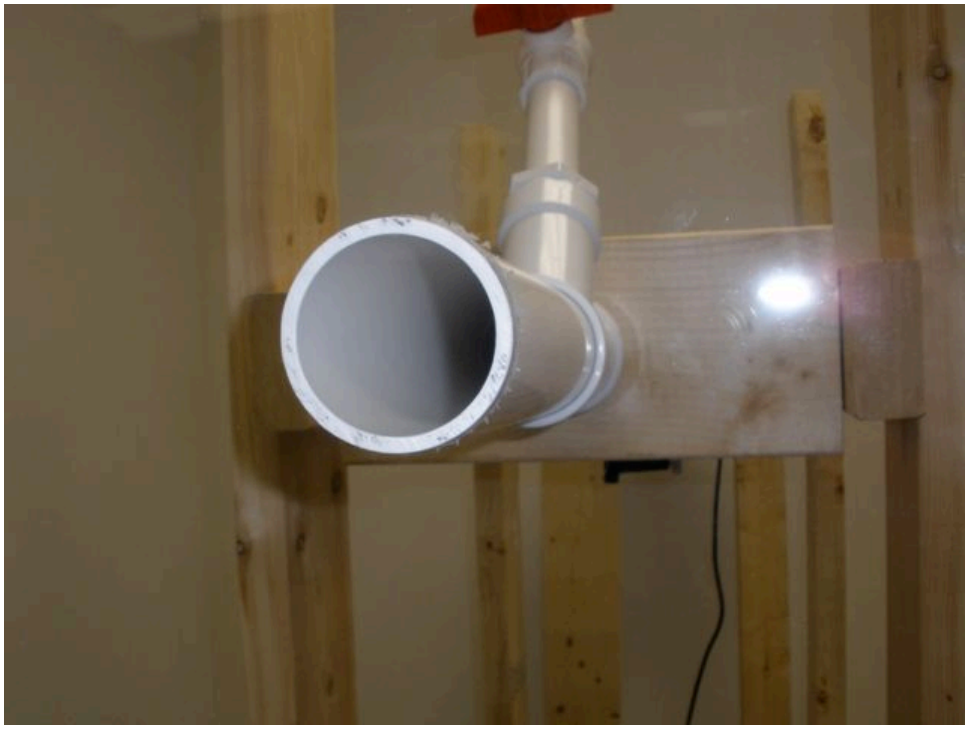

Figure 9. PVC Jet Nozzle

From the 45º-wye connection, the flow continues on its way to the jet nozzle. The flow from the blower travels along the x-axis, toward the Particle Entrapment System, picking up any particles released from the Particle Injection System, and through a final, 10.5 inch length of 2-in ID PVC pipe. This pipe attaches the Jet Propulsion Apparatus to the Particle Entrapment System and serves as the round jet nozzle, as seen in Figure 9, above. The center of the nozzle's opening is located 4 feet above the Particle Entrapment System's floor, and 2 feet from either of the sidewalls, making it completely centered on the nozzle-side wall of the tunnel.

Particle Entrapment System

As seen below, in Figure 10, the Particle Entrapment System was housed by a 5-sided, clear, acrylic (Plexiglas) enclosure. The unit measured 16 feet long, 8 feet tall, and 4 feet wide. The structure was designed to create a static environment around the nozzle, allowing a free jet to be created upon activation of the blower. Dimensions were set by conducting numerical calculations and CFD simulations to determine the area needed around the nozzle where wall effects were negligible [44]. All walls were constructed from 4' x 8' x 0.236" acrylic sheets,

purchased from McMaster-Carr. The unit was connected with steel brackets and reinforced with two wooden 4" x 4" x 8' beams, located on the end of the tunnel, opposite the nozzle. The tunnel face opposite the nozzle was also the only one without a Plexiglas wall. This was to mitigate recirculation of jet airflows and to ensure no pressure buildups within the entrapment system.

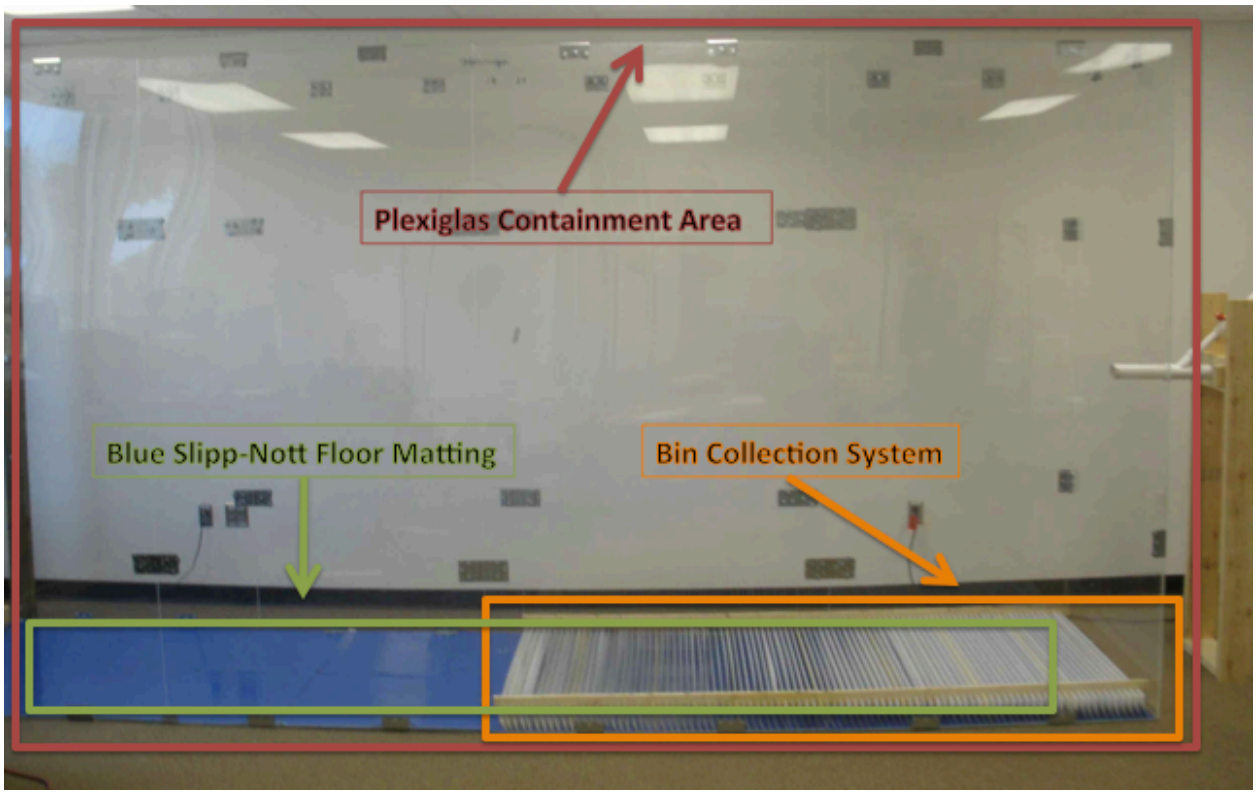

Figure 10. Particle Entrapment System & Labeled Subsystems

The floor of the Particle Entrapment System was designed after a tedious trial-and-error period. In order to gain valuable data about the particles' dispersion distance, it was critical to "trap" each particle as soon as it made contact with the floor surface. Any bouncing or rolling after initial contact would make any data for that particle invalid. To accomplish this, the bin collection system in Figure 11 was constructed. Four interchangeable "fin pallets" were built out of vertical window blinds and 1" x 2" x 4" wooden beams. Each window blind fin was glued into slots in the wooden beams, spaced at 1-inch intervals. These fin pallets, placed on the tunnel floor, had slight curves to ensure particles did not bounce out of each "bin". Blue industrial adhesive mats from Slipp-Nott, Inc. were placed underneath the pallets to serve three purposes:

- Create a better seal between the bin fins and the Plexiglas floor
- Provide some shock-absorbency for particle impact, reducing momentum and bounce height
- Turn the floor into an adhesive surface to trap smaller, low-mass, particles upon contact

Using relatively thin materials to build the fin pallets, and decreasing the hardness of the floor surface, particles would be trapped in 1-inch bins, spaced along the x-axis of Figure 2.

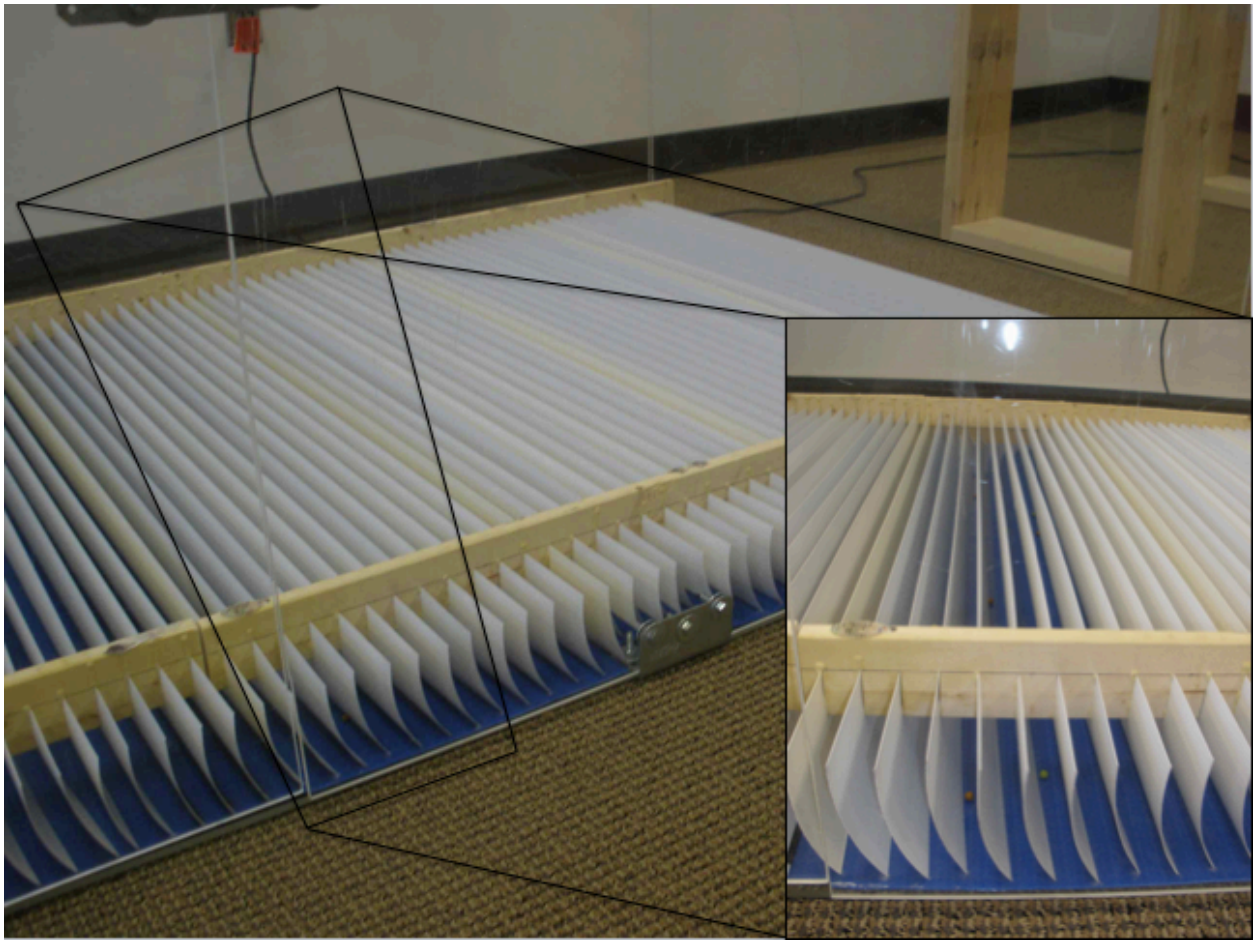

Figure 11. Bin Collection System

To minimize disturbing particle location after the completion of an experimental run, the particles were counted from the side of the Particle Entrapment System. By lying on the floor, it was possible to count and record the number of particles in each bin, as seen in Figure 12.

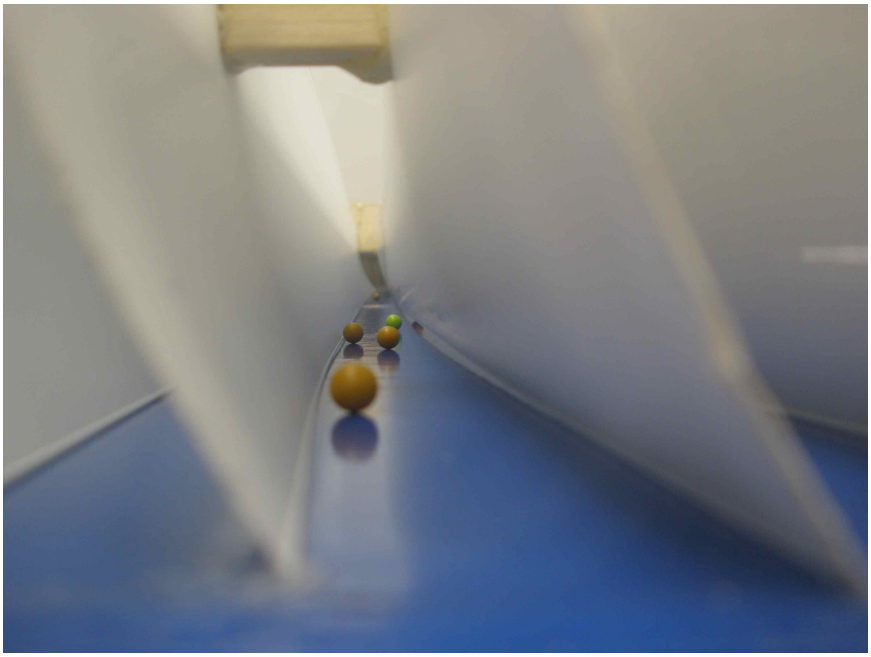

Figure 12. Single-Bin Count View

This, combined with a second count from a slightly elevated position, as seen in the blowout of Figure 11, resulted in 100% particle accountability for most experiments. In the event 100% of the particles were not counted in these two passes, it was possible to switch to the other side (wall side), to complete the count. Regardless of the number of counting passes, each particle was found and measured in every experimental run.

Instruments of Measurement

The flowmeter in the Jet Propulsion Apparatus is a model 1-71-R-300-I, dial-indicating flowmeter, built by RCM Industries. This wafer-type flowmeter, shown in Figure 13, was designed for 40-300 SCFM flows and was professionally calibrated in 2010. In accordance with manufacturer's instructions, the flowmeter was installed with 12 diameters of pipe on either end (minimum specification called for 10 diameters) [45]. For each experiment performed, the flowmeter reading was noted. The flowmeter always recorded values between 143 SCFM and 145 SCFM, which was in line with the manufacturer's specifications for the Shop-Vac blower [43]. The value was 145 SCFM over 90% of the time and did not visibly fluctuate during particle injection and flight.

Figure 13. 40-300 SCFM Dial-Indicating Flowmeter

After the experiments discussed in this paper had been performed, additional information was desired regarding the pipe's flow characteristic. For this purpose, a handheld pitot tube anemometer was purchased to measure airspeeds at the jet nozzle. The HD350 unit from Extech Industries is shown below in Figure 14. The unit's anemometer is 0.25 inches thick and has a measuring range of 1-80.0 m//s [46].

Figure 14. HD350 Extech Heavy-Duty Pitot Tube Anemometer

& Differential Pressure Monitor

To gather accurate information regarding particle diameters and physical characteristics, a Tekton 7168 Outside Mircrometer was purchased. The micrometer, shown in Figure 15, measured 0-1 inches via a vernier scale. The micrometer was calibrated before each particle type was measured and again after every 50 measurements.

Figure 15. Tekton 7168 Outside Micrometer

Particle Characteristics:

Glass Particles

While multiple types of particles were tested in this experiment, the majority of these were made out of Type 3000 Soda-Lime glass [47]. Six different sizes were used, as seen in Figure 16:

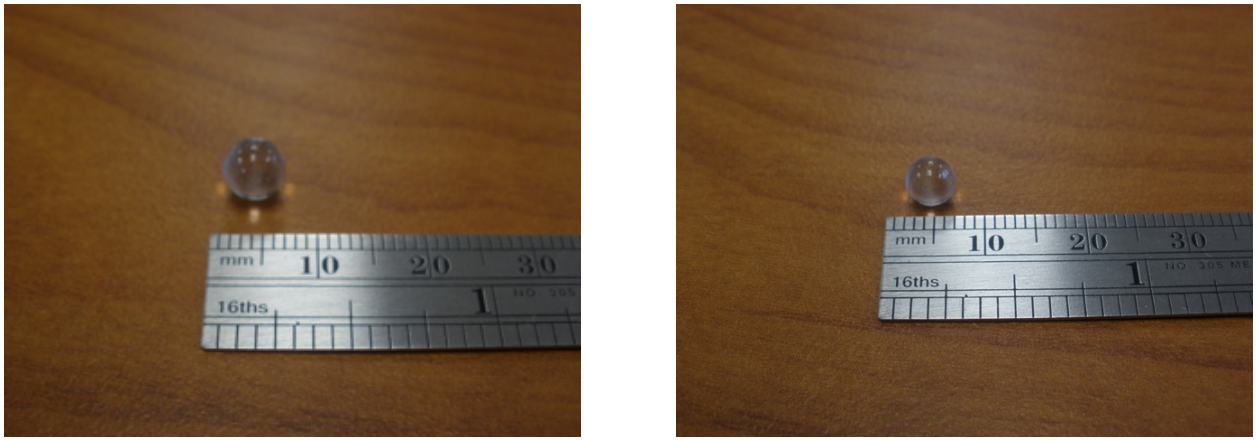

(a) (b)

(c)

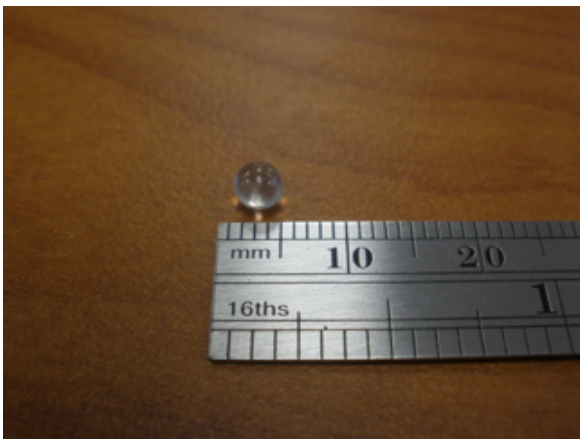

(d)

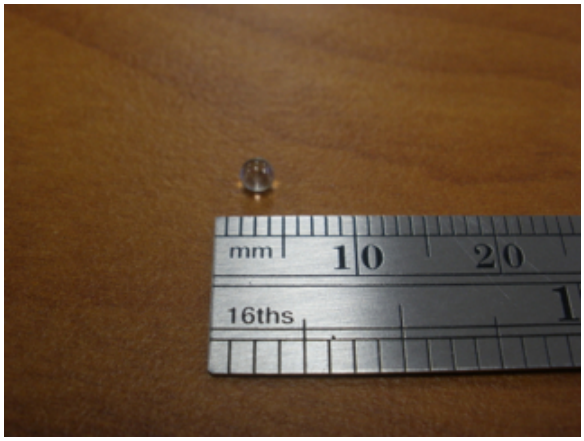

(e)

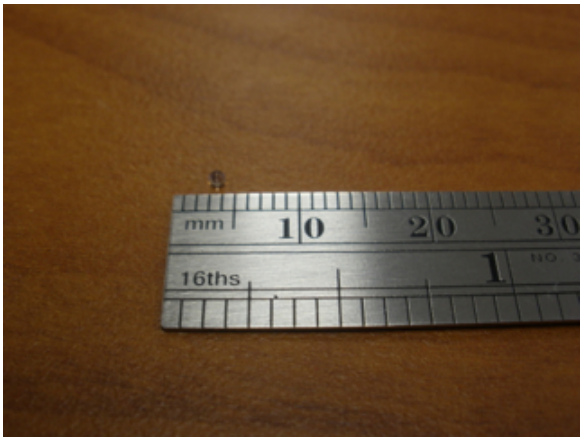

(f)

Figure 16. Glass Particles: (a) G_6 Particle, (b) G_5 Particle, (c) G_4 Particle, (d) G_3.5 Particle, (e) G_2.5 Particle, and (f) G_1 Particle

Although the manufacturers provided particle diameters and errors, there was some question as to the validity of those values, when examined in the TPaNS Lab. The micrometer, mentioned earlier, was used to test a random sample of 200 individual particles from each particle type/size. This dimensional analysis, when combined with known density values, and particle Reynolds number equations from Eq. 1 and 3, allowed for the creation of Table 2.

	Glass Properties					
Particle ID	G_6	G_5	G_4	G_3.5	G_2.5	G_1
Material	Glass	Glass	Glass	Glass	Glass	Glass
Supplier	BioSpec	Lab Depot	Lab Depot	BioSpec	BioSpec	BioSpec
d_p (Mean) (mm)	5.994781	5.009248	3.97543	3.645599	2.601925	1.167473
d_p (St. Dev.) (mm)	0.08376	0.06377	0.05866	0.17763	0.14746	0.09596
Volume (m^3)	1.128E-07	6.581E-08	3.290E-08	2.537E-08	9.223E-09	8.332E-10
ρ_p (kg/m^3)	2500	2500	2500	2500	2500	2500
m_p (kg)	2.820E-04	1.645E-04	8.224E-05	6.342E-05	2.306E-05	2.083E-06
V_s (m/s)	1.923E+01	1.758E+01	1.566E+01	1.500E+01	1.267E+01	8.488E+00
Re_p	7.648E+03	5.842E+03	4.130E+03	3.627E+03	2.187E+03	6.573E+02
Regime	Newton	Newton	Newton	Newton	Newton	Transition
Dispersal Type	Mono-	Mono-	Mono-	Mono-	Mono-	Mono-
No. Sampled	200	200	200	200	200	200

Table 2. Glass Particle Dimensional Analysis Results

Note that the glass pellets on the right of Table 2, "G_1", are identified as existing in the Transition Regime. Normally this would require a C_D value greater than 0.44 to be used for the V_s calculation. However, after comparing these particles with experimental and theoretical data presented in Munson on pages 382 and 526, they are found to be close enough to the Newtonian Regime that the $C_D \approx 0.44$ approximation is still valid [4]. This is also true for the ZS_1 and Z_1 particles to be presented in Table 3.

Other Particles

As discussed earlier, particles of other material types were used for other entrainment comparisons. The four other types include plastic, chrome steel, zirconia-silica, and zirconia, as seen in Figure 17:

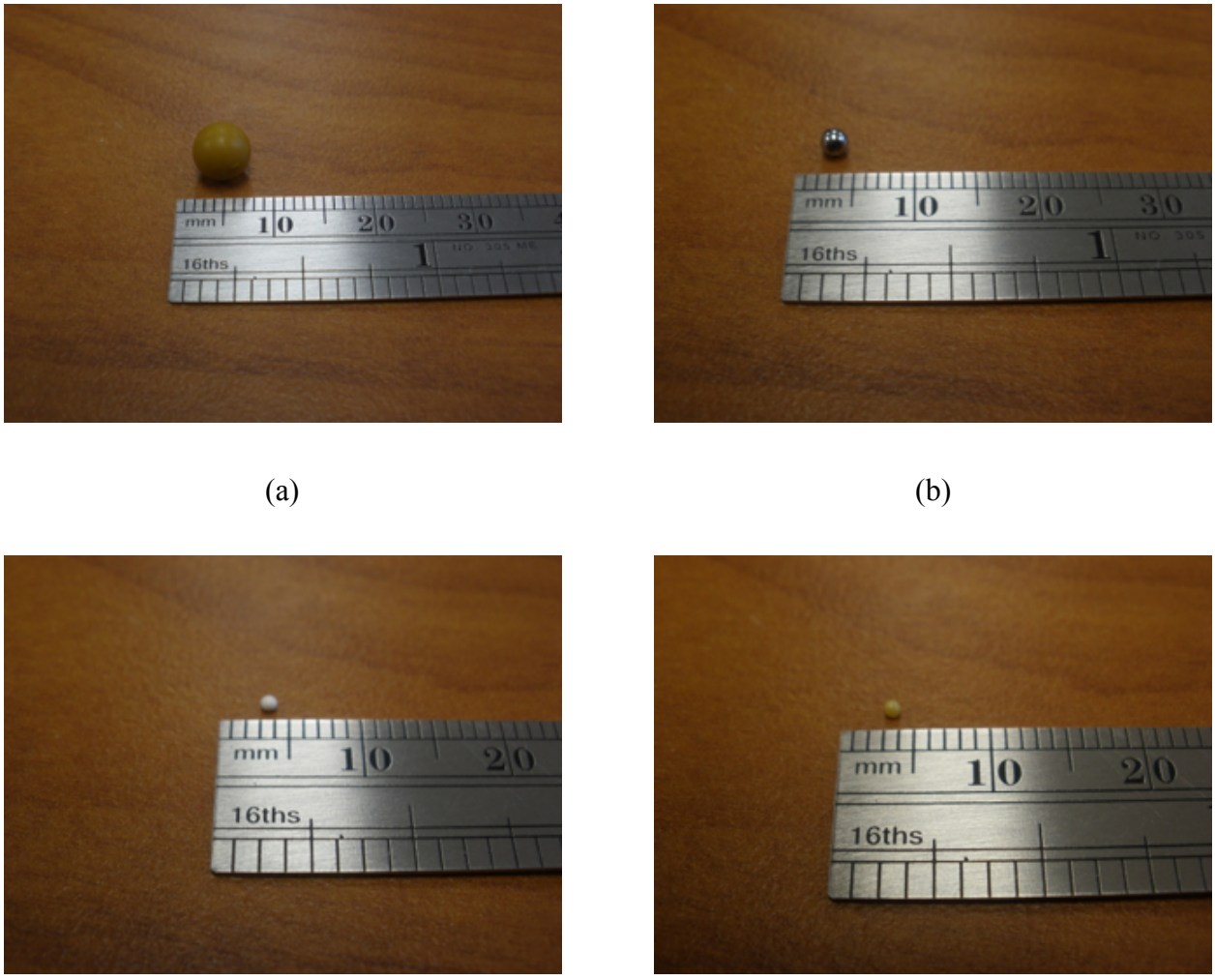

Figure 17. Other Particles: (a) AS_6 Particle, (b) CS_2.3 Particle, (c) ZS_1 Particle, and (d) Z_1 Particle

The plastic particles were used for low-cost proof-of-concept trials, low density experiments, and coupling/particle-to-particle studies. The chrome steel, zirconia-silica, and zirconia particles were used to compare the effects of changing density and/or mass. These particle dimensions and particle Reynolds number values are indicated in Table 3, below.

	Particle Properties			
Particle ID	AS_6	CS_2.3	ZS_1	Z_1
Material	Plastic	Chrome Steel	Zirconia-Silica	Zirconia
Supplier	Crossman	BioSpec	BioSpec	BioSpec
d_p (Mean) (mm)	5.9217	2.3833	1.1206	1.0722
d_p (St. Dev.) (mm)	0.0254	0.0087	0.0684	0.0715
Volume (m^3)	1.087E-07	7.088E-09	7.368E-10	6.454E-10
ρ_p (kg/m^3)	1103.706	7900	3700	5500
m_p (kg)	0.00012	5.60E-05	2.73E-06	3.55E-06
V_s (m/s)	12.70101	21.55704	10.11611	12.06456
Re_p	4988.7	3407.7	751.9	858.0
Regime	Newton	Newton	Transition	Transition
Disperse	Mono-	Mono-	Mono-	Mono-
No. Sampled	200	200	200	200

Table 3. Other Particle Dimensional Analysis Results

The plastic particles were Airsoft pellets, sold by Crossman Corporation. The chrome steel, zirconia-silica, and zirconia pellets were sold by BioSpec, Inc. (available at BioSpec.com). Finally, the glass particles were sold by both BioSpec, Inc., and Lab Depot, Inc. (available at LabDepotInc.com).

Jet at Nozzle Air Conditions:

After the experimental trials of the various particles were completed, the velocity of the airflow was carefully measured inside the Jet Propulsion Apparatus. This was accomplished using the anemometer from Figure 14, using the procedure outlined below:

1. Identify center of nozzle using a square, level, and engineer rule.
2. Draw vertical centerline above and below nozzle, on Plexiglas wall.

3. Bolt wooden block to Plexiglas wall, below the nozzle, along the centerline.
4. Clamp pitot tube to wooden block, aligned with centerline, with inlet along the bottom of the PVC pipe (nozzle). This is the "0.125-inch" position, due to pitot tube width.
5. Turn on and "zero" hand-held anemometer.
6. Activate blower.
7. Wait 60 seconds for airflow to reach stationarity.
8. Begin recording air velocity, using mean-value measurement.
9. Record for 60 seconds.
10. End recording.
11. Turn off blower.
12. Record anemometer's mean value for the given pipe height.
13. Unclamp pitot tube, raise 0.125 inches, and re-clamp. Be sure clamp does not allow pitot tube to move.
14. Repeat Steps 5 – 13 until the "1.875-inch" position has been reached and recorded.
15. Clear and turn off anemometer.

The above procedure was conducted 5 separate times. The results were compared and found to be very similar in each run (within the uncertainty range for the anemometer). The 5 tests were averaged for each measurement position, to produce the plot in Figure 18.

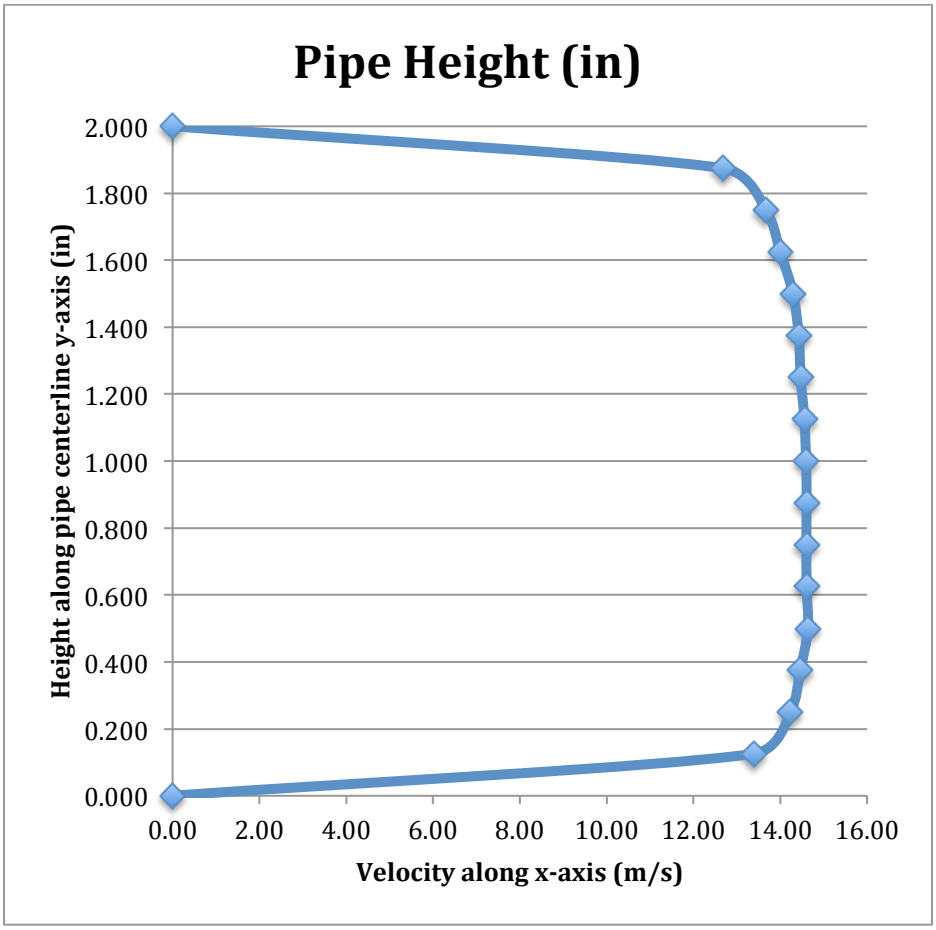

Figure 18. Airflow Velocity Profile at Nozzle Opening

The velocity profile shown in Figure 18 was consistent with the airflow rate from the jet nozzle to the inline flowmeter. The flowmeter, however, was registering a much higher value. Upon further examination, the flowmeter appeared to be restricting the flow and slowing the blower. Although the airspeed was decreased by the flowmeter, the velocity average of the air in the particle path remained relatively steady. From the 45º-wye connection to the jet nozzle, the average airspeed was 14.29 m/s. This average airspeed matched the additional measurements taken with a non-calibrated, vane-type, handheld anemometer, used to verify the reliability of the anemometer. Finally, based on measurements of temperature and pressure in the TPaNS Lab, the air properties used for the flow are described in Table 4.

Air	
ρ_f (kg/m^3)	1.204
T (K)	293.15
P (N/mm^2)	0.101325
μ (kg/(m*s))	1.81519E-05
v (m^2/s)	0.00001511

Table 4. TPaNS Lab Air Properties

Experimental Procedure:

The procedure used in this set of experiments was very specific, to ensure similar lab conditions and consistent, accurate results. The experimental procedure used is identified below:

1. Confirm experimental rig was cleared and reset for experiment.
2. Don double hearing protection.
3. Turn on blower.
4. Load particles into particle hopper.
5. Wait 45 seconds to ensure flow reaches stationarity.
6. Open red globe valve to release particles into Jet Propulsion Apparatus.
7. Look into particle hopper and verify all particles have deployed.
8. Close red globe valve.
9. Turn off blower.
10. Count particles bin-by-bin, moving from the bin closest to the jet nozzle, to the bin furthest away. Perform this action from the position shown in Figure 12, recording results on a lab test sheet after each bin is counted.
11. Re-count particles bin-by-bin, moving from the bin closest to the jet nozzle, to the bin furthest away. Perform this action from the position shown in the blowout image of

Figure 11. Confirm each bin's count with that already recorded on the lab test sheet. Correct if necessary.

12. Sum the results of the lab test sheet. If the sum is less than the amount of particles released in Step 6, switch to the opposite side of the Particle Entrapment System and repeat steps 10-12. If sum is greater than the amount of particles released in Step 6, proceed to Step 13, but discard any experimental results, as the experiment was contaminated.
13. Remove each pallet of the bin collection system.
14. Use lab vacuum to clean entire Particle Entrapment System. NOTE: Care must be taken here to ensure a clean tunnel where no debris may affect future experimental runs.
15. Replace each pallet of the bin collection system. As pallets are returned to experimental positions, ensure each vane is tight and straight, to ensure each bin is exactly 1 inch apart.
16. Complete experiment and enter results from lab test sheet into experimental database on the computer.

This procedure was used for every experiment described in the following chapters. A minimum of 20 experiments were conducted for each particle type (Particle ID).

CHAPTER 3 – Experimental Results

Introduction:

Using the procedure outlined in Chapter 2, 301 experiments were conducted to determine the distance of dispersion for the particles discussed in Tables 2 and 3. The following sections present the results of those experiments and describe observations of various particle paths. Analysis and discussion of these results are found later in Chapter 4.

Although the Particle Entrapment System was built to accommodate particles traveling up to 16 feet, all of the particles tested in this series of experiments fall within the 0'9" bin and the 8'0" bin. All of the dispersion plots will be cut off along the x-axis, to never exceed the 100-inch bin, for this reason. Figure 19, below, shows a summary plot of all data collected, from the 0-inch bin, to the 100-inch bin.

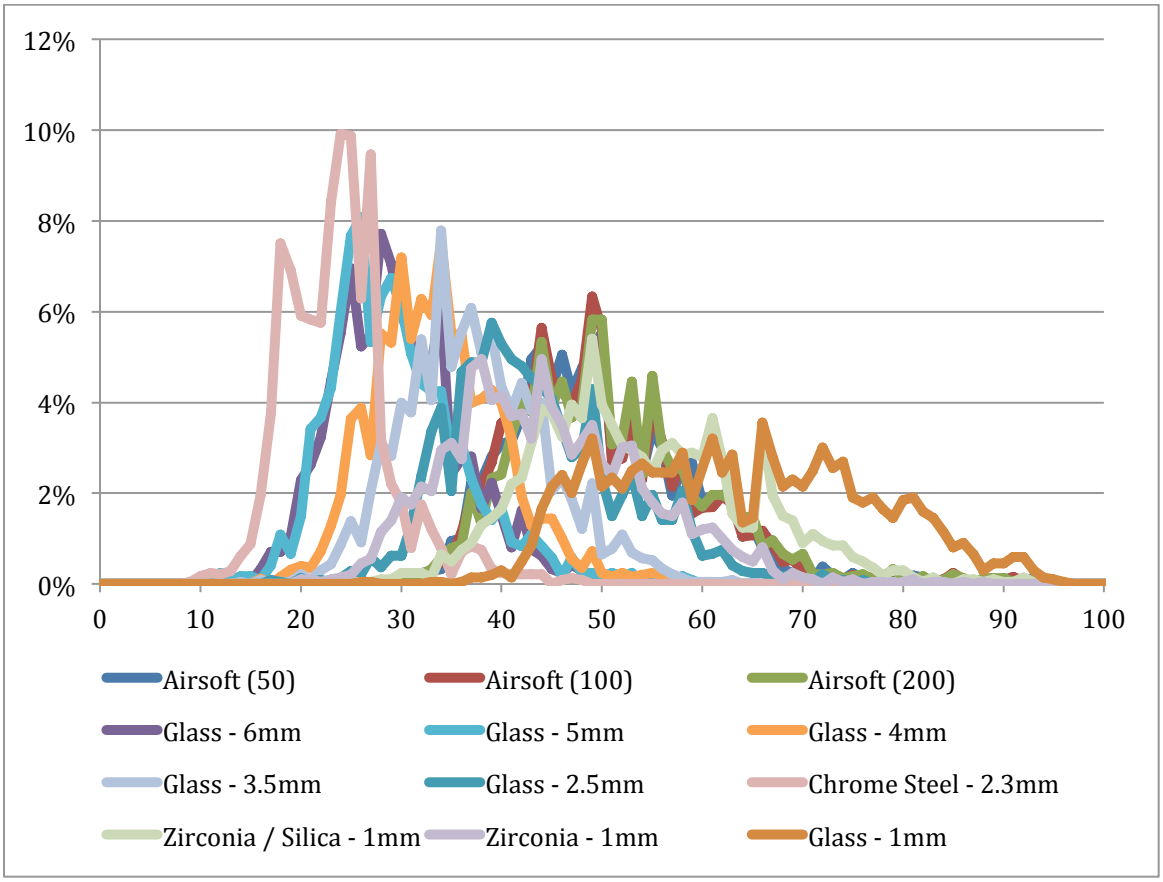

Figure 19. Summary Plot of Cumulative Particle Dispersion Distances

Airsoft Particles (AS_6):

The first particle type to be tested was the plastic airsoft particles (AS_6). These cheap, large particles can be purchased at any "big box" superstore. The TPaNS Lab went through over 15,000 AS_6 particles during the building of earlier prototype rigs and the experiments discussed in this paper. Their bright colors and large size make the particles easy to spot and visibly track during flight – good qualities in a proof-of-concept particle. The dispersion data collected was found useful for two reasons. First, the plastic material provided a low-density value, which could be compared to the 6mm glass particle (G_6). Second, the availability of so many particles at low cost, made them an ideal type for a comparison of various test particle-counts. Airsoft particles were tested 50 at a time, 100 at a time, and 200 at a time. This was to see if

dispersion data changed with various particle-counts due to the phase-coupling types described in Table 1.

Initially, the AS_6 particles were tested at 100 particle-counts. 100 was chosen as the standard amount for all other particles in this study. The results of this series of experiments are presented in Figure 20 and Table 5.

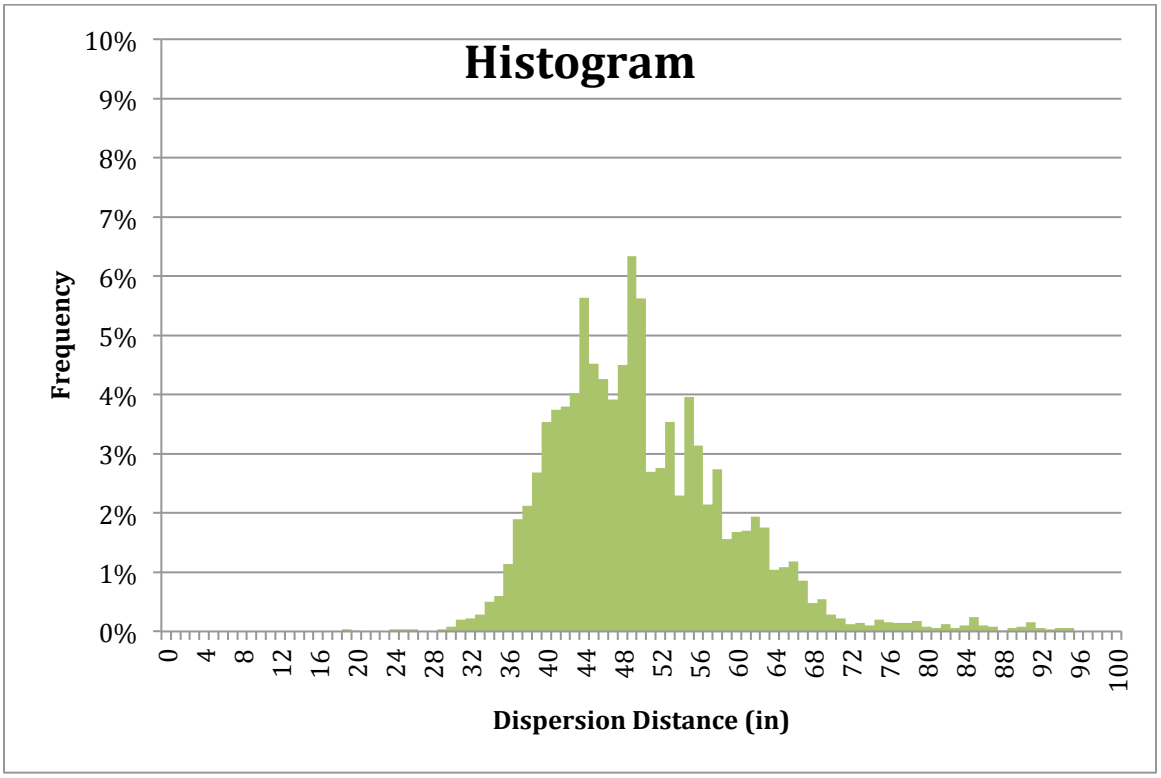

Figure 20. AS_6 Cumulative Dispersion Plot (100 Particle-Count)

Upon completion of the 100 particle-count experiments, 200 particle-count runs were started. These experiments were followed by a study of the 50 particle-count runs (results shown in Figures 21 and 22). While the AS_6 experiments were performed rapidly, due to their large size and visibility aiding the counting process, with over 100 experiments conducted, it took multiple weeks to reach completion.

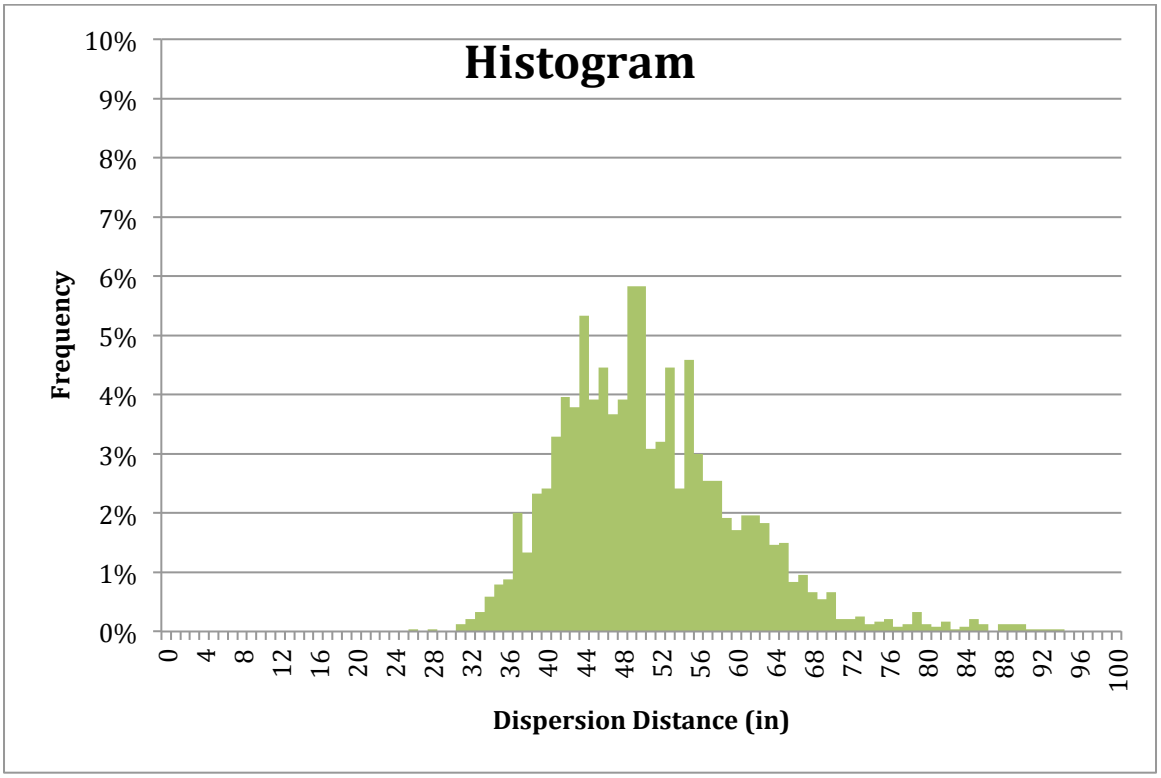

Figure 21. AS_6 Cumulative Dispersion Plot (200 Particle-Count)

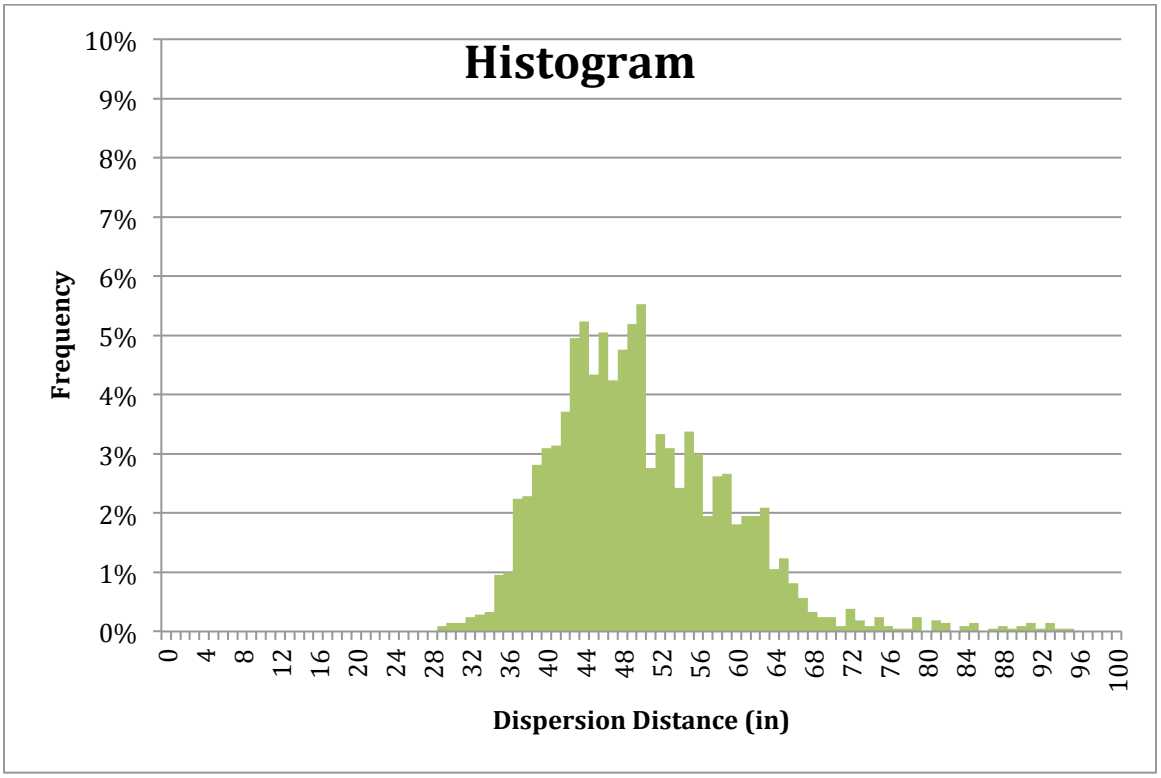

Figure 22. AS_6 Cumulative Dispersion Plot (50 Particle-Count)

Particle bouncing was a concern when measuring the larger particles (4mm – 6mm). With the larger mass, momentum was more likely to carry particles up and out of the bins. However, from observation and video recordings of the particle dispersion, there was very little bouncing observed in the AS_6 experiments. The only exception to this was with the 200 particle-count tests. With so many particles hitting the fin pallets, approximately 3-4 particles bounced, out of the 200.

Type:	Airsoft	Airsoft	Airsoft
Hopper Size:	50	100	200
# of Particles:	2100	5000	2400
Mean (in):	50.04285714	50.1332	50.94125
Median (in):	49	49	50
Mode (in):	50	49	49
Stand. Dev. (in):	9.476737217	9.632965097	9.627638333
Skewness:	1.058753807	1.02932539	0.921632446
Kurtosis:	2.238009847	2.118953219	1.552681368

Table 5. AS_6 Cumulative Dispersion Data

Glass Particles (G_X):

Upon completion of the AS_6 study, glass particles of various sizes were examined. These particles had densities more than two times that of the AS_6 particles. All of the glass particles were launched with particle-counts of 100. A minimum of 2,000 particles were tested for each particle type. Figures 23-28 present the results of these experimental runs.

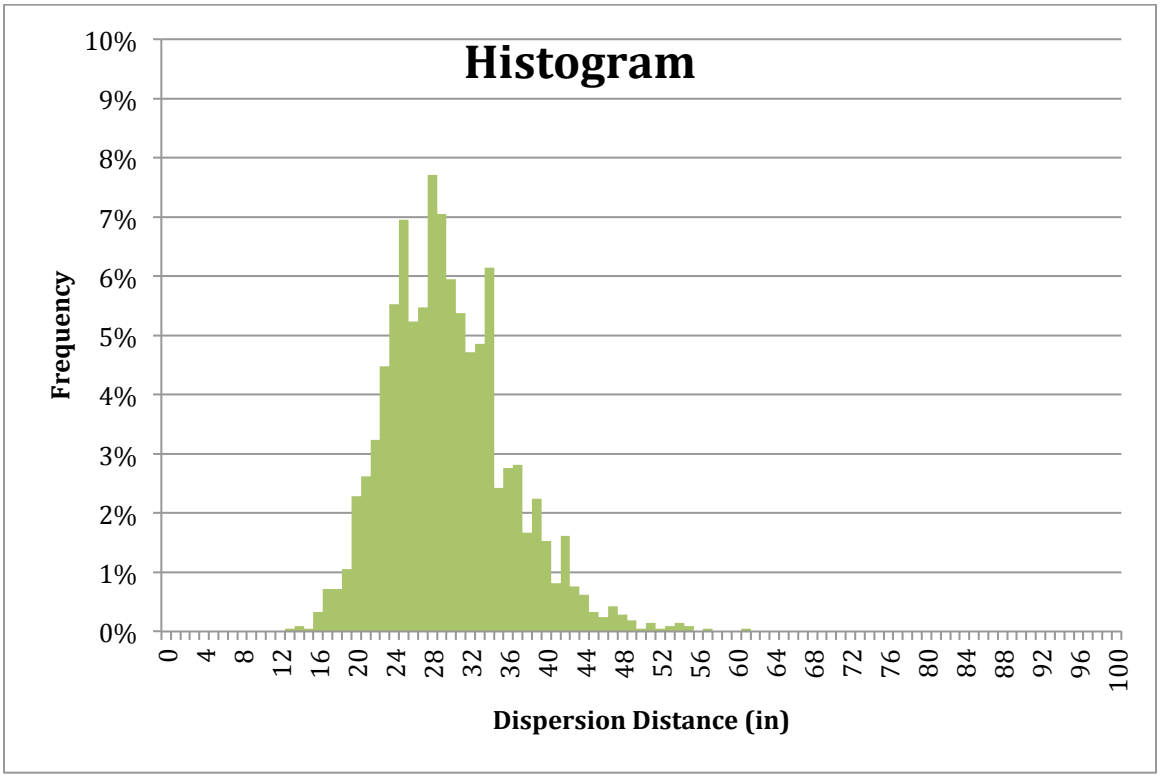

Figure 23. G_6 Cumulative Dispersion Plot

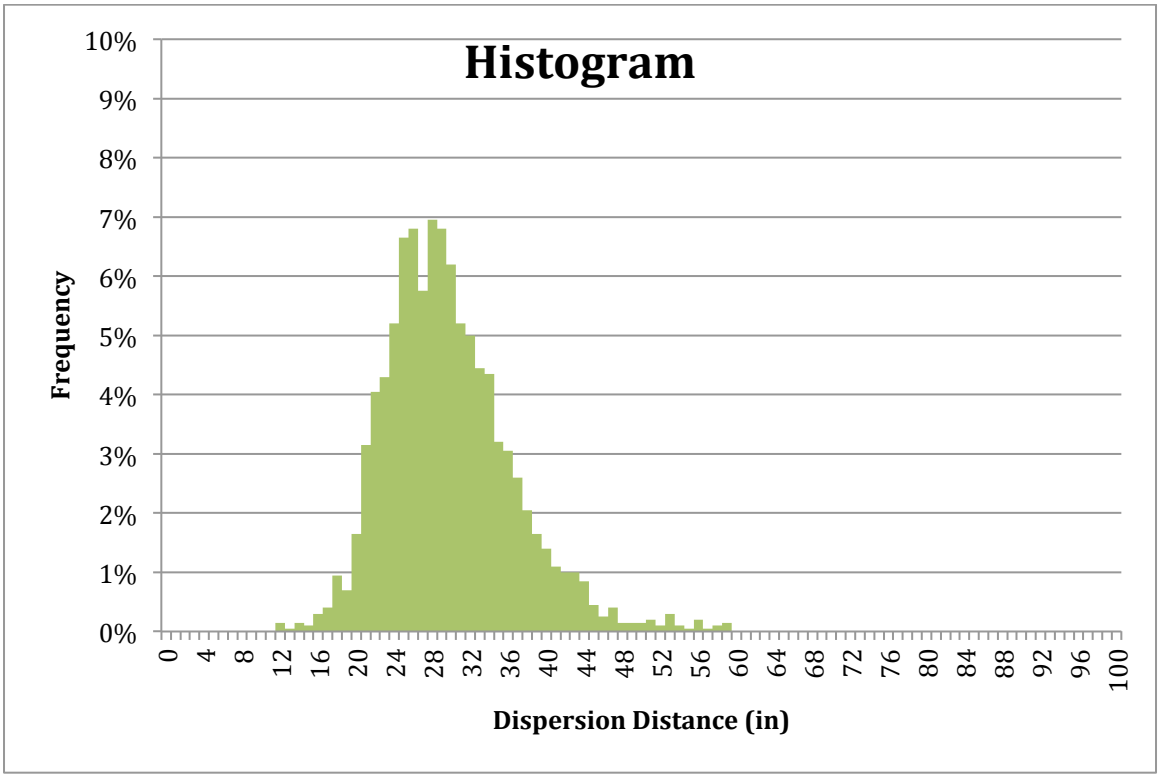

Figure 24. G_5 Cumulative Dispersion Plot

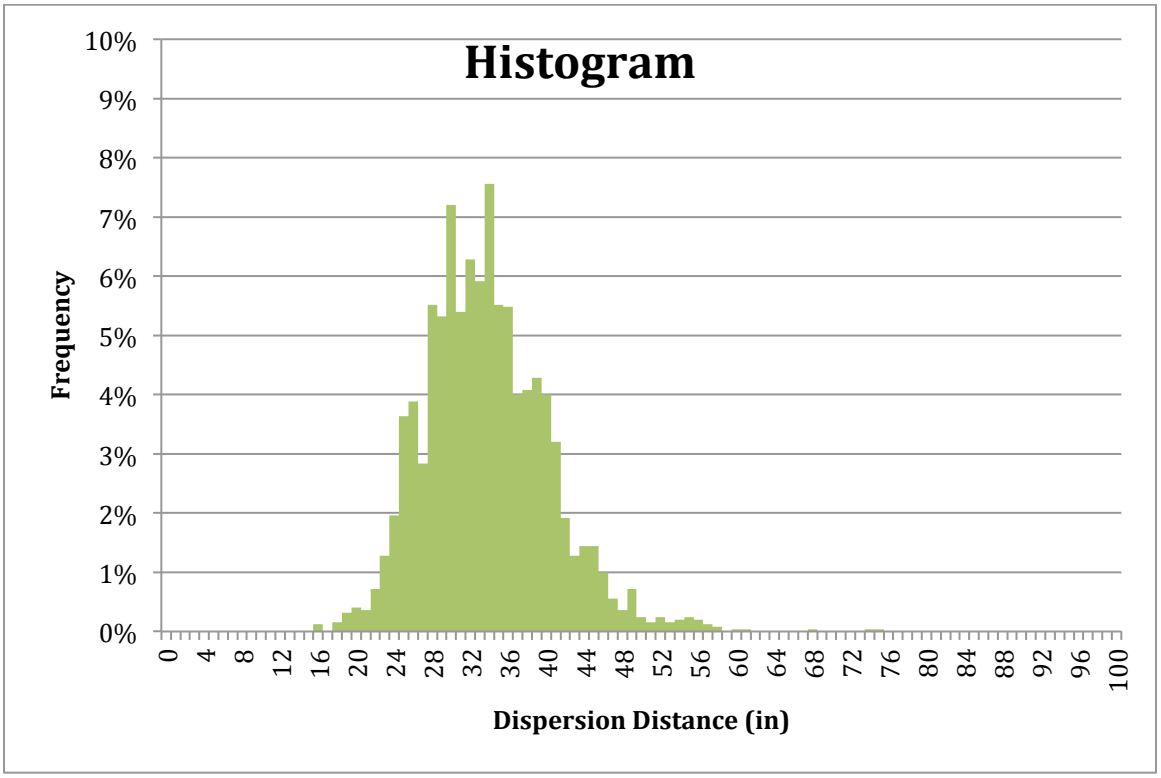

Figure 25. G_4 Cumulative Dispersion Plot

As with the AS_6 particles, there was concern of bouncing with the G_4, G_5, and G_6 particles. There was minimal bouncing with the G_4 and G_5 particles; however, there was visible bouncing with the G_6 particles. Upon further examination with use of an AVCHD video camera, loaned to the TPaNS Lab by Virginia Tech Innovation Space, it was discovered that for the few particles that bounced, they always bounced vertically, landing in the same initial bin.

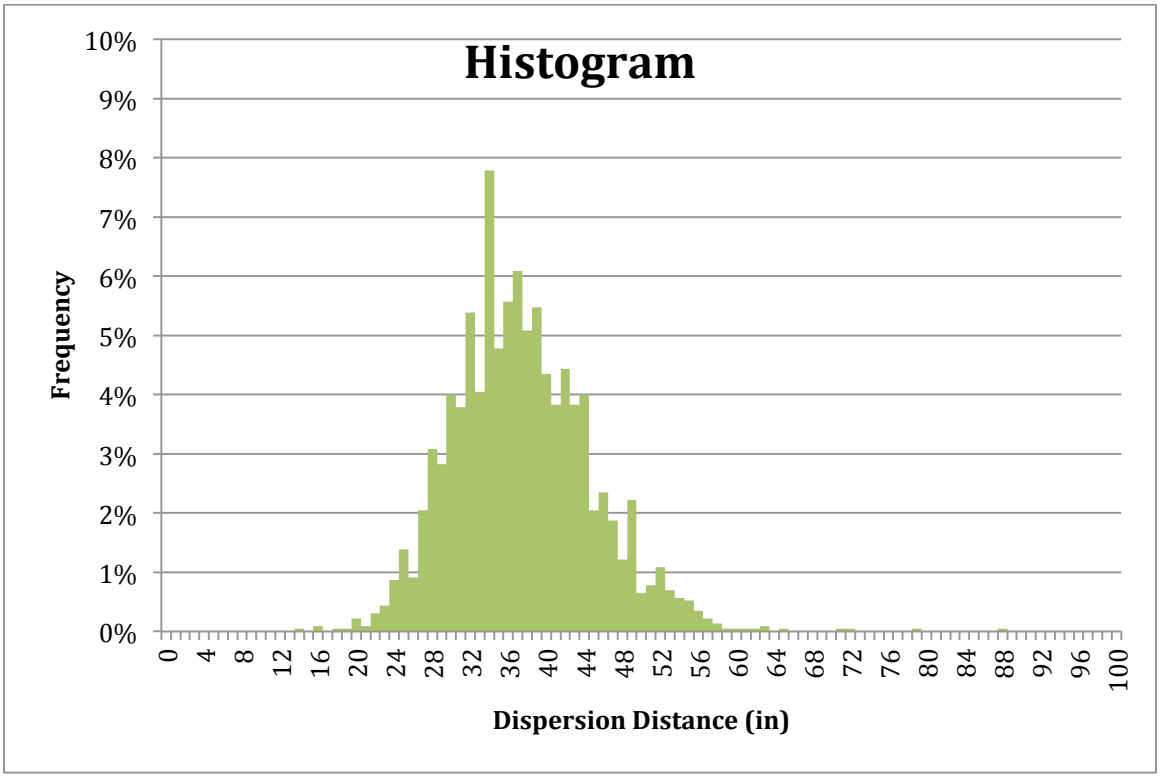

Figure 26. G_3.5 Cumulative Dispersion Plot

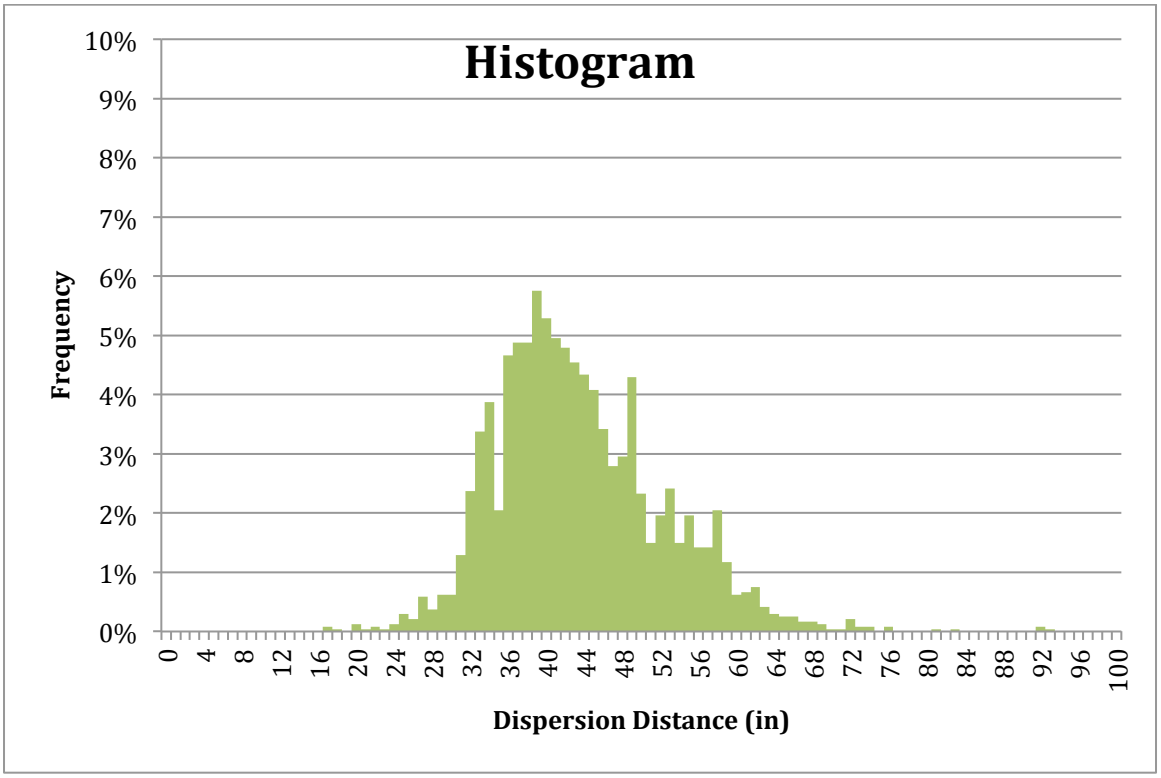

Figure 27. G_2.5 Cumulative Dispersion Plot

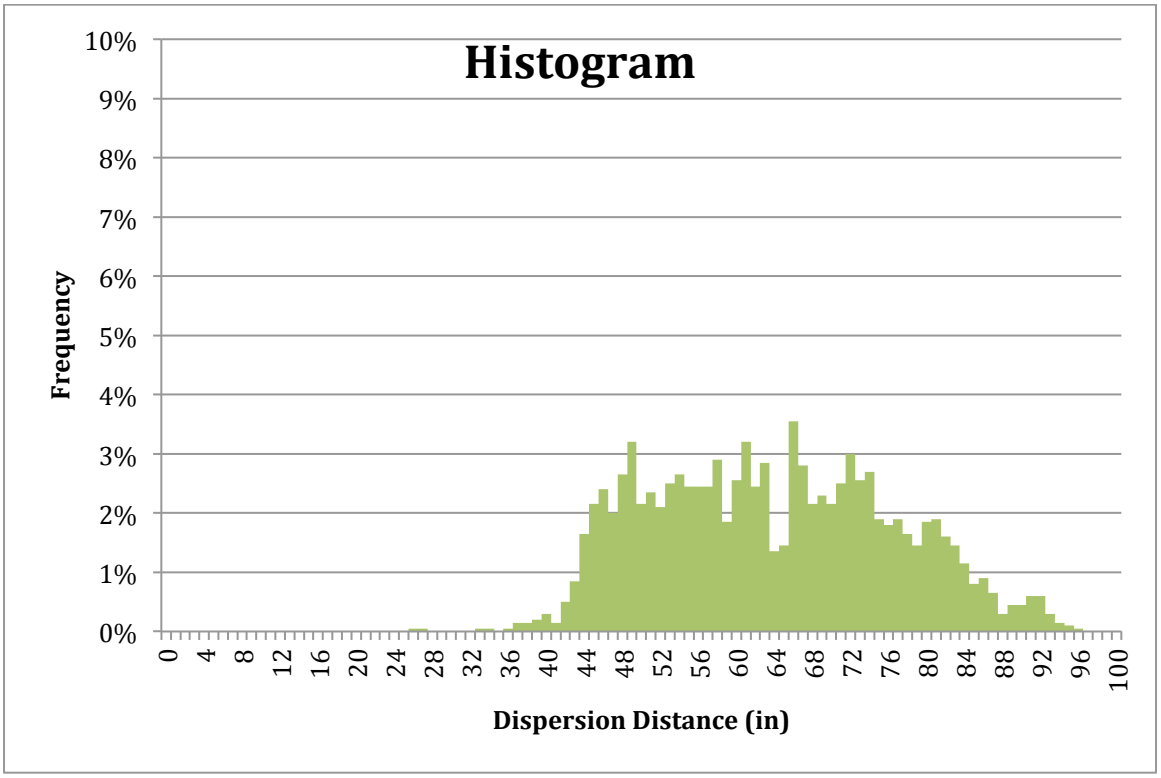

Figure 28. G_1 Cumulative Dispersion Plot

It was expected that the glass particles would disperse further in the x-direction with decreasing diameter, due to the large ρ_p/ρ_a ratio. This presumption was confirmed when the statistical data was reviewed in Table 6, below.

Type:	Glass - 6	Glass - 5	Glass - 4	Glass - 3	Glass - 2	Glass - 1
Hopper Size:	100	100	100	100	100	100
# of Particles:	2100	2000	2500	2300	2400	2000
Mean (in):	29.700	29.766	33.746	37.465	43.527	63.724
Median (in):	29	29	33	37	42	63
Mode (in):	28	28	34	34	39	66
Stand. Dev. (in):	6.444	6.768	6.612	7.313	8.885	12.800
Skewness:	0.669	0.880	0.751	0.619	0.743	0.167
Kurtosis:	0.861	1.541	1.840	1.686	1.391	-0.788

Table 6. G_X Cumulative Dispersion Data

Other Particles:

Lastly, particles of different materials were experimented with, to help gain a better understanding of the effect of mass and density to dispersion distance. The "heaviest" material type examined in this study was that of the Chrome Steel, with ρ_p=7900 kg/m^3. This is more than 3x that of the glass particles, and 7x that of the AS_6 particles. The results of the CS_2.3 particle experiments are presented below, in Figure 29 and Table 7.

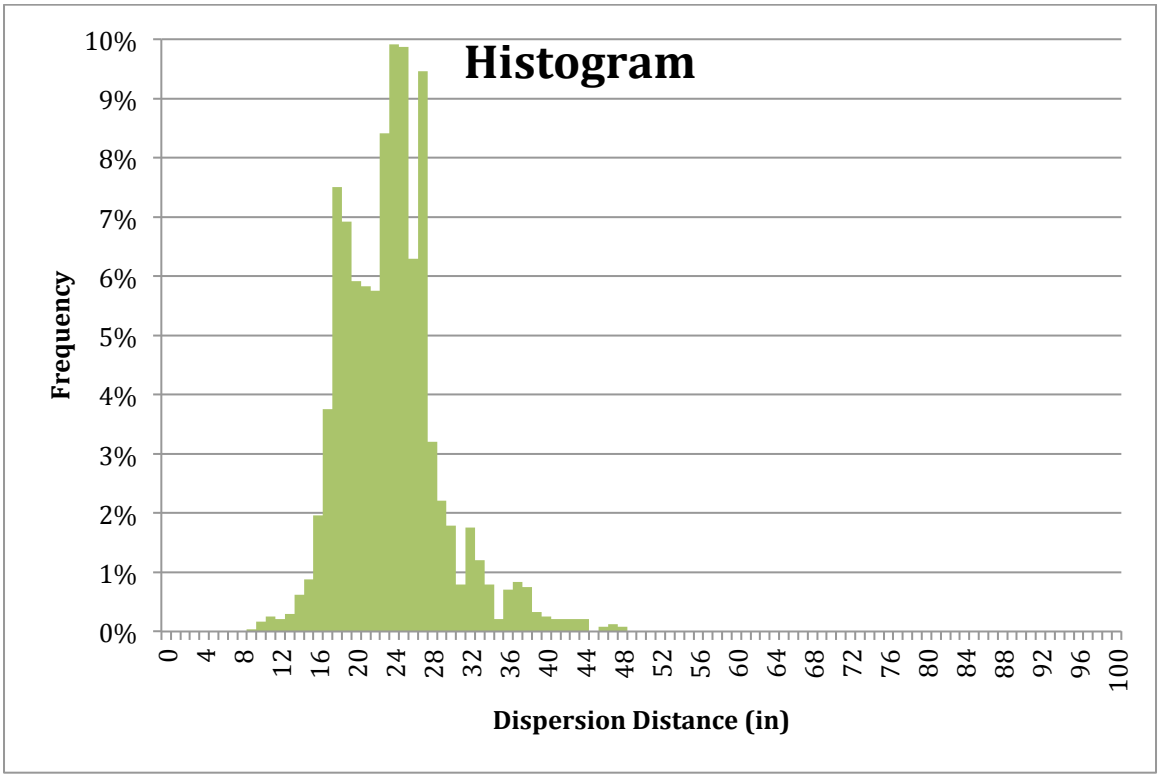

Figure 29. CS_2.3 Cumulative Dispersion Plot

Type:	CS_2.3
Hopper Size:	100
# of Particles Tested:	2400
Mean (in):	23.78416667
Median (in):	24
Mode (in):	24
Stand. Dev. (in):	5.3140
Skewness:	0.9184
Kurtosis:	1.9807

Table 7. CS_2.3 Cumulative Dispersion Data

The two remaining particle types were ZS_1 and Z_1. These two materials were more dense than glass, but of such small size, that they were expected to travel quite far, relative to the

earlier particles tested. Lab members were not sure if heavier particles at such small size would be inclined to disperse further, due to momentum, or if they would fall out of the jet stream faster, due to increased gravitational force. After examining the data of Figures 30 and 31, it was clear that at 1mm, the particles were able to entrain further, the lighter they were. Experimental data of the Zirconia and Zirconia-Silica particles is presented in Table 8.

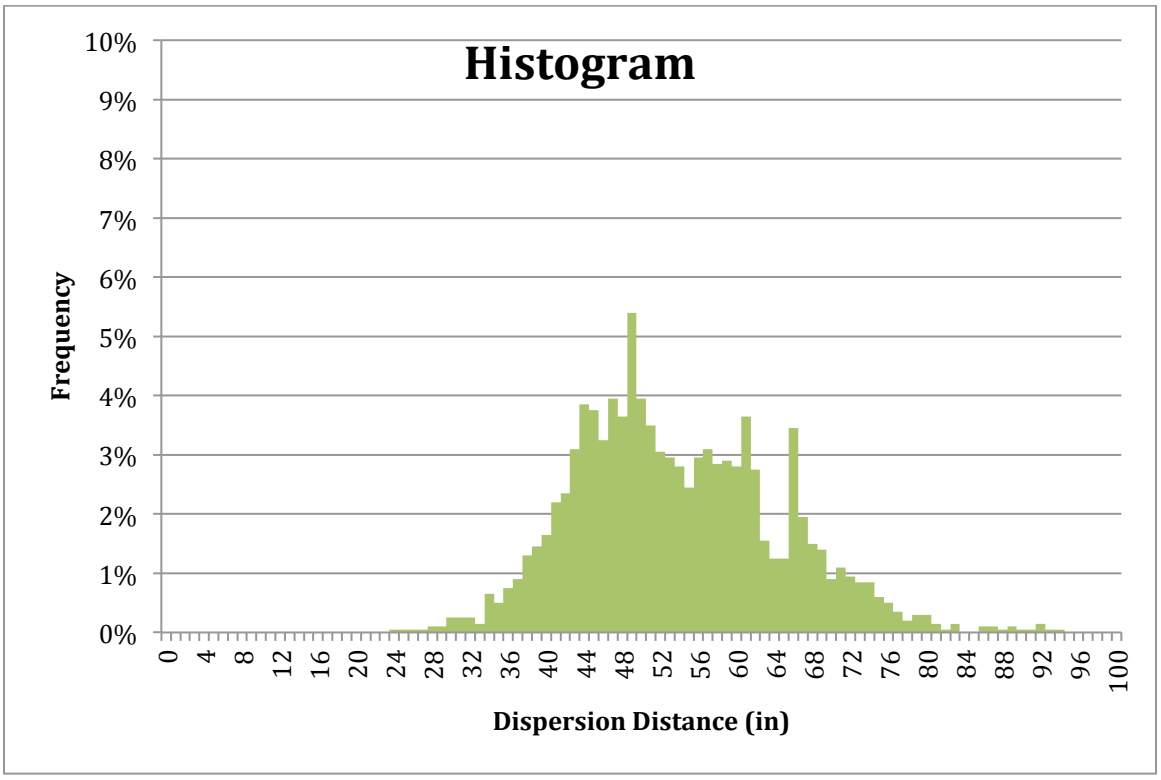

Figure 30. ZS_1 Cumulative Dispersion Plot

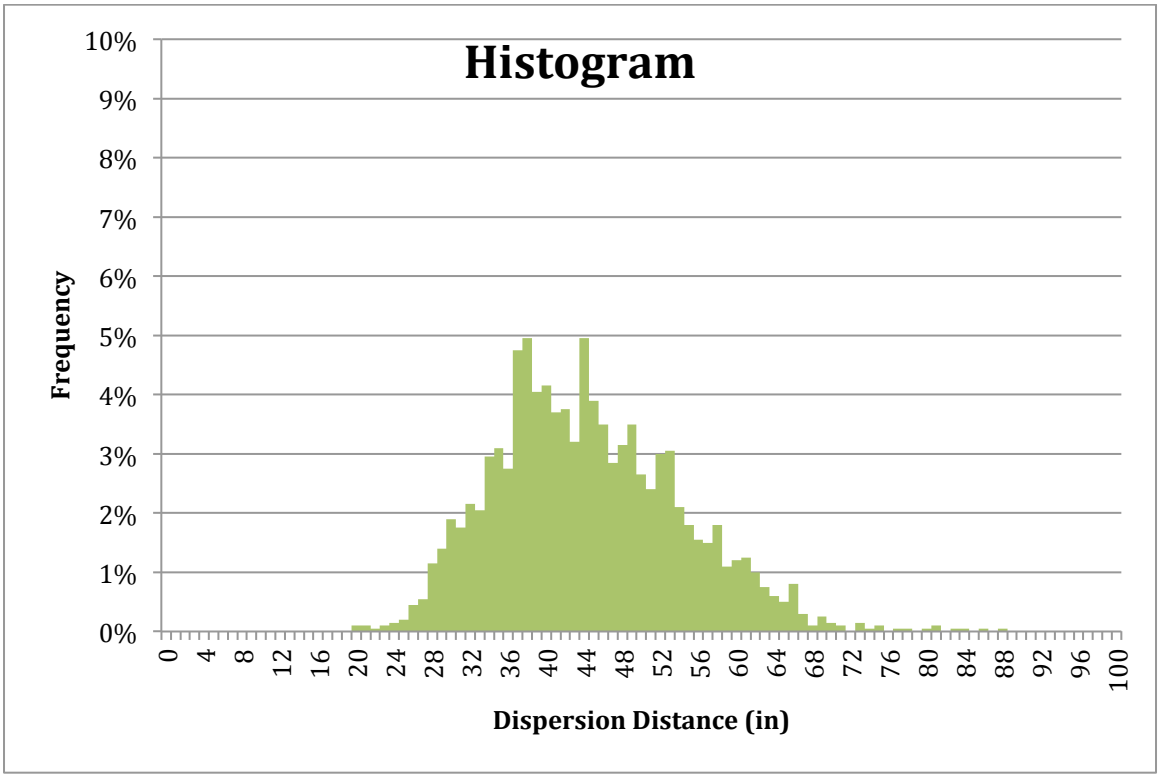

Figure 31. Z_1 Cumulative Dispersion Plot

Type:	Zirc/Sil - 1	Zirc - 1
Hopper Size:	100	100
# of Particles:	2000	2000
Mean (in):	53.7755	44.4505
Median (in):	52	44
Mode (in):	49	38
Stand. Dev. (in):	10.75187896	9.851907419
Skewness:	0.442352149	0.540343226
Kurtosis:	0.123512908	0.378012919

Table 8. 1mm Particle Cumulative Dispersion Data

CHAPTER 4 – Experimental Discussion & Analysis

Introduction:

The experimental results in Chapter 3 presented several interesting trends and raised some new questions. This chapter will review these findings and present some numerical analysis of the deposition data. Each test type will be discussed first individually, then more collectively for trend analysis.

3-Point Moving Average & Cumulative Distribution:

Airsoft Particles (AS_6)

As mentioned earlier, there were more AS_6 particles tested than any other particle type. As seen in Figures 20-22, the distribution plots were unique in how many small peaks were present. Although the mean and standard distribution of the plots had settled (changing less than 0.2%) after 1,500 particles, experiments were continued to see if the distribution plots would begin to smooth out. For AS_6, they did not.

Once it was determined that the distribution plots were unlikely to smooth out naturally with more experiments, a numerical smoother was applied to the data. Figure 32(b) is a distribution plot of the same data as Figure 22, but with a 3-point moving average applied. In addition to the smoothed data plot, a cumulative distribution plot is provided in Figure 32(a) to better characterize the data's form, compared to a normal distribution.

(a)

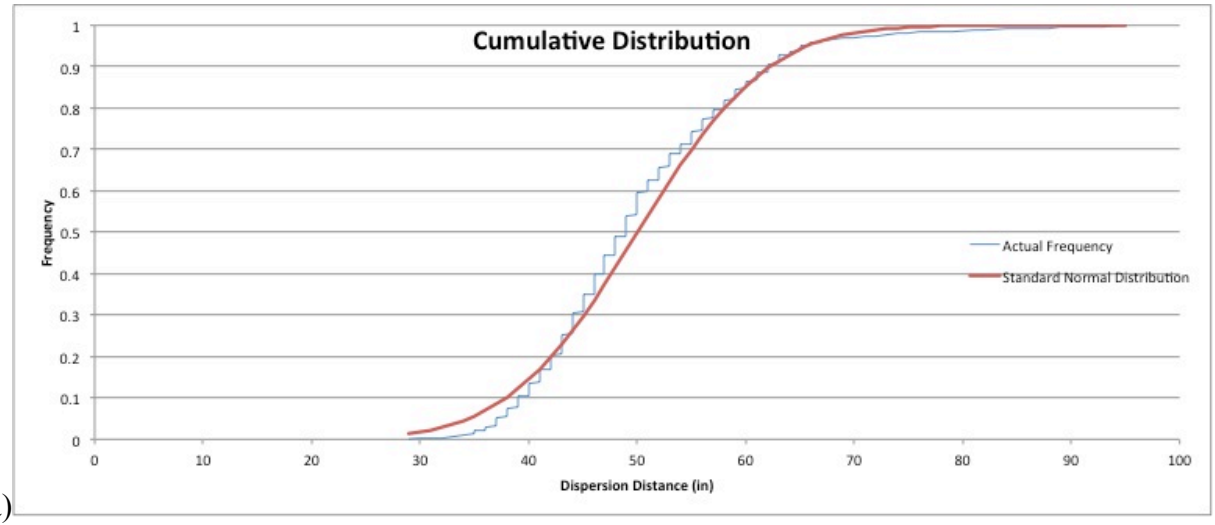

(b)

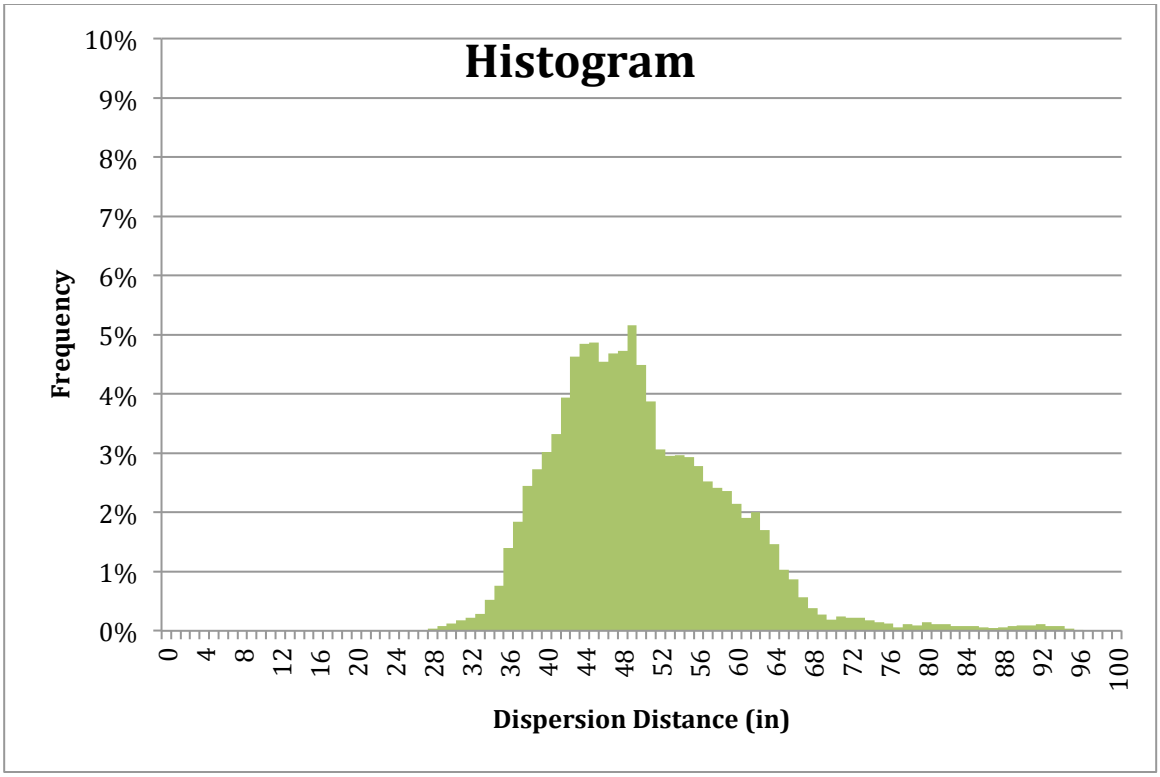

Figure 32. AS_6 (50 Particle-Count): (a) Cumulative Distribution Plot and (b) 3-Point Moving Average Distribution Plot

After 42 experiments and 2,100 particles, it is clear that the distribution is not Gaussian. Rather, the data shows a tail away from the nozzle and a positive skewness value. The mean distance is located at 50 inches, which is also the location of the largest peak.

As seen in Figure 33, the AS_6 (100 particle-count) data is very similar to that of the 50 particle-count in Figure 32. This data set involved 50 experiments and 5,000 particles. Several weeks were spent collecting these results to verify that the smaller peaks would not go away with more experimental runs, as discussed earlier. The data were initially collected by conducting two separate experimental types, 2,500 particles each, and comparing the results. The plots were put side-by-side and compared, revealing a difference of less than 0.1% between the two means and standard distributions. Additionally, the major and three-largest minor peaks (located at 44, 55, and 62 inches) were located at the same locations.

(a)

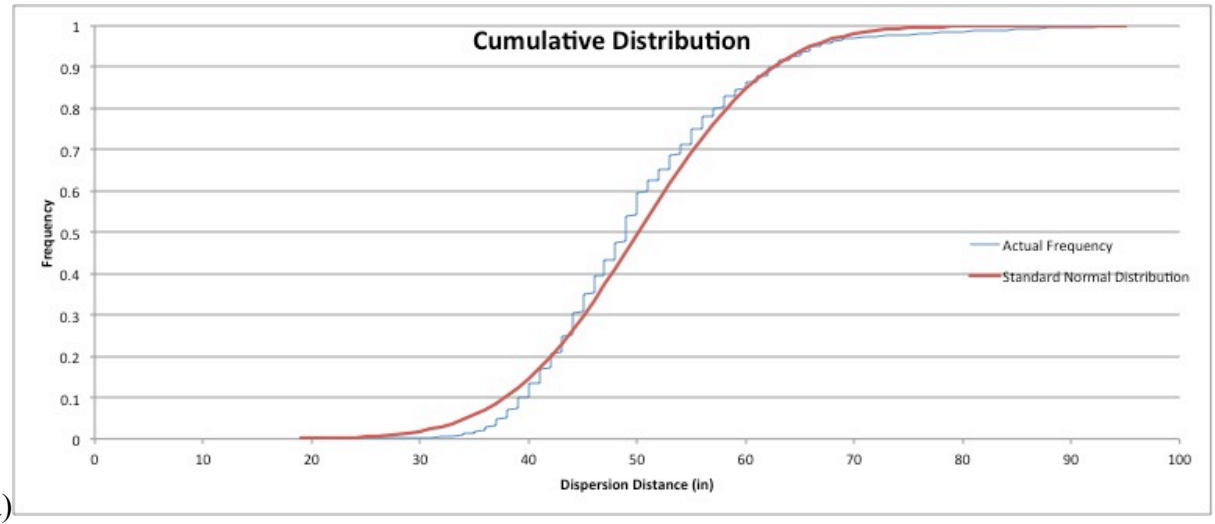

(b)

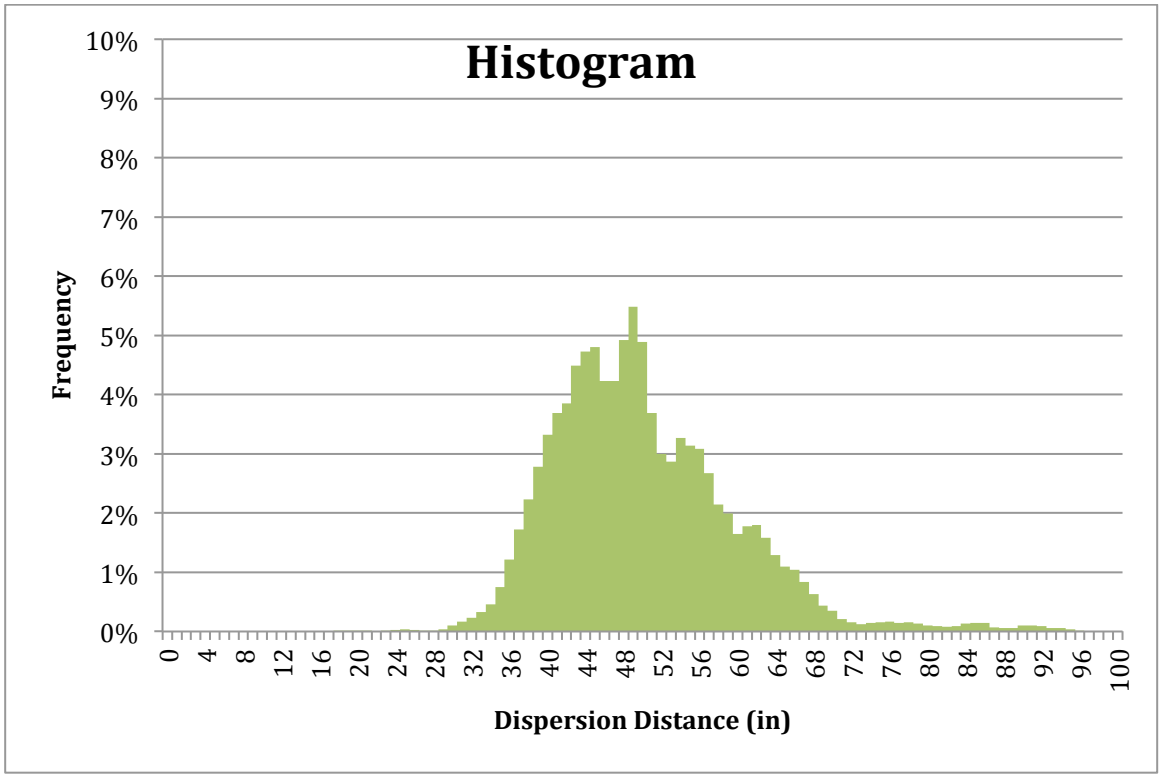

Figure 33. AS_6 (100 Particle-Count): (a) Cumulative Distribution Plot and (b) 3-Point Moving Average Distribution Plot

Once again, seen in Figures 21 and 34, the AS_6 (200 particle-count) has a mean and maximum peak located at the 50-in bin. The minor peaks are once including the 44-in, 55-in, and 62-in bins. The distribution continues to show a tail away from the jet and have positive skewness.

(a)

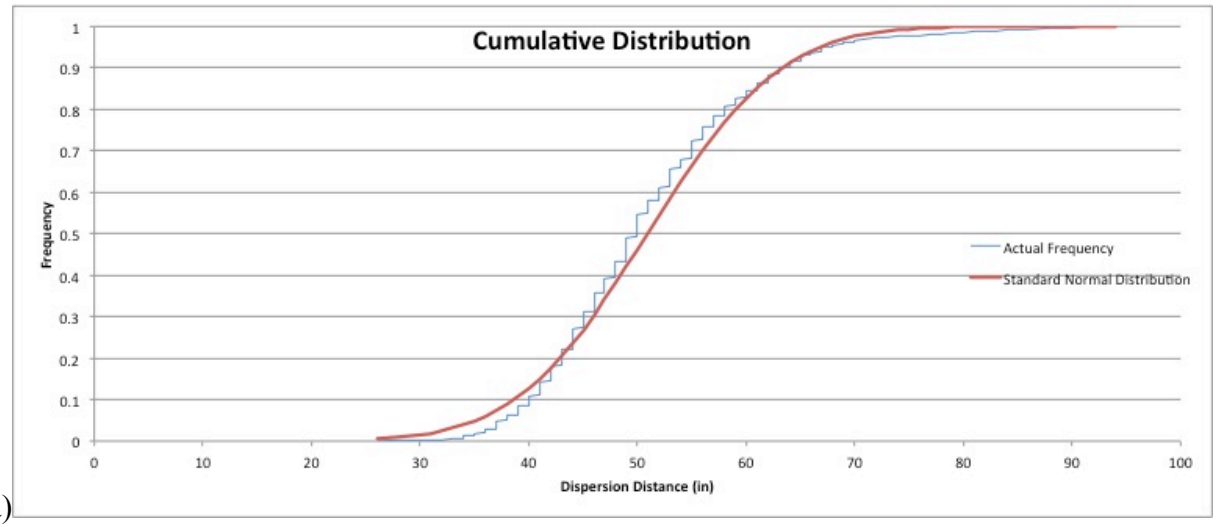

(b)

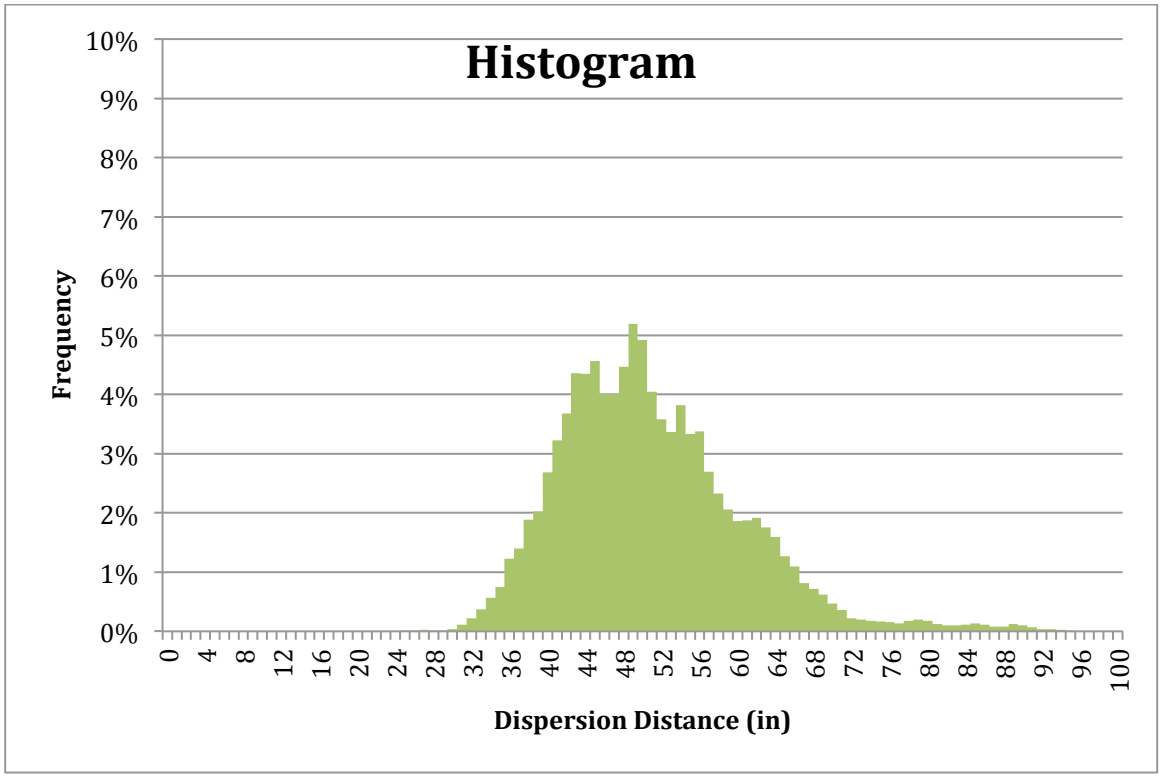

Figure 34. AS_6 (200 Particle-Count): (a) Cumulative Distribution Plot and (b) 3-Point Moving Average Distribution Plot

Glass Particles (G_X)

Upon first glance at Figures 23 and 35, the plots look similar to Figures 20 and 33, due to the position of the minor peaks. However, the G_6 particle plots are shifted significantly to the

left. The G_6 particles did not travel nearly as far as the AS_6, regardless of the similar diameters. In addition to the shorter particle path, the standard deviation of the results is significantly less. Just from the quick comparison of the AS_6 and G_6 particles, it is clear that particle diameter is not the sole factor in a particle's ability to entrain in a jet flow.

(a)

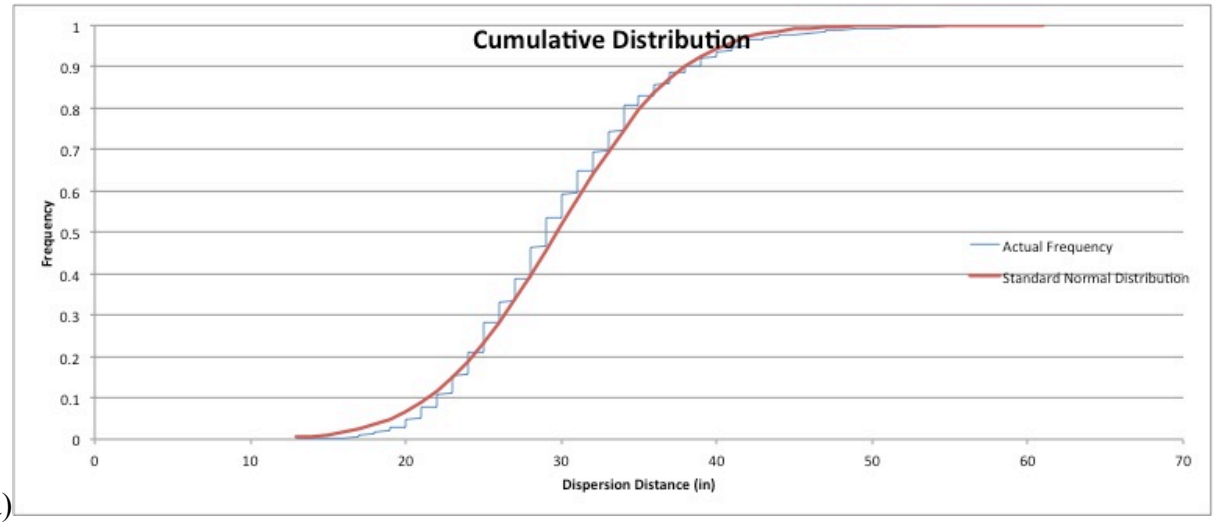

(b)

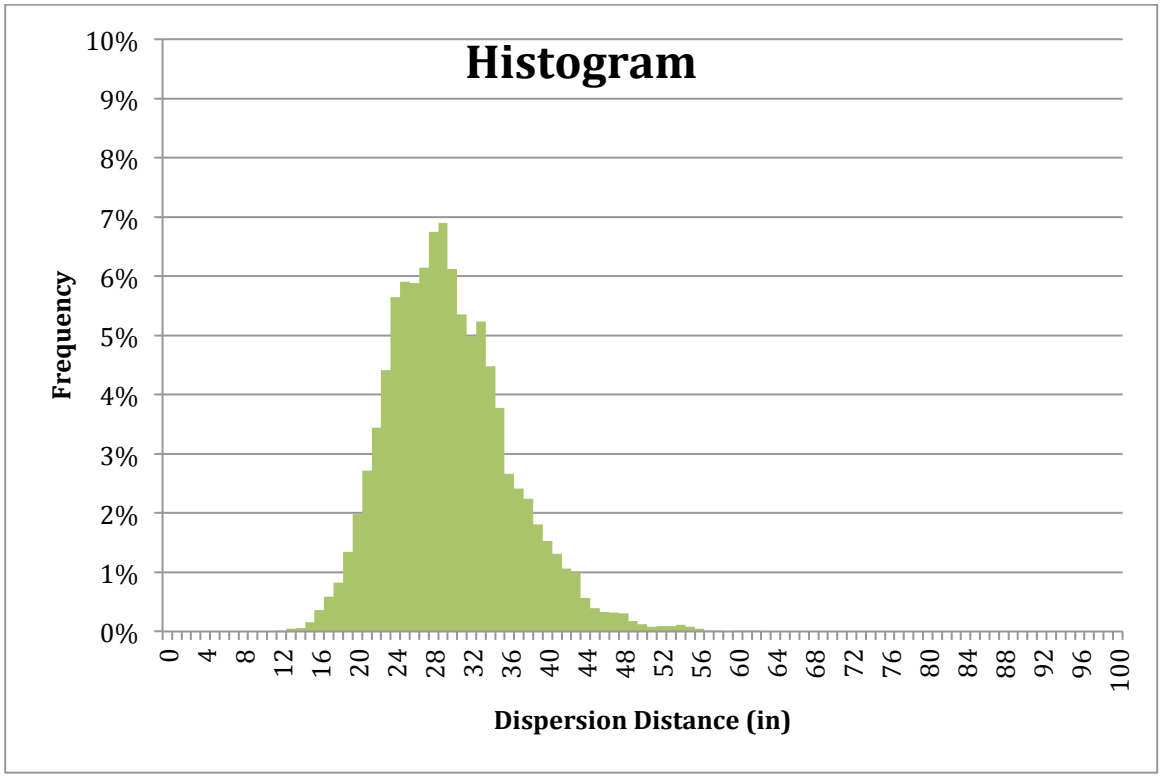

Figure 35. G_6: (a) Cumulative Distribution Plot and (b) 3-Point Moving Average Distribution Plot

Figures 24 and 36 represent the data from the first particle type with a diameter reduction. The G_5 particles have a diameter 1mm less than the G_6 and AS_6, and present a mean-value very similar to that of the G_6 particles. One feature different in the G_5 plot is a reduction of the number of minor peaks. The distribution plot in Figure 24 shows a peak at the 28-in bin, with a significant minor peak located just 2 inches closer to the jet nozzle. Once the smoothing function is applied, all minor peaks are eliminated and the curve becomes very clear.

(a)

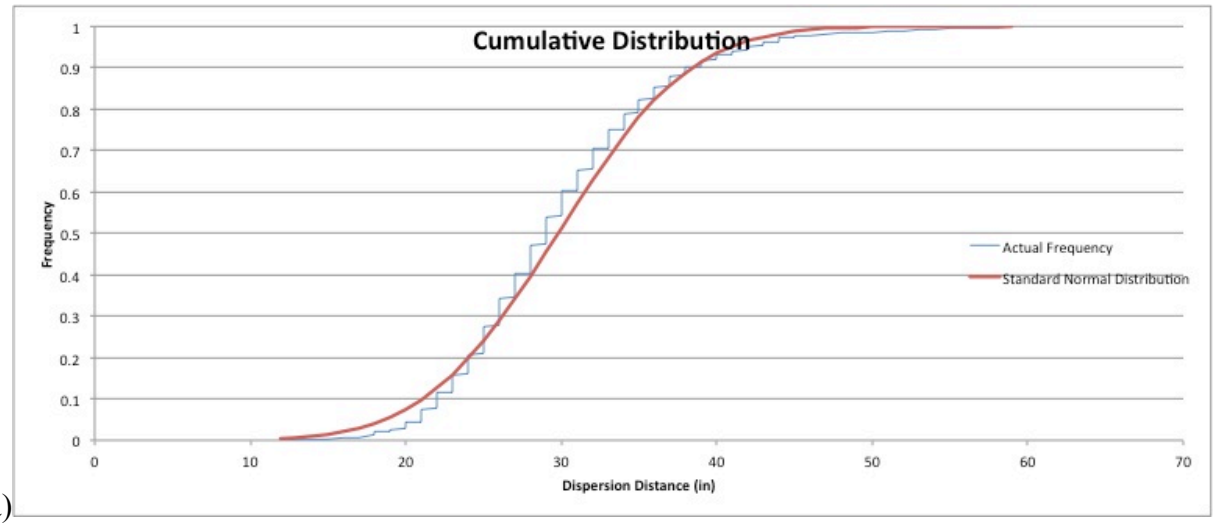

(b)

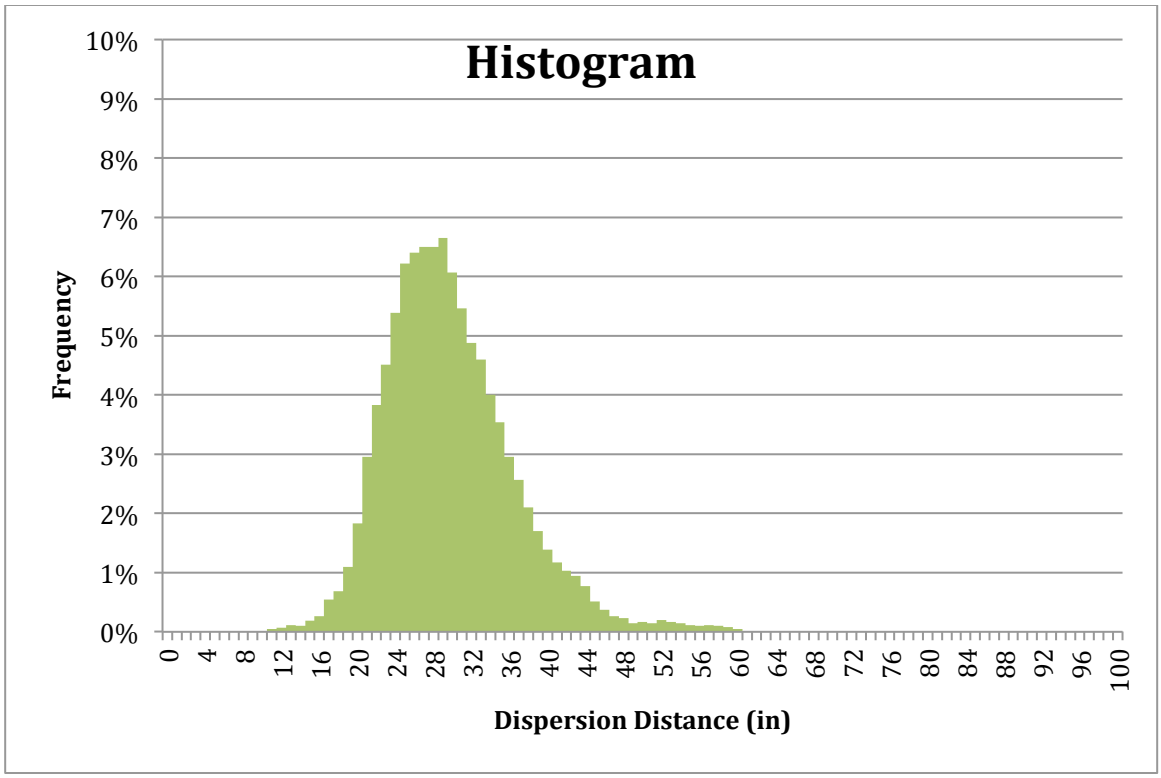

Figure 36. G_5: (a) Cumulative Distribution Plot and (b) 3-Point Moving Average Distribution Plot

With another 1mm d_p reduction, the minor peaks reappear, visible in Figures 25 and 37. The mean dispersion distance increases 4 inches and takes on a shape much more similar to a normal distribution, as seen in Figure 37(a). At this point, enough different data types have been

analyzed to establish that one bin is not more "attractive" to the particles than another, as the peaks are located at different points.

(a)

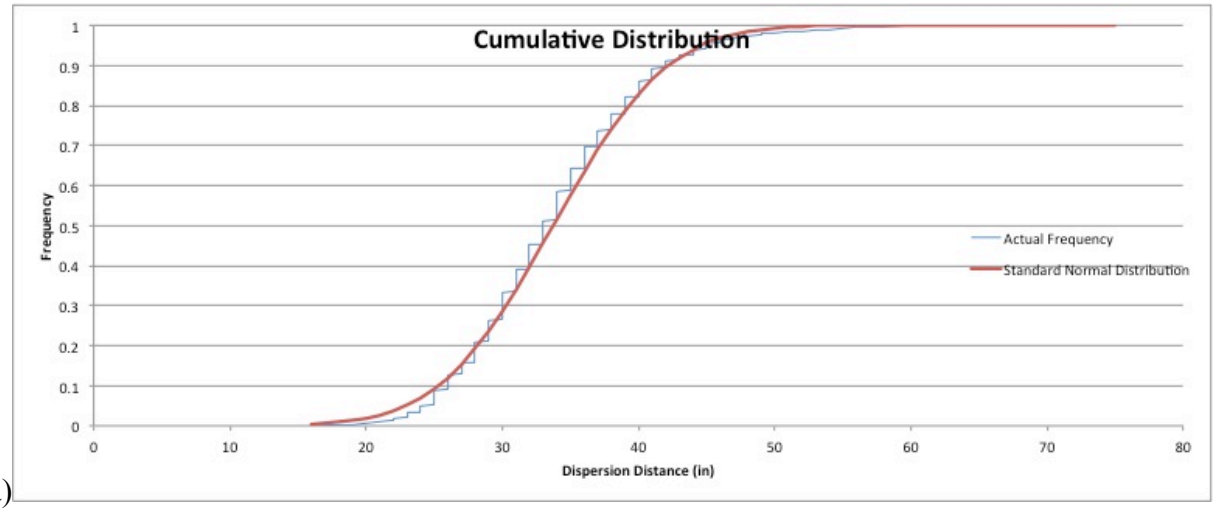

(b)

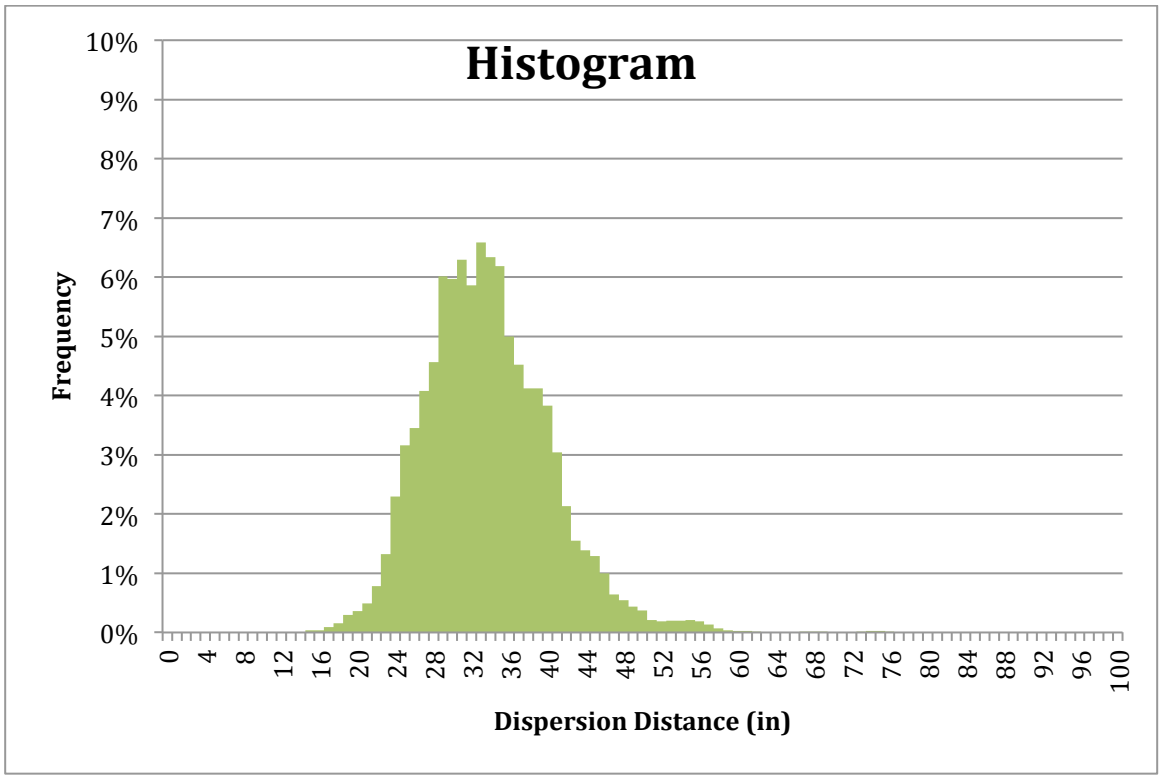

Figure 37. G_4: (a) Cumulative Distribution Plot and (b) 3-Point Moving Average Distribution Plot

As seen in Figures 26 and 38, the 3.5mm, G_3.5 particles have a mean dispersion distance 3.8 inches beyond the G_4 particles. Once again, the particle dispersion histogram is similar to the normal curve, but maintains a positive skewness.

(a)

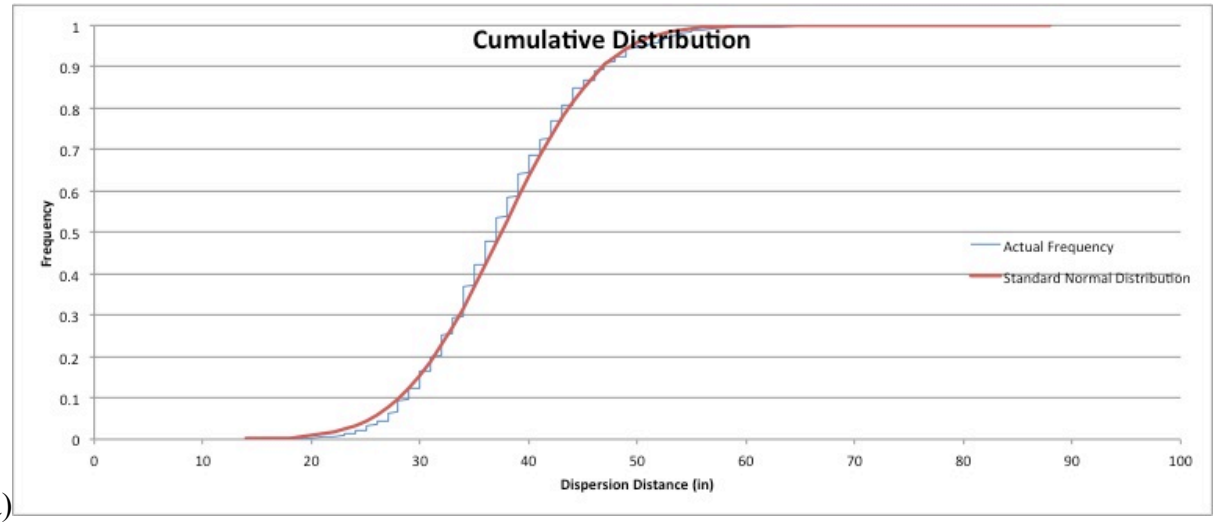

(b)

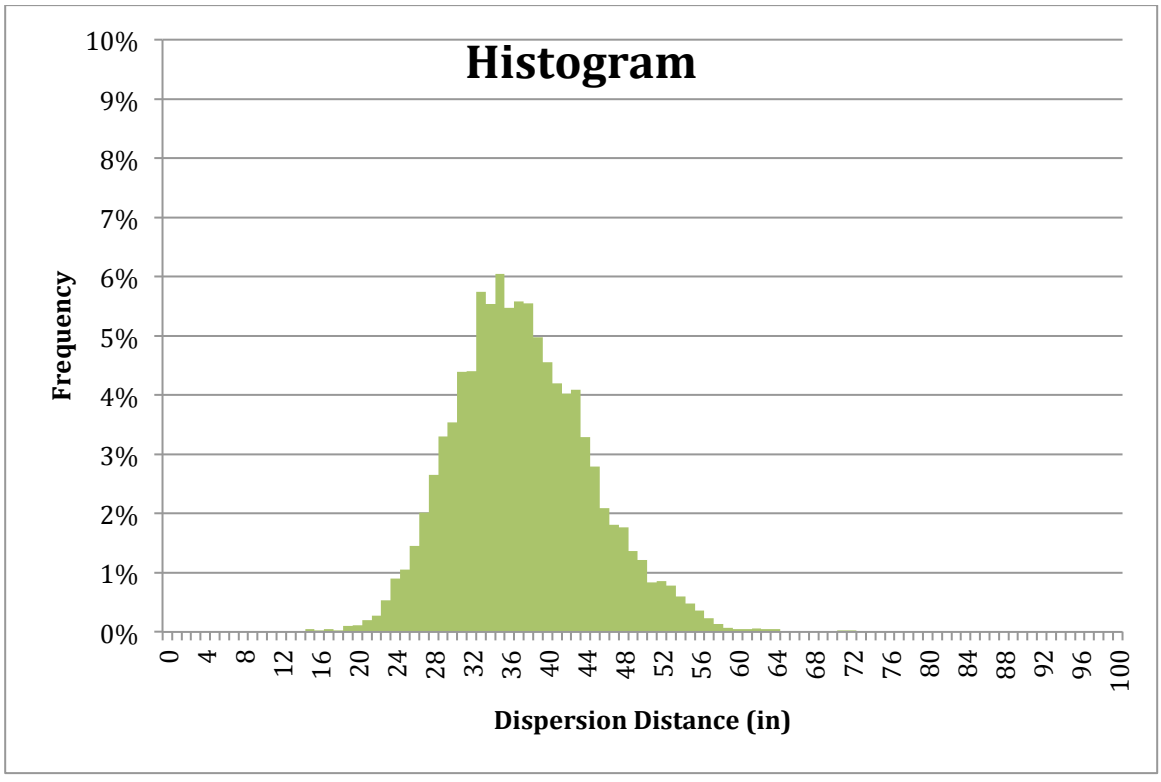

Figure 38. G_3.5: (a) Cumulative Distribution Plot and (b) 3-Point Moving Average Distribution Plot

The G_2.5 particles, as indicated in Table 2, are the smallest of the glass particles to reside in the Newtonian regime. The positive skewness is very visible with the G_2.5 particles of Figures 27 and 39. Additionally, the mean and standard distribution increase significantly. Figure 39(a) shows how statistically significant the histogram's steep lead-in curve is. The minimum particle velocity clearly rises as d_p decreases. If this were not true, at least a few of these particles would fall in the bins closer to the nozzle and the lead-in tail would be more like that of the lead-out.

(a)

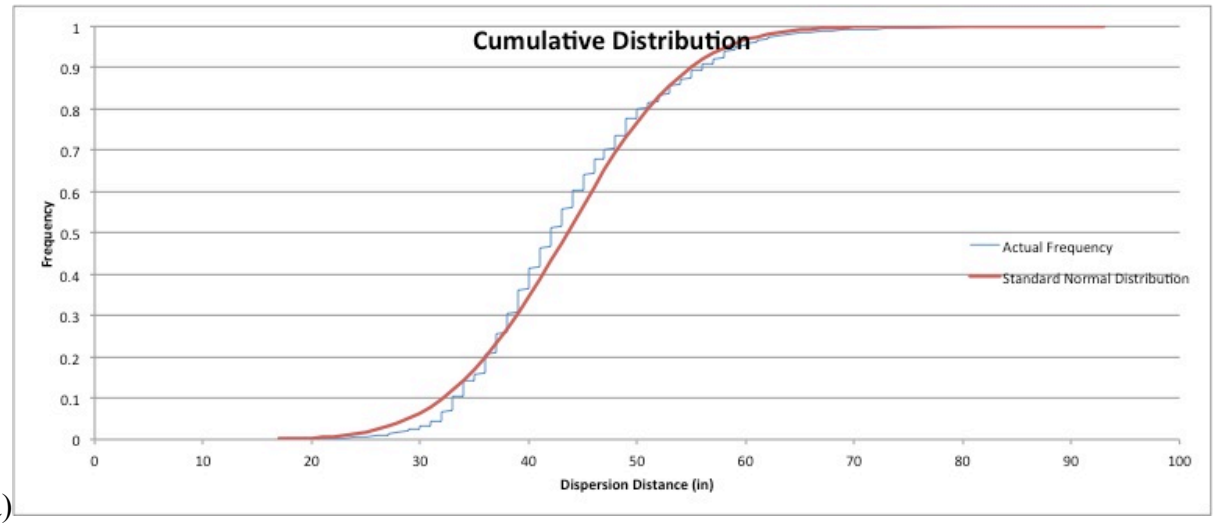

(b)

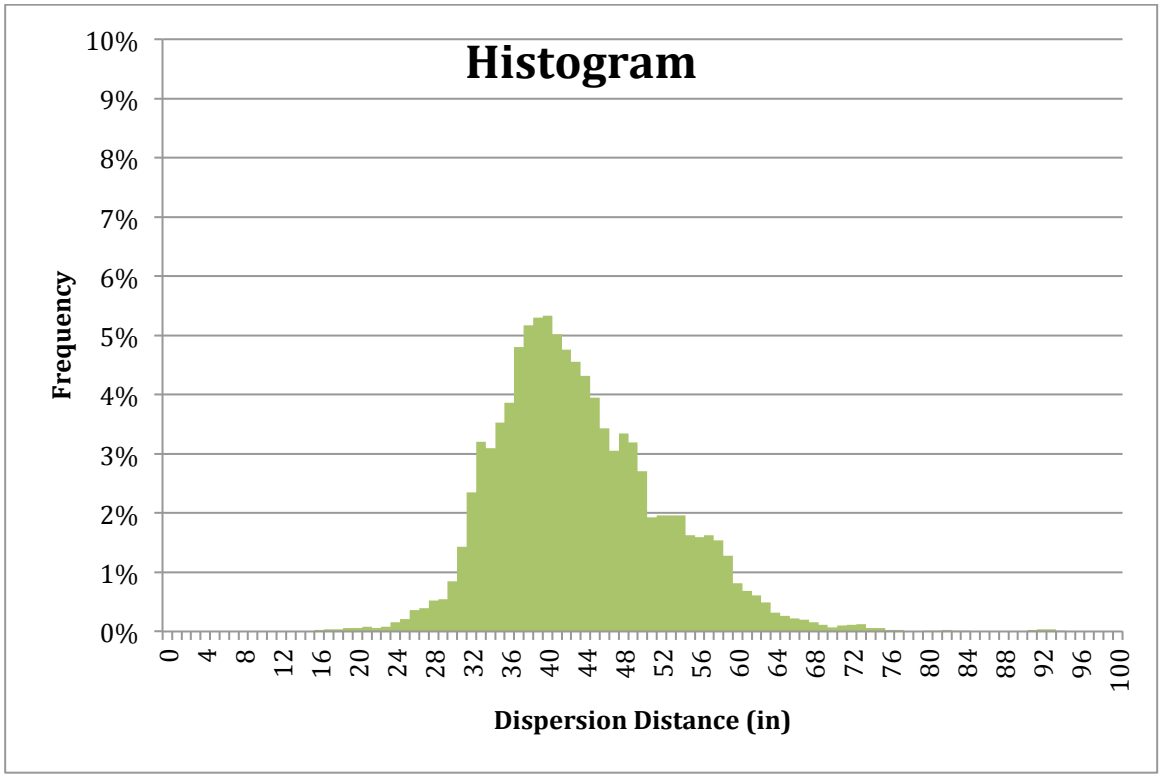

Figure 39. G_2.5: (a) Cumulative Distribution Plot and (b) 3-Point Moving Average Distribution Plot

The experiments with the G_1 particles included a new type of behavior. The shape of the histogram plots in Figures 28 and 40(b) is much broader of those by the AS_6 particles, or any of the other glass particle type. The mean dispersion distance and standard deviation are greater than any other particle type described in this paper. While the difference between the characteristics of Figure 40(a) and those of the above particle types may be due to G_1 particles existing just inside the transition regime, it is suspected it is actually due to increased entrainment. Prolonged time in the turbulent jet stream would increase the particle dispersion distance and increase mixing of particles, prior to the deposition. This turbulent mixing may have caused the increased standard deviation and broader shape of Figures 28 and 40(b).

(a)

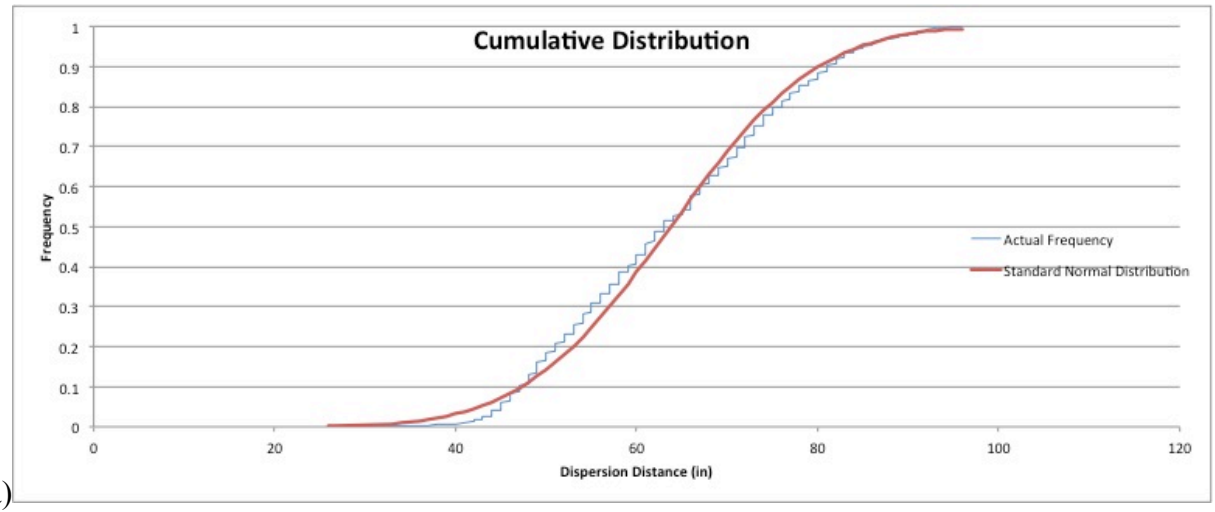

(b)

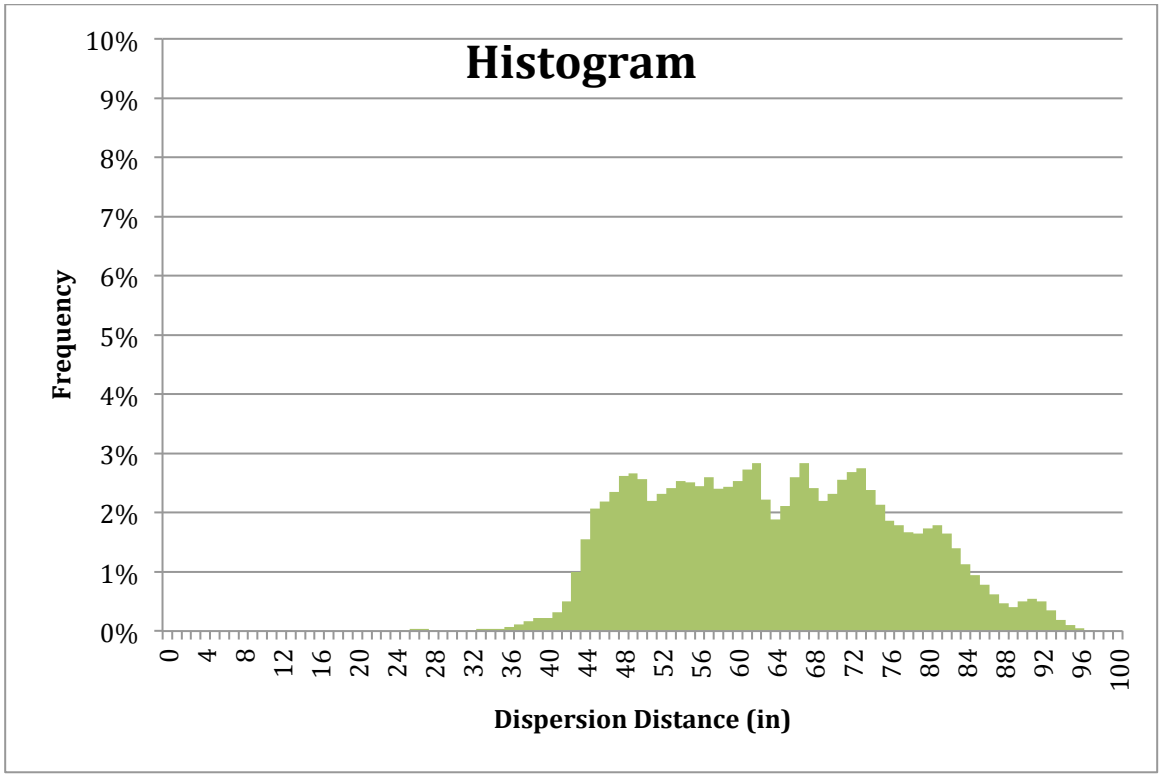

Figure 40. G_1: (a) Cumulative Distribution Plot and (b) 3-Point Moving Average Distribution Plot

Other Particles

The CS_2.3, ZS_1, and Z_ histograms shown in Figures 29-31 and 41-43 show the importance of particle material when considering mean dispersion distance. The chrome steel

composition of the CS_2.3 particles had a density more than 3x that of the glass. Even at 2.3mm, the CS_2.3 particles seemed to "plummet" out of the jet nozzle. Figures 29 and 41 show the unusual shape of the CS_2.3 distributions. The three peaks in Figure 29 were found in almost every experimental run. No bouncing of these particles was observed, and as mentioned earlier, the glass particles have shown there is no one bin that is significantly more "attractive" to particles than another. Regardless of the unusual shape and peak characteristics of the CS_2.3 particle distributions, the mean dispersion distance and low standard deviation further indicate the importance of particle material when considering entrainment properties.

(a)

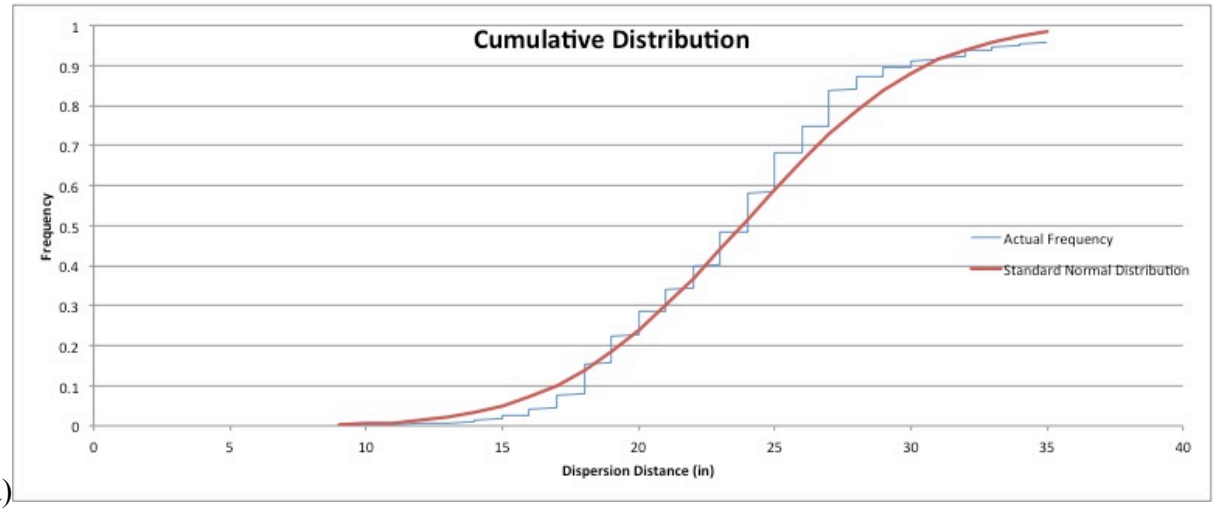

(b)

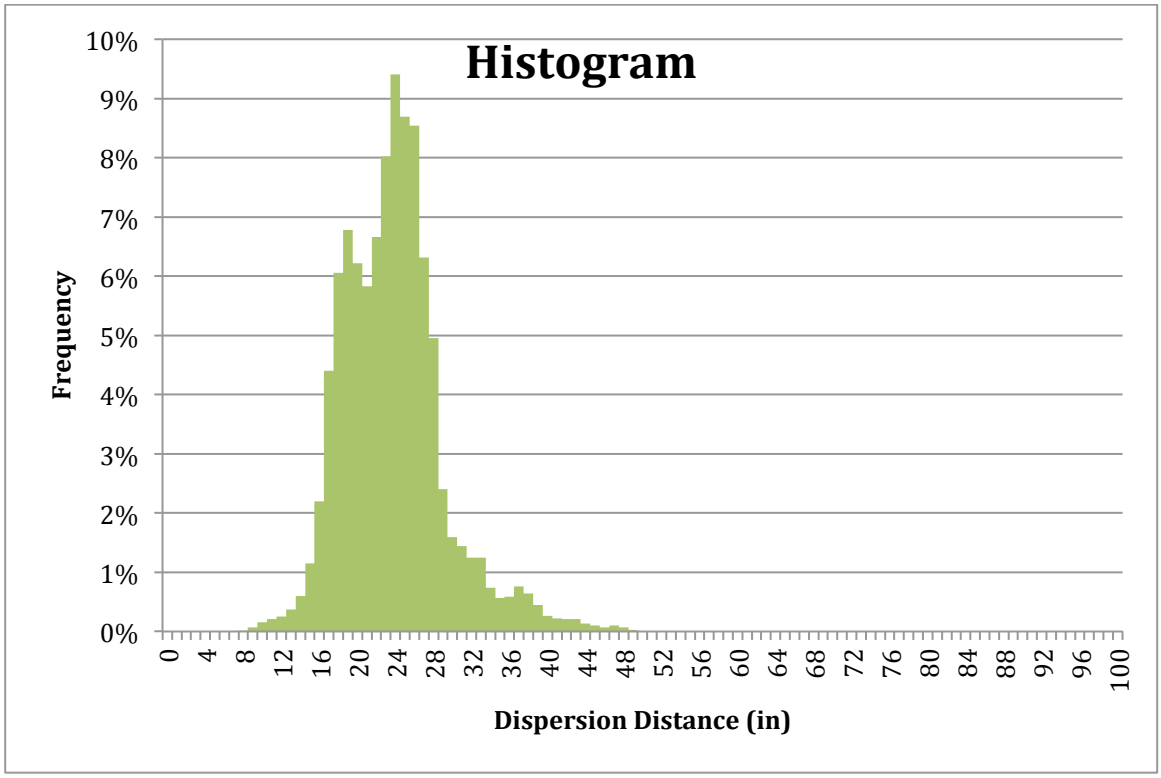

Figure 41. CS_2.3: (a) Cumulative Distribution Plot and (b) 3-Point Moving Average Distribution Plot

In Figures 30, 31, 42, and 43, distribution data is presented for the ZS_1 and Z_1 particle experiments. While there are some minor peaks in these plots, the overall shape is easy to discern. Something unique about these plots is the nature of the histogram slopes. Unlike the curved slopes of the earlier particle types, the ZS_1 and Z_1 histograms feature nearly linear slopes on both sides of the plots. This is particularly noticeable with Figures 31 and 43.

(a)

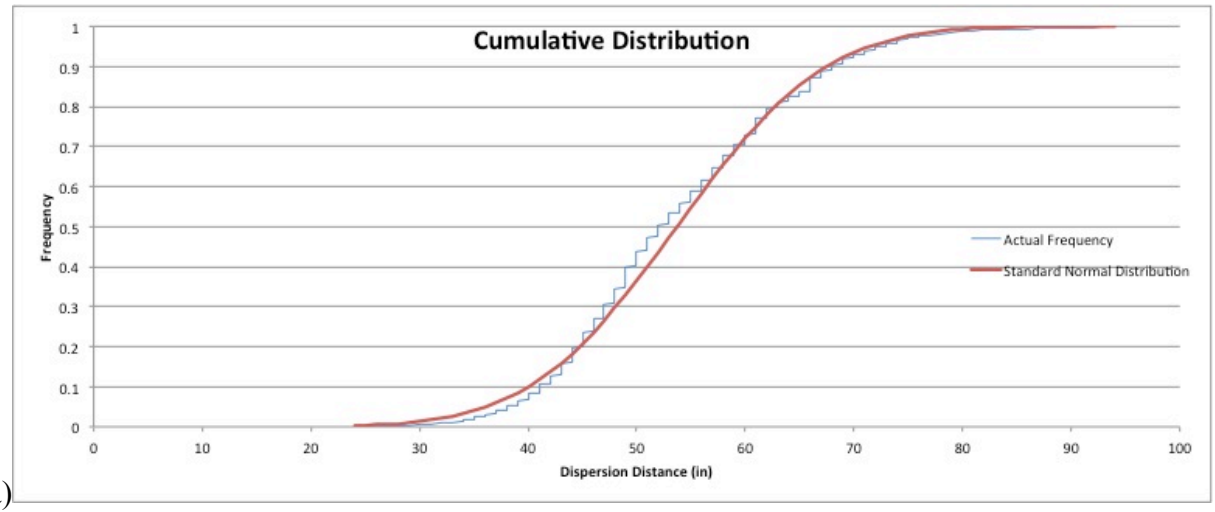

(b)

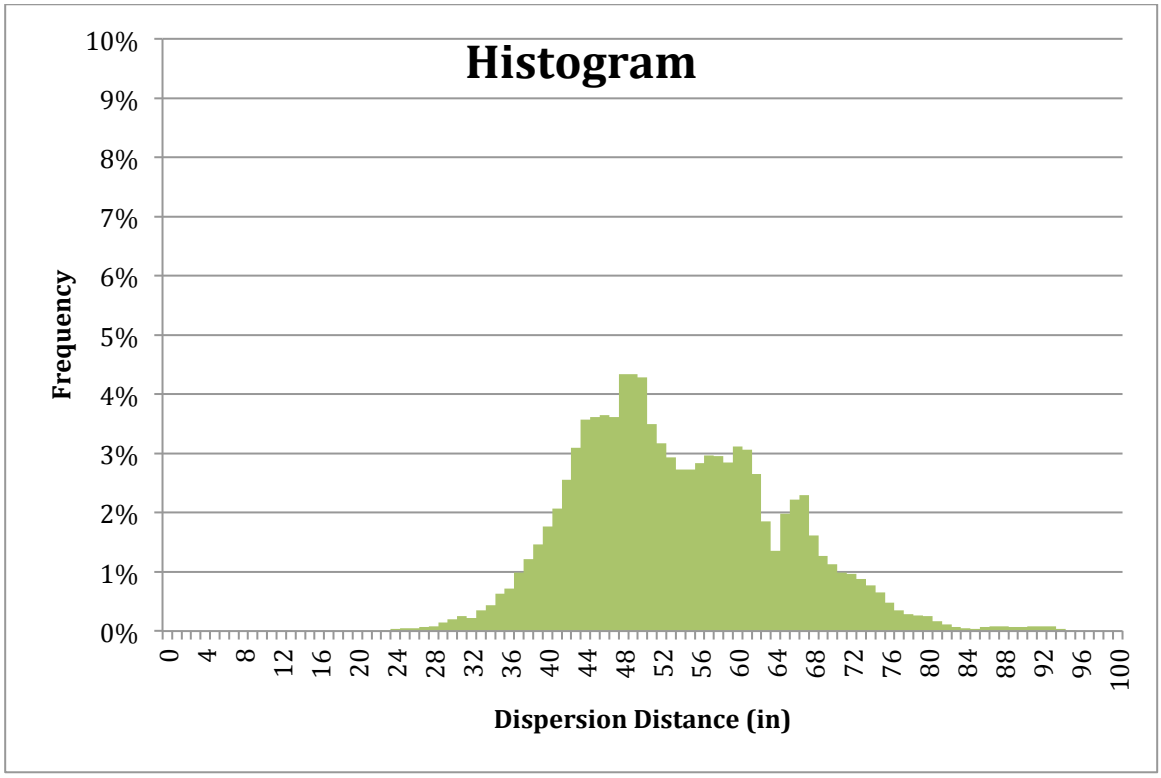

Figure 42. ZS_1: (a) Cumulative Distribution Plot and (b) 3-Point Moving Average Distribution Plot

(a)

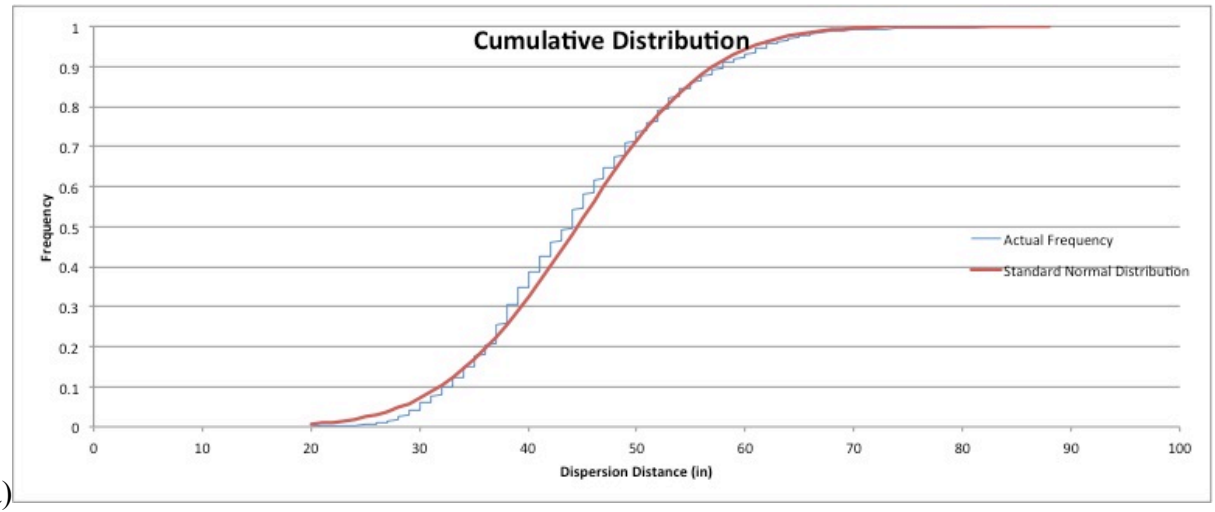

(b)

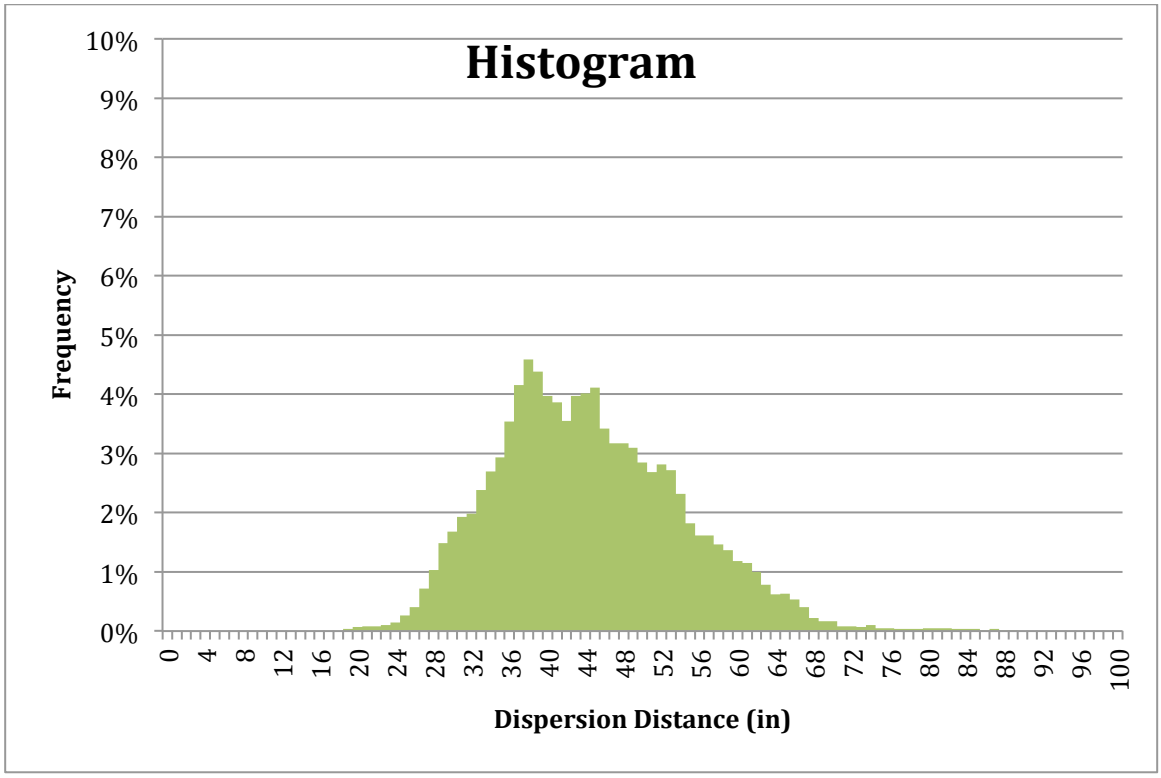

Figure 43. Z_1: (a) Cumulative Distribution Plot and (b) 3-Point Moving Average Distribution Plot

Both the ZS_1 and Z_1 particle types have small d_p values and exist in the transition regime. While their mean dispersion distance values are greater than most of the glass particles,

they both are lower than that of the G_1 type. A closer comparison of the G_1, ZS_1, and Z_1 particles will be discussed later in the chapter.

Comparison of Data:

Effect of Particle-Count

As seen in Table 5 and Figure 44, there was negligible difference in the dispersion data between the 50, 100, and 200 particle-counts with AS_6 spheres. All three experiment types resulted with mean values within the error ranges of each other, as the measuring method used a series of 1-in bins. The slightly higher mean distance of the 200 particle-count set can likely be attributed to the 3-4 bounces (which would very-slightly raise the mean dispersion distance).

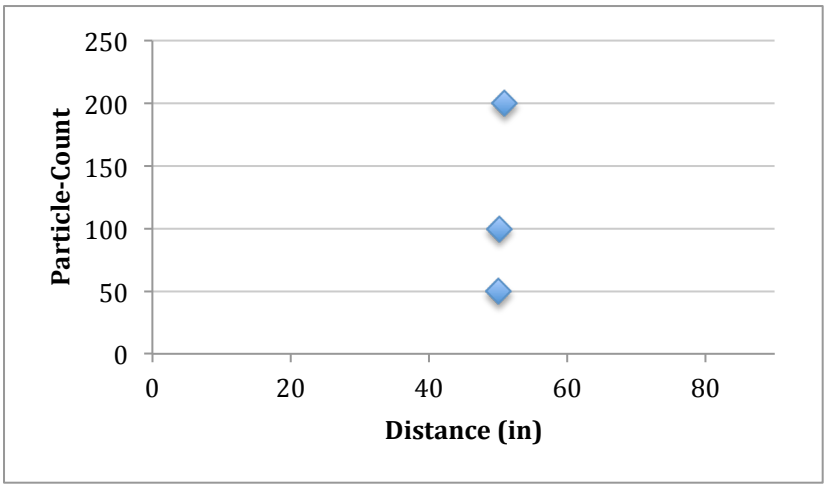

Figure 44. Mean Dispersion Distance vs. AS_6 Experimental Particle-Count

The AS_6 airsoft particles were compared, as of all the particles tested, AS_6 were considered the most likely to be affected by coupling effects. This consideration was due to their large volume fraction. As the other particle types discussed in this paper have smaller volume fractions, the effect of particle-count on entrainment properties is likely minimal, if even existent.

Effect of Particle Characteristics

While it has already been discussed that particle diameter has an effect on dispersion distance, Figure 45 shows that there is a nonlinear effect on distance. The greater the particle diameter, the less distance the particle will travel. Additionally, it is apparent that diameter is not the only factor, as shown in Figure 46.

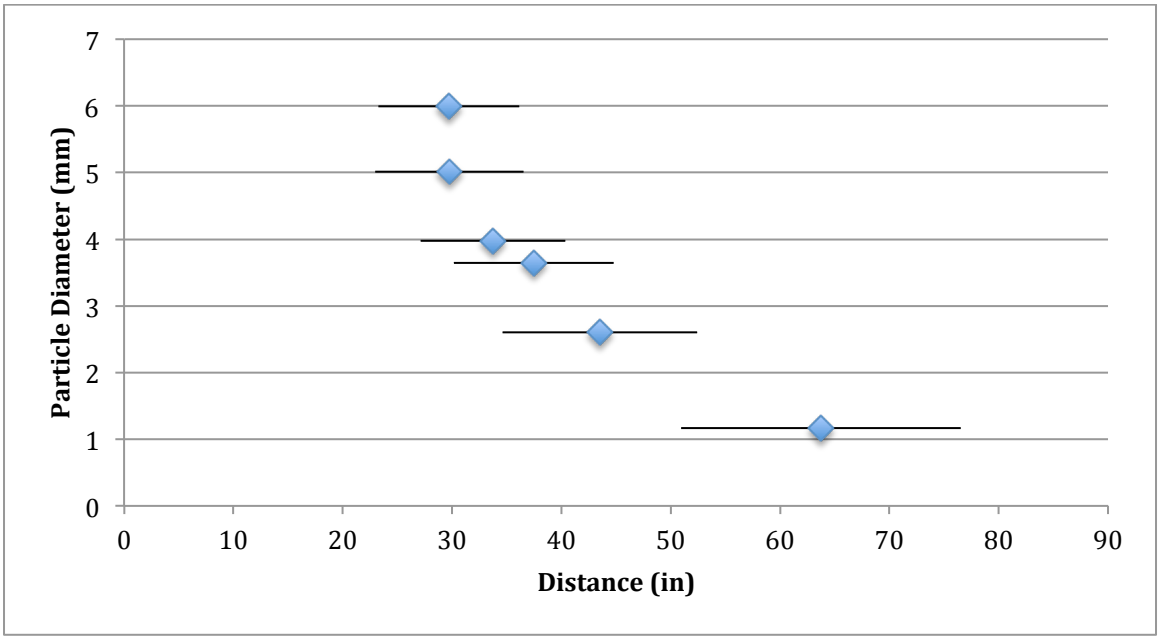

Figure 45. Mean Dispersion Distance vs. Glass Particle Diameter

Figure 45 shows all six glass particle types and their respective mean dispersion distances. The "error" bars in the plot indicated the standard deviation of each particle type's distribution. Figure 45 is relevant as all the particles were launched with the same experimental conditions, with only particle size changing. It is unclear, however, whether the increased dispersion distance is actually caused by a size parameter (diameter, surface area, cross-sectional area, or volume), or by particle mass.

A plot of 1mm particle densities vs. mean dispersion distance is provided in Figure 46, below. The green, red, and purple lines connect the particles shown with similar sizes. The 6mm line includes the G_6 and AS_6 mean dispersion distances. The red, 2.5mm line connects the G_2.5 and CS_2.3 particle types. Lastly, the purple line connects the Z_1, ZS_1, and G_1

mean dispersion distances. This comparison helps determine the importance of particle density in entrainment ability.

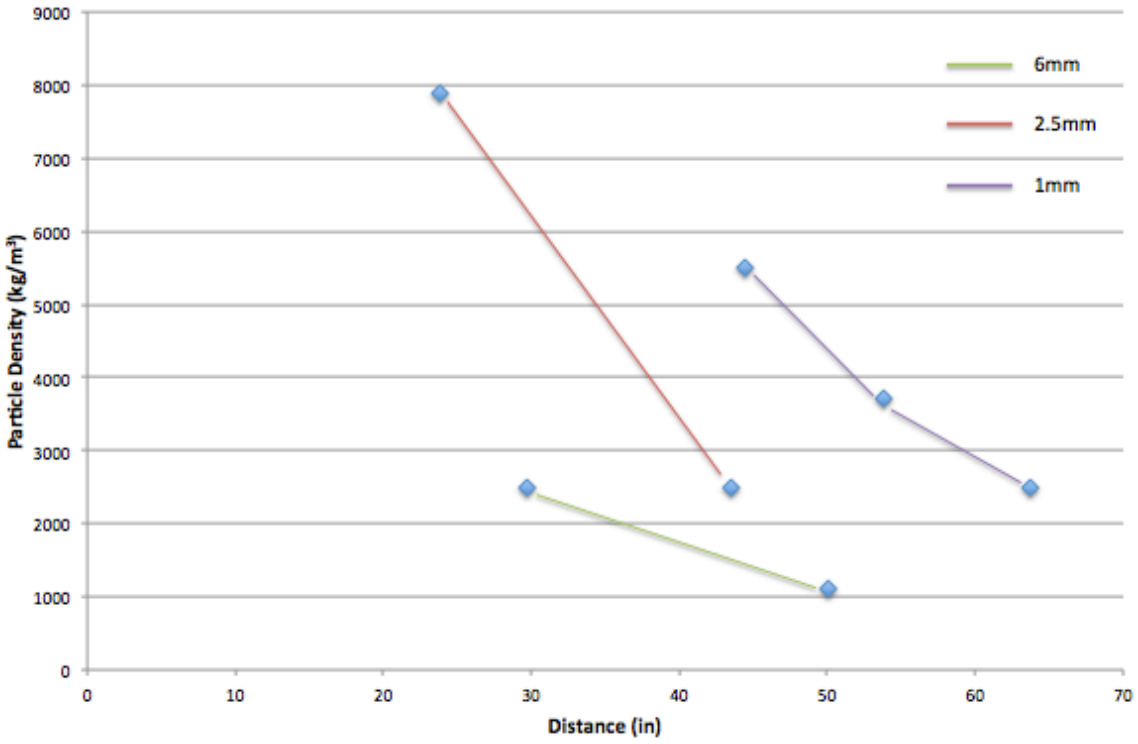

Figure 46. Mean Dispersion Distance vs. 1mm Particle Densities

Unfortunately, there are not enough data points at any specific particle size to fully understand the magnitude of importance in particle density. What is clear, however, is that a reduction of particle density, with all other characteristics fixed, will increase particle dispersion distance. As both Figures 45 and 46 indicate increases of dispersion distance with particles of decreasing mass, a mass vs. dispersion distance plot must be examined.

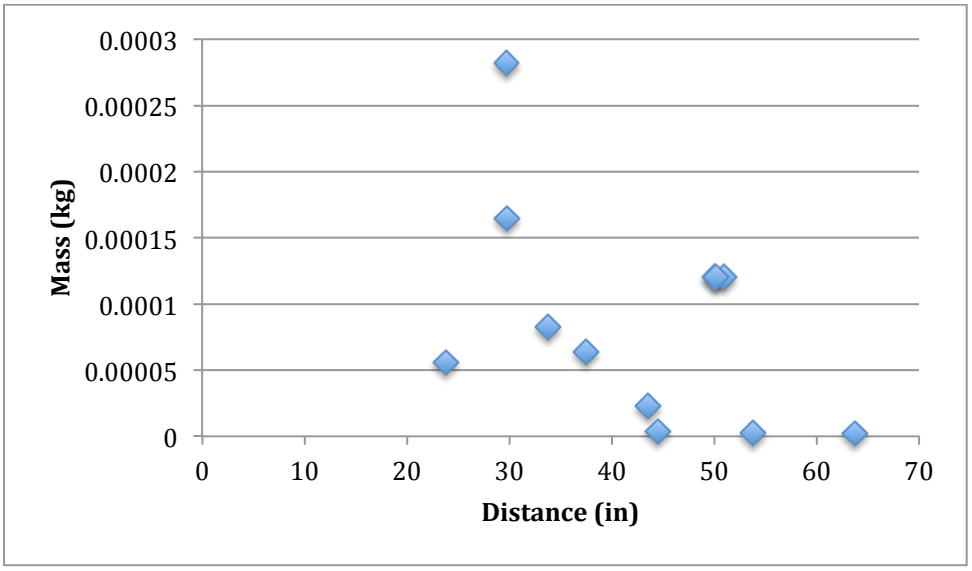

Figure 47. Mean Dispersion Distance vs. Particle Mass

Figure 47 presents a particle mass vs. dispersion distance plot including all particle types. As seen above, the data points are scattered all over the plot. This plot is important for that reason. Since there is no common trend in this plot, it proves mass is not the sole factor in determining dispersion distance. Figure 47, combined with the relationship observations from Figures 45 and 46 indicate that both particle size and density affect a particle's linear dispersion.

This conclusion makes sense, as the prominent vertical forces acting on a Newtonian particle in flight are gravity and lift. Lift force is dependent on particle size and gravitational force is dependent on particle mass (density x volume). As particle flight requires a balance between these forces, it is logical that they both would impact a particle's entrainment ability.

Discussion:

Every cumulative density function (CDF) in this chapter was found to be similar to a Normal Distribution. However, all of the CDF's also shared certain traits indicating a non-Gaussian form. To verify numerically the non-Gaussian form of the plots, the Kolmogorov-Smirnov Test was conducted. This test examines the likelihood of two sets of data being from

the same source. The CDF's for all experiment types were examined to find the largest difference (D) value, as seen in Figure 48.

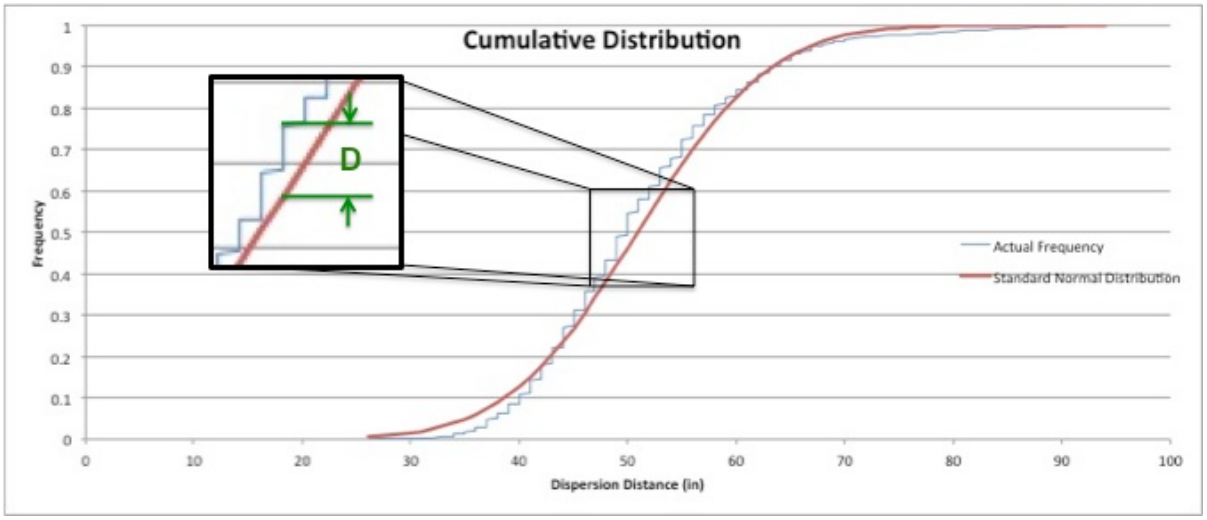

Figure 48. G_3.5 Maximum Difference (D) Value

Once the D value has been identified, a critical value, C, is calculated using Eq. (12),

$$C = \sqrt{\frac{N_1 \cdot N_2}{N_1 + N_2}} \cdot D \tag{12}$$

where N_1 is the number of data points available for the standard normal curve and N_2 is the number of sample points from the experimental results. Lastly, C is used to determine an uncertainty value, a. The lower this value, the less likely the two sample sets come from the same source

$$a = 2\sum_{i=1}^{\infty}(-1)^{i-1}e^{-2i^2C^2} \tag{13}$$

Using the Kolmogorov-Smirnov Test, uncertainty and confidence values were determined for every class of experiments discussed. Each experiment had a confidence value of at least 99%, indicating that it is very unlikely any of the results are Gaussian.

As it is unlikely the experimental results are from a normal distribution, the nature of the difference must be considered. The plots all have steep lead-ins, positive skewness values, and long "tails" along the upper end of the x-axis. If the particles were experiencing only a projectile

motion, the distribution plots would be Gaussian and there would likely be a mix of positive/negative skewness values. The following is a proposed explanation for common traits observed in this study.

To better understand the motion of the experimental particles, Chris Sebesta, a fellow TPaNS researcher, helped create a CFD model of the Jet Propulsion Apparatus. Two datasets were requested: (1) nature of the airflow prior to becoming a jet and (2) typical particle locations at nozzle, relative to the cross-sectional area. Figures 49 and 50 include the results of the CFD simulations [48].

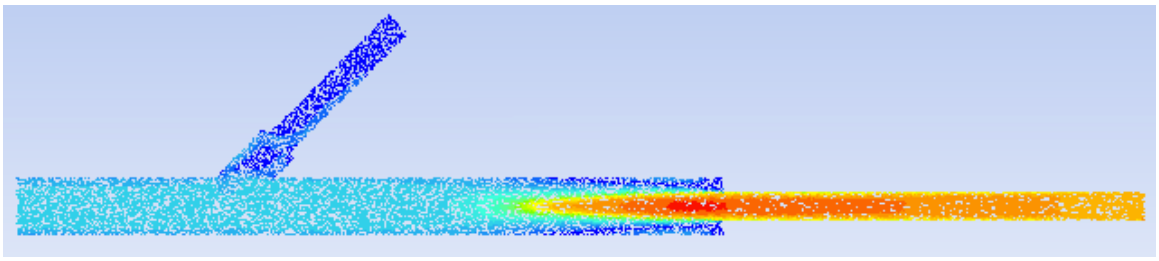

Figure 49. CFD Simulation of Airflow Velocity at Center Plane [44, 48]

Figure 50. CFD Simulation of G_1 Particle Injection Path [44, 48]

The color spectrum of Figure 49 uses blue to represent minimum velocity and red for maximum velocity. Figure 50, on the other hand, has a time-step color-coding. Dark blue is t=0 and red indicates the time of final particle ejection [48]. Both images indicate particles traveling with the flow at the jet's start, with an even mix of particles throughout the nozzle's cross-sectional plane. This mixed flow is exactly what was hoped for in this series of experiments and is the foundation for the theory described in Figure 51.

As stated above, the distributions of the various particle types all have shapes similar to Gaussian. They all additionally show a positive skewness and extended "tail" to the right. Figure 51 is a sketch of what may be the cause of these traits.

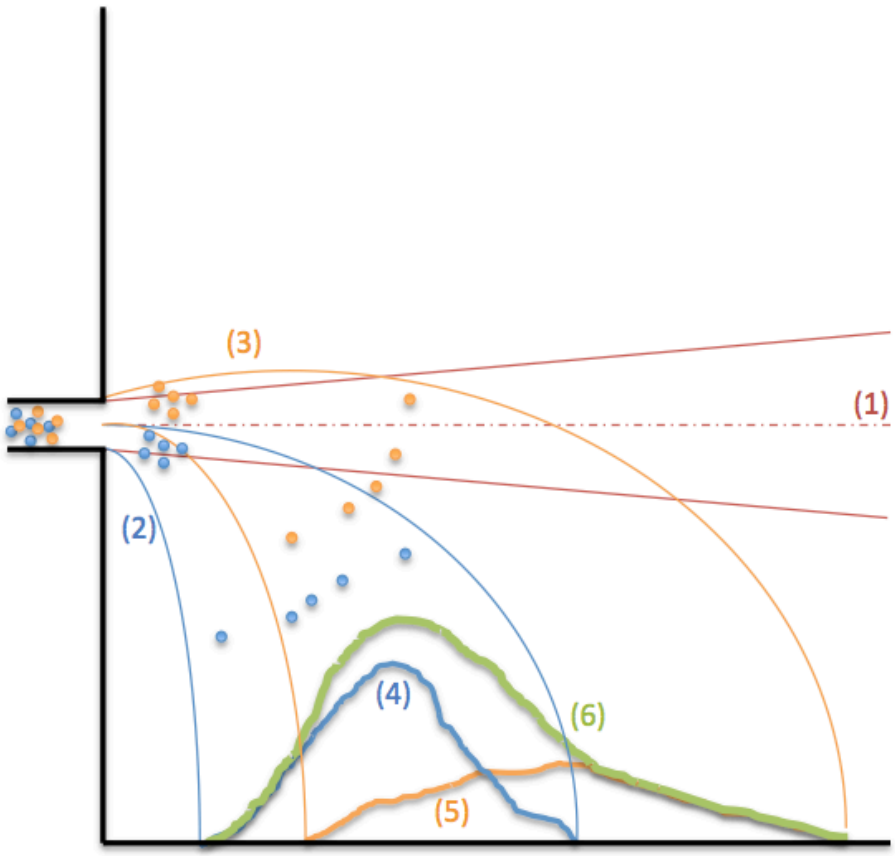

Figure 51. Theory Sketch of Non-Gaussian Dispersion Distribution Plots

Figure 51 is a sketch of the side-view of the jet and Particle Entrapment System, showing theoretical particle paths. The first notable item in the sketch is (1), showing the jet's distribution. The solid red lines indicate the angle of air dispersion and a dashed red line is placed along the jet's centerline. This dashed line should be considered a plane passing through the page. There are two regions of particle transport. The lower region (2), exists in the portion of the nozzle and jet below the mid-plane (1). The upper region (3), is colored orange and consists of all particles ejected above the mid-plane (1).

It is possible that the particles fired out the nozzle in the lower region follow a ballistic trajectory, shown by the blue curves of (2). When these particles land on the tunnel's floor, they

are patterned in a Gaussian manner. This Gaussian pattern is represented by the dark blue curve of (4).

Unlike the lower particles, those exiting the jet nozzle above the mid-plane of (1) follow a different path. These upper particles follow an extended path along (3), as they exist for a longer period of time in the jet flow, and all cross the maximum air-velocity point at mid-plane. Additionally, the upper half of an axisymmetric jet includes a larger amount of upward-oriented air vectors than the lower. This encourages additional lift on the particles in the upper-region. Once the particles finally fall out of the jet stream, they will have experienced more turbulent mixing and longer travel times, causing a more deviated landing, as indicated by (5).

Combined, (4) and (5) are summed to create the overall particle distribution of (6), which is representative of the particles measured in this paper's study. This combination of two different distributions would result in a plot with several Normal distribution qualities, while experiencing a positive skewness and right-side tail. This possible explanation is also supported by the increasing nature of distribution standard deviation vs. particle diameter, as seen in Figure 52. As the particle size increases, the propulsive forces of the jetstream also increase, extending the "tail", and increasing the standard distribution.

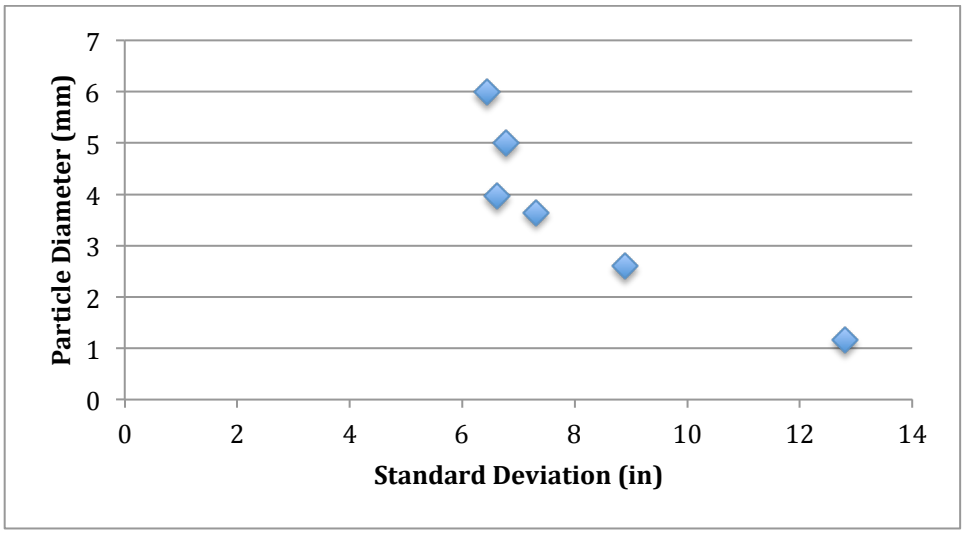

Figure 52. Dispersion Distance Standard Deviation vs. Particle Diameter

In future experiments, the tests would need to be repeated with a means of tracking only upper-region particles. This would be difficult to accomplish experimentally, as most means of separation would disrupt the jet flow's uniform distribution. For this reason, initial studies should be conducted via CFD simulation. With software such as FLUENT, it would be easy to run two different simulations with the upper and lower regions separated (as long as an adequate particle transport code is in possession). If the CFD simulations support this theory, particle image velocimetry (PIV) should be used to track the particle velocity vectors during transport. With CFD and PIV experimentation, this theory could be adequately proven or disproven.

CHAPTER 5 – Summary and Conclusions

Summary:

The research objectives for this study called for the creation of an experimental rig to study particle transport and the behavior of particles injected into axisymmetric jets. This was completed with the system described in Chapter 3 and Figure 3. The 301 experiments conducted with this rig produced experimental data capable of validating CFD codes modeling particle transport in axisymmetric jets. At the time of this paper's submission, other members of the TPaNS Lab were already incorporating the data into new multiphase flow codes. Lastly, particle size, density, mass, and particle-count properties were examined to help identify which elements are relevant in maximizing entrainment and dispersion distance. All three research objectives outlined in Chapter 1 were accomplished, analysis was performed, and future research paths were identified to enhance the engineering communities understanding of particle flows in jets.

Conclusions:

While many new questions arose from the results of this study; there were some well-founded conclusions that may prove useful when working with particles in gas flows in the future.

When considering Newtonian particles in a jet flow, particle concentration will have to be very high before two or four-way coupling effects become relevant. There was no situation in this study where particle-particle interaction proved to affect the outcome of a trial's dispersion mean.

If all other flow conditions are fixed, and a spherical Newtonian particle's size is decreased, it is much more likely to have an increased dispersion distance.

If all other flow conditions are fixed, and a spherical Newtonian particle's density is decreased, it is more likely to have an increased dispersion distance.

Neither size, nor density, nor mass, are the sole parameters in determining particle dispersion distance.

There may exist multiple regions of particle transport within a jet, but further research is necessary.

CHAPTER 6 – Recommendations

Introduction:

Time and financial resources significantly limited the scope and accuracy of this research. The Transport Phenomena and National Security (TPaNS) Lab had only been in existence for 15 months at the time of this paper, so resources were limited. The quality of the data documented here was adequate; however, the lab team came up with some good ideas for lab / research improvement, should further resources be available in the future. Ideas deemed to be most practical are summarized in this chapter.

Experimental Approach:

Three changes in the Experimental Rig of Figure 3 were thought of in the month prior to this paper's submission, should additional time and financial resources become available. These changes would affect the:

- Bin Collection System
- Particle Injection System
- Air Flow Velocity Measurement Method

First, the Bin Collection System could be improved further, to reduce bouncing, rolling, and ease-of-measurement recording. The system was adequate for Newtonian particles, but would prove problematic for particles larger than $Re_p = 8{,}000$ or smaller than $Re_p = 600$. The larger particles would either bounce too much or damage the fin pallets, due to their large mass / size. The smaller particles would have diameters too small to be trapped by the fin pallets. Additionally, even if the smaller particles were adequately trapped, it would be difficult to count them, as they would require 20/10, or better, vision to identify each particle.

One way to improve the Bin Collection System would be to glue the fins directly to the tunnel floor and slope the floor to one side, perpendicular to the jet flow. This would prevent rolling and would gather each bin's particles in one spot, allowing for easy counting. The fins could be trimmed along the top to ensure their height was equal and a hinged tab could be cut into the Plexiglas wall to allow fast and easy resetting of the experimental rig.

Another way to improve the bin collection system would require a quality machining lab and additional resources, but would decrease experimental time significantly and make counting smaller particles possible. A series of wide, rectangular funnels could be built, also in 1-inch increments, to sort the particles into collection cups or area. An example side-view is shown in Figure 53. Such a system would maintain a completely uniform tunnel in the z-direction (side to side), while allowing for easier and more accurate low-Transition/Stokes regime flow measurements in a lab environment.

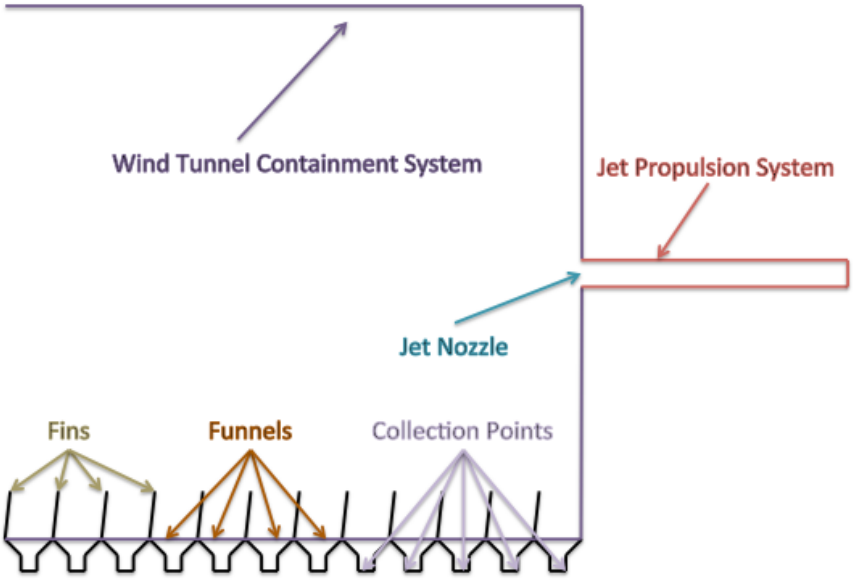

Figure 53. Future Fin Cup Side-View

The particle injection system is reasonably designed, given the regime of the tested particles. However, if smaller particles are to be test, some geometric conditions of the injection system must change. Throughout this paper, particles were injected through a reverse-45º insertion pipe. Two concerns for smaller particles lie within the insertion pipe air-flow and the PVC connection gaps. Given the current experimental rig geometry, there is roughly a 1 m/s air-

flow up and out of the injection system. Newtonian particles are heavy enough to fall through this flow and entrain into the pipe flow, prior to ejection. However, Stokes regime particles may not experience this gravitational superiority.

Miller Plastic Products, Inc., manufactures PVC eductors, which could be modified to not just reduce the outward airflow, but reverse it, creating a suction to draw the particles down the injection pipe [49]. Using long wooden cotton swabs, acrylic glue could be applied to fill the interior connection gaps of the pipe, minimizing the "sticking" of any particles upon injection. Such an upgrade to the injection system could be completed for under $200.

Lastly, to better understand the nature of the airflow throughout the experimental rig, a series of modifications should be made. First, the inline flowmeter from Figures 6 and 13 should be removed from the system. With the lab's pitot tube anemometer, the flowmeter is no longer necessary and restricts the flow from the blower. Second, for each variation of the Jet Propulsion Apparatus, the pitot tube anemometer should be used to measure the velocity profile before and after each connecting piece. To complete this efficiently, the measurements should be taken, as the system is being put together. The next change to the system would involve building an add-on to the Jet Propulsion Apparatus frame. By adding a small wooden plank over the frame, the TPaNS Lab smoke machine could be attached and have the ability to pump smoke into the particle hopper. Additionally, a laser sheet generator should be placed on top of the Particle Entrapment System. This, combined with the smoke injection, would allow for several types of flow visualization in the tunnel, with or without particles. Such a system is described and photographed in a paper by J.L. Wright et al. [50].

Continuation of Current Research:

For an immediate expansion of current research, the experimental rig could be modified slightly to accommodate another dimension of tests to determine the affect of airflow velocity, nozzle diameter, nozzle height, and jet angle on entrainment values. All of the below modifications can be made using the materials on-hand in the TPaNS Lab.

Airflow Velocity & Nozzle Diameter

There are two separate ways to modify the airflow velocity of the Jet Propulsion Apparatus. First, by removing the inline flowmeter, as described above, the speed of the airflow will instantly increase. With the additional two feet of space available, a globe valve and 1-in ID PVC pipe could be used to create a throttling system for the apparatus. This modification would increase the maximum air speed and allow for testing particle dispersion distance with varying air speed.

Second, the nozzle diameter could be reduced to 1-in ID. By decreasing the pipe's cross-section area, the air speed would increase, while maintaining a constant flow rate. This modification would allow for studying a new set of jet conditions. If such a change were made, it would be important to retest all of the particles, understanding that there could be no direct comparison of test results. Jet properties are dependent on nozzle diameter, so such a modification would cause a change of two separate variables.

Nozzle Height & Jet Angle

The Jet Propulsion Apparatus was designed to have the nozzle height easily changed. By cutting a new hole above or below the nozzle's current 4-ft location, and shifting 8 screws in the apparatus stand, the jet piping can be set to a height between 6 inches and 72 inches. When cutting the new hole, care should be taken to keep the circular Plexiglas piece intact, as it will be needed to fill in the hole currently supporting the nozzle.

The jet angle can be modified in a similar fashion. The jet can have its angle changed by lifting or lowering the piping within the apparatus stands. As long as the jet angle is changed by 30º or less, the injection system will continue to work for the current particles. Before making changes of 15º or more, new CFD models should be tested to ensure none of the walls in the tunnel affect the jet's flow.

Future Research:

As the TPaNS Lab continues to grow and develop, this research will advance and gain more practical applications. First, this data should be used in conjunction with the CFD models being designed for the same geometry by other members of the research team. CFD is a valuable tool, but should always be used in conjunction with physical experimentation. The experiments described in this paper will allow several different configurations of the CFD model to be tested and calibrated, making if possible to move on to even better models, hopefully for smaller particles.

Second, as more money and personnel are assigned to the experimentation side of the TPaNS research group, he experimental rig can be modified or redesigned to accommodate the testing of smaller particles. Particle image velocimetry (PIV) should be incorporated into the design and some sort of trapping mechanism should be installed at the end of the Particle Entrapment System. The trapping mechanism should contain test particles to within the test section, as not to contaminate the lab environment. This will be critical once the particles begin to entrain for longer periods of time, as inhalation could prove hazardous to lab personnel.

If nothing else, the lab's experiments should be continued to study more particles in the transition regime. These particle types have not been studied adequately by the engineering community and could have real-world benefits to industries such as mining, pollution tracking, and lubrication. None of the particles included in this paper's research traveled beyond 8-ft, and it is unlikely that other transition regime particles would surpass the 16-ft limit of the Particle Entrapment System. It would be very feasible to continue this paper's Newtonian research into the transition regime, given more time.

Appendix A – Error Analysis

Measurement Error:

Table 9 lists error analysis data for the various measurement devices used in this paper. Given a restricted budget, the best measurement devices possible were used to determine the values discussed.

Device	Measurement	Range	Resolution	Accuracy
HD350 Extech Anemometer & Pressure Monitor	Differential Pressure	0-5000 Pa	1 Pa	±0.3% FS
HD350 Extech Anemometer & Pressure Monitor	Velocity	1-80.00 m/s	0.01 m/s	±0.3% rdg
HD350 Extech Anemometer & Pressure Monitor	Temperature	273.15-323.15 K	0.1 K	±1 K
Tekton 7168 Outside Micrometer	Length	0-1 in	0.0001 in	±0.0001 in
RCM Dial-Indicating Flowmeter	Flowrate	40-300 SCFM	0.5 SCFM	±3% rdg
Engineer Rule	Length	0-6 in	0.00625 in	±0.005 in
Fin Pallet System	Length	0-192 in	1 in	±1 in

Table 9. Measurement Error Data for All Devices

Bibliography

[1] Higgins, J. A., Cooper, M., Schroeder-Tucker, L., Black, S., Miller, D., Karns, J. S., Manthey, E., Breeze, R., and Perdue, M. L., 2003, "A Field Investigation of Bacillus anthracis Contamination of U.S. Department of Agriculture and Other Washington, D.C., Buildings during the Anthrax Attack of October 2001," Applied and Environmental Microbiology, 69(1), pp. 593-599.

[2] Settles, G. S., 2006, "Fluid Mechanics and Homeland Security," Annual Review of Fluid Mechanics, 38, pp. 87-110.

[3] Hinds, W. C., 1999, Aerosol Technology: Properties, Behavior, and Measurement of Airborne Particles, John Wiley & Sons, Inc, New York, NY.

[4] Munson, B. R., Young, D. F., and Okiishi, T. H., 2006, Fundamentals of Fluid Mechanics, John Wiley & Sons, Hoboken, NJ.

[5] Hayden, K. S., Park, K., and Curtis, J. S., 2003, "Effect of particle characteristics on particle pickup velocity," Powder Technology 131(1), pp. 7-14.

[6] Saffman, P. G., 1965, "The lift on a small sphere in a slow shear flow," Journal of Fluid Mechanics, 22(2), pp. 385-400.

[7] Crowe, C. T., Schwarzkopf, J. D., Sommerfeld, M., and Tsuji, Y., 2011, Multiphase Flows with Droplets and Particles, CRC Press.

[8] Ferguson, J. R., and Stock, D. E., ""Heavy" Particle Dispersion Measurements with Mono- and Polydisperse Particle Size Distributions," Proc. Winter Annual Meeting of the American Society of Mechanical Engineers, T. O'Hern, ed., ASME, pp. 53-58.

[9] Elghobashi, S., 1994, "On predicting particle-laden turbulent flows," Applied Scientific Research 52.4, pp. 309-329.

[10] Crowe, C. T., Troutt, T. R., and Chung, J. N., 1996, "Numerical Models for Two-Phase Turbulent Flows," Annual Review of Fluid Mechanics, 28, pp. 11-43.

[11] Cushman-Roisin, B., 2010, Environmental Fluid Mechanics, John Wiley & Sons, Inc., New York, NY.

[12] Kotsovinos, N. E., 1976, "A note on the spreading rate and virtual origin of a plane turbulent jet," Journal of Fluid Mechanics, 77(2), pp. 305-311.

[13] Kotsovinos, N. E., 1978, "A note on the conservation of the axial momentum of a turbulent jet," Journal of Fluid Mechanics, 87(1), pp. 55-63.

[14] Pope, S. B., 2005, Turbulent Flows, Cambridge University Press, New York, NY.

[15] Birkhoff, G., 1957, Jets, Wakes, and Cavities, Academic Press Inc., New York, NY.

[16] Lin, S. P., 2003, Breakup of Liquid Sheets and Jets, Cambridge University Press, Cambridge, UK.

[17] Chhabra, S., T. N. Shipman, and Prasad, A. K., 2005, "The entrainment behavior of a turbulent axisymmetric jet in a viscous host fluid," Exp. Fluid, 38(1), pp. 70-79.

[18] Wygnanski, I., and Fielder, H., 1969, "Some measurements in the self-preserving jet. ," Journal of Fluid Mechanics, 38(3), pp. 577-612.

[19] Hussein, H. S., Capp, S., and George, W. K., 1994, "Velocity measurements in a high-Reynolds-number, momentum-conserving, axisymmetric, turbulent jet.," Journal of Fluid Mechanics, 258, pp. 31-75.

[20] Panchapakesan, N. R., and Lumley, J. L., 1993, "Turbulence measurements in axisymmetric jets of air and helium. Part 1. Air jet.," Journal of Fluid Mechanics, 246, pp. 197-223.

[21] Panton, R. L., 2005, Incompressible Flow: 3rd Ed., John Wiley & Sons, Hoboken, NJ.

[22] Waite, L., and Fine, J., 2007, "Applied Biofluid Mechanics," Mc-Graw-Hill, pp. 15-16.

[23] Fields, M. A., 1963, "Entrainment into an Air Jet Laden with Particles," The British Coal Utilization Research Association Members Information Circular No. 273.

[24] Ricou, F. P., and Spalding, D. B., 1961, "Measurement of Entrainment by Axisymmetrical Turbulent Jets," Journal of Fluid Mechanics, 11, pp. 21-32.

[25] Tatterson, D. F., Marker, T. L., and Forgac, J. M., 1987, "Particle effects on free jet entrainment. ," The Canadian Journal of Chemical Engineering, 65, pp. 361-365.

[26] Chen, F., Yu, S. C. M., and Lai, A. C. K., 2006, "Modeling particle distribution and deposition in indoor environments with a new drift-flux model," Atmospheric Environment, 40, pp. 357-367.

[27] Gao, N. P., and Niu, J. L., 2007, "Modeling particle dispersion and deposition in indoor environments," Aerosol Science, 41, pp. 3862-3876.

[28] Zhao, B., Chen, C., and Tan, Z., 2009, "Modeling of ultrafine particle dispersion in indoor environments with an improved drift flux model," Aerosol Science, 40, pp. 29-43.

[29] Zhao, B., and Wu, J., 2006, "Modeling particle deposition from fully developed turbulent flow in ventilation duct," Atmospheric Environment, 40, pp. 457-466.

[30] Sextro, R., Lorenzetti, D., Sohn, M., and Thatcher, T., "Modeling the Spread of Anthrax in Buildings," Proc. Indoor Air 2002, Indoor Air 2002, pp. 506-511.

[31] WInters, W. S., and Chenoweth, D. R., 2002, "Modeling dispersion of chemical-biological agents in three dimensional living spaces," Sandia National Laboratories, Albuquerque, NM.

[32] Musser, A., and Persily, A. K., 2002, "Multizone modeling approaches to contaminant-based design," American Society of Heating, Refrigeration and Air-Conditioning Engineers, 108(2).

[33] Zhao, B., Yang, C., Yang, X., and Liu, S., 2008, "Particle Dispersion and Deposition in Ventilated Rooms: Testing and Evaluation of Different Eulerian and Lagrangian Models. ," Building and Model(43), pp. 388-397

[34] Zhang, Z., and Chen, Q., 2007, "Comparison of the Eulerian and Lagrangian methods for predicting particle transport in enclosed spaces," Atmospheric Environment, 41(25), pp. 5236-5248.

[35] Mi, J., Nobes, D. S., and Nathan, G. J., 2001, "Influence of jet exit conditions on the passive scalar field of an axisymmetric free jet," Journal of Fluid Mechanics, 432, pp. 91-125.

[36] Hardalupas, Y., Taylor, A. M. K. P., and Whitelaw, J. H., 1989, "Velocity and Particle-Flux Characteristics of Turbulent Particle-Laden Jets," Proceedings of the Royal Society A, 426, pp. 31-78.

[37] Fleckhaus, D., Hishida, K., and Maeda, M., 1987, "Effect of laden solid particles on the turbulent flow structure of a round free jet," Experiments in Fluids, 5, pp. 323-333.

[38] Longmire, K, E., and K., E. J., 1992, "Structure of a particle-laden round jet," Journal of Fluid Mechanics, 236, pp. 217-257.

[39] Casciola, C., Gualtieri, P., Picano, F., Sardina, G., and Troiani, G., 2010, "Dynamics of inertial particles in free jets," 2nd International Conference and Advanced School on Turbulent Mixing and Beyond, Physica Scripta, Rome, Italy, pp. 1-7.

[40] Gualtieri, P., Picano, F., and Casciola, C. M., 2009, "Anistropic clustering of inertial particles in homogeneous shear flow," Journal of Fluid Mechanics, 629, pp. 25-39.

[41] Chung, J. N., and Troutt, T. R., 1988, "Simulation of particle dispersion in an axisymmetric jet," Journal of Fluid Mechanics, 186, pp. 199-222.

[42] Crowe, C. T., Gore, R., and Troutt, T. R., 1985, "Particle dispersion by coherent structures in free shear flows," Particulate Science and Technology, 3, pp. 149-158.

[43] 2011, "Shop-Vac: Series LB - Wet/Dry Vacuum User Manual," Shop-Vac Corporation.

[44] "FLUENT v6.3.12," ANSYS® Academic Research, Release 14.0.

[45] 2010, "Installation, Operation and Maintenance Manual: Threaded and Wafer Style Flowmeters. M1, Rev H.," RCM Industries Concord, CA.

[46] 2010, "Heavy Duty Pitot Tube Anemometer and Differential Pressure Manometer: Model HD350: User Guide," Extech Instruments: A FLIR Company, Waltham, MA.

[47] 2011, "Material Safety Data Sheet," OSHA, ed., BioSpec Products, Inc., Bartlesville, OK.

[48] Sebasta, C., 2012, "Modeling the Effect of Particle Diameter and Density on Dispersion in an Axisymmetric Turbulent Jet," Master of Science, Virginia Polytechnic Institute and State University, Blacksburg, VA.

[49] "Custom Plasting Machining, Plastic Fabrication, Plastic Parts by Miller Plastics," http://www.millerplastics.com.

[50] Wright, J. L., Jin, H., Hollands, K. G. T., and Naylor, D., 2006, "Flow visualization of natural convection in a tall, air-filled vertical cavity," International Journal of Heat and Mass Transfer, 49(5-6), pp. 889-904.